64-3

RADC-TDR-63-338
FINAL REPORT

64-3

MECHANISMS OF FAILURE IN SEMICONDUCTOR DEVICES

TECHNICAL DOCUMENTARY REPORT NO. RADC-TDR-63-338

September 1963

Applied Research Laboratory
Rome Air Development Center
Research and Technology Division
Air Force Systems Command
Griffiss Air Force Base, New York

Project No.5519, Task No.551902

(Prepared under Contract No. AF30(602)-2778 by the Department of Electrical Engineering, College of Engineering, Syracuse University Research Institute, Syracuse 10, New York, by Glenn M. Glasford, W. Howard Card, Richard L. Anderson, Rajendra P. Nanavati.)

FOREWORD

This report covers approximately a one-year effort expended on Contract No. AF 30(602)-2778 which has been carried out as part of the Physics of Failure program of the Rome Air Development Center. The beginning of the work in this program was conducted under Contract No. AF 30(602)-2177 and the results of this earlier effort are reported in its final report, RADC-TDR-62-271 (Syracuse University Research Institute Report No. EE 751-625TN-3) entitled, THEORETICAL AND EXPERIMENTAL STUDIES RELATING TO MECHANISMS OF FAILURE OF SEMICONDUCTOR DEVICES.

Two reports which cover a portion of this effort which overlaps the previous contract appear in the publication, PHYSICS OF FAILURE IN ELECTRONICS, edited by M. F. Goldberg and Joseph Vaccaro, Rome Air Development Center, Spartan Books, Inc., 1963, which consists of the Proceedings of the Symposium on the Physics of Failure in Electronics. September 26 and 27, 1962, sponsored by the Applied Research Laboratory of Rome Air Development Center and the Armour Research Foundation. One of these reports was "Some Physical Mechanisms Contributing to Tunnel Diode Failure," by R. P. Nanavati, and the other was "Electrical Detection of Surface Effects in Transistors," by W. Howard Card.

Later informal reports were given by G. M. Glasford and W. Howard Card on the current contract at the Contractors Progress Briefing, RADC Reliability Program, Hughes Aircraft Company, Fullerton, California on January 31, 1963 on the progress on the current contract.

AIR FORCE, Cato Show Prtg. Co. 9 20 63 - 147 -

In this document, the work reported on in Section 2 and 3 is essentially the work of Dr. W. Howard Card assisted by Anton Mavretic; that in Section 4 of Dr. R. L. Anderson assisted by Adolpho Lopez; and that of Section 5, the work of Dr. Rajendra P. Nanavati assisted by Carlos D'Andrade.

Appendix I is a summary of a Master's thesis entitled, "Investigation of Germanium-Gallium Arsenide Tunnel Heterodiodes," by Kieske Yawata and Appendix II is a summary of the Master's thesis entitled, "Tunnel Diode Capacitance as a Function of Applied Voltage," by Carlos D'Andrade. These summaries include all results of the respective theses which are pertinent to the work of the Contract.

The Project Engineer of Rome Air Development Center in charge of this work has been Mr. Regis Hilow. His understanding and cooperation are gratefully acknowledged.

The secondary report number for this document is EE959-630TDR-1.

ABSTRACT

Extensive studies of low frequency noise in resistors and semiconductor devices have been made for the express purpose of exploring any correlation between low frequency excess noise and device deterioration or other anomalous behavior. New techniques for making noise measurements have made it possible to distinguish between two types of noise, one which is more or less regular which has been called clean noise and the other called burst noise which is irregular and statistically nonstationary. Present results indicate that burst noise is associated with chemical processes and is related to drift of electrical parameters. It is tentatively concluded that burst noise is also related to irreversible processes which are precursors of device failure, although further studies are required to definitely establish this connection.

Further studies have been made of gallium arsenide tunnel diode failure. Infrared radiation from diodes biased in the injection region has been measured and related to true injection current. The voltage-current characteristic of a number of diodes as a function of time have been recorded. From these measurements a quantitative relationship among radiation, injection current and degradation rate has been established. From these results and from other experiments, including capacitance measurements, an increased understanding of failure processes in gallium arsenide tunnel diodes has evolved.

PUBLICATION REVIEW

This report has been reviewed and is approved. For further technical information on this project, contact Mr. Regis Hilow, RASGR, Ext. 5264.

Approved: for DAVID F. BARBER
Chief, Applied Research Laboratory
Directorate of Engineering

Approved: for WILLIAM P. BETHKE
Director of Engineering

FOR THE COMMANDER:
IRVING J. GABELMAN
Director of Advanced Studies

TABLE OF CONTENTS

SECTION 1

INTRODUCTION

1-1. Background

At the time this group became involved in the Physics of Failure Program of the Rome Air Development Center, it was apparent that no one group or contractor could hope to explore all possible aspects of failure mechanisms. It seemed that the best contribution to the total effort was to build on and extend the work which had been done on previous contracts.

On the preceding contract (No. AF 30(602)-2177) we had made some studies of microplasma breakdown phenomenon in p-n junctions and studies on the electrical detection of surface effects in transistors. We had begun a study of low frequency noise in semiconductor devices and had developed a unique sampling correlator for making low frequency noise measurements. In addition, we had developed a technique for fabricating tunnel diodes and had begun a study of their mechanisms of failure.

All of this work was reported on in the report, RADC-TDR-62-271, THEORETICAL AND EXPERIMENTAL STUDIES RELATING TO MECHANISMS OF FAILURE OF SEMICONDUCTOR DEVICES.

Of the work which had been done on the preceding contract, two particular areas of activity showed evidence that further work might lead to tangible results in the understanding and control of failure mechanisms. These were (1) Low frequency noise studies and (2) Failure studies of Gallium Arsenide Tunnel Diodes. These two areas have received the bulk of the effort on the current contract which covers the period of 1 March 1962 to May 1, 1963.

1-2. Low Frequency Noise in Electronic Devices

In Section 2 and Section 3 to follow, the theoretical and experimental studies of low frequency noise are discussed in complete detail. We believe that some significant contributions have been made in both the understanding and measurement of noise and its possible connection with device failure.

In particular, the techniques which we have developed for the measurement of low frequency noise has made possible the differentiation between two types of noise, the more-or-less regular type, and a much more erratic type which we have classified as "burst" noise. It is the so-called "burst" noise on which our attention has been focused, and which we now believe to be related to irreversible chemical processes which are involved in device degradation and ultimate failure.

1-3. Failure Mechanisms in Tunnel Diodes

For some time there has been considerable attention paid to the problem of failure of gallium arsenide tunnel diodes with an attempt to understand the mechanisms of failure and to eliminate the causes. Preliminary efforts on this problem are described in the report referred to in Section 1-2 in which a tentative theory of failure was proposed. For some time, after the initial shock of the knowledge of the wholesale failure of GaAs tunnel diodes had worn off, and the applications were confined to the low voltage non-failure region, there was a minimum effort expended on the failure problem of these units in various segments of the semiconductor industry. Now with the renewed interest in GaAs with respect to lasers and other devices it appears that our own judgement in maintaining a continuous (although small) effort on this problem has been justified.

There have been two, more or less independent approaches to this problem which are reported on independently in Section 4 and Section 5.

Section 4 is devoted to the measurement of radiation from GaAs tunnel diodes, a careful experimental correlation of radiation with injection current and deterioration rate under conditions of relatively high forward voltage bias. An explanation of the probable cause of failure based specifically on these experimental results is presented.

Section 5 is devoted to continued efforts to evolve a comprehensive theory of tunnel diode failure. It contains modifications of the preliminary theory presented in the previous report, as based on further experimental evidence based on a variety of tests and measurements.

1-4. Supplementary Material

During the course of the contract two studies, in part directly related to the contract, and in part, something of a peripheral nature were made. Both of these are summarized in two Appendices.

One of these relates to development of Germanium-Gallium Arsenide Heterodiodes. Work in this area is proceding currently as part of other contracts.* We are following this work closely with respect to the Mechanisms of Failure aspects.

The other such study is a comprehensive analysis of tunnel diode capacitance experimentally and theoretically. By the careful development of a unique measuring system, it has been found possible to measure tunnel diode capacitance throughout the region of interest without the "scattering"

*G-24905--National Science Foundation, "Heterojunctions", Dr. R.L. Anderson.
AF 30(602)-3059--Rome Air Development Center, "Heterojunction Devices," Dr. R. L. Anderson.

of points previously found in the vicinity of the peak. At the same time a comprehensive theory has been developed, taking into account all free charges in this region with agrees with measurements. Preliminary evidence suggests that changes in capacitance in this region are precursers of device failure.

SECTION 2

THEORY OF EXCESS NOISE IN SEMICONDUCTOR DEVICES

2-1. Physics of Failure Investigations

Investigations into the physics of failure of semiconductor devices generally follow either of two attacks. By the first method, when a device fails in a particular way, studies are undertaken to find what physical, chemical or other process accounts for the observed device failure. This method is followed, for example, in the investigations of gallium arsenide device failure reported in Sections 4 and 5 of this report. For clearly defined failure modes investigations of this sort can bring quick and valuable results. Most physics of failure investigations in the past have followed this approach.

In the second method of attack particular anomalous, erratic, or unexplained characteristics of a device are investigated for two purposes. First, the relationship of the characteristic under study to the performance and long-time behavior of the device are determined. Second, attempts are made to account for the characteristic under study in terms of physical and chemical processes. If the mechanism under study contributes to failure, then, ideally, the completion of this investigation will allow this failure mode to be eliminated.

These two lines of attack fit different situations. The first is obviously suitable when the failure mode is endemic in the population, as is the case for GaAs tunnel diodes. The second may be the only practicable method when failures are relatively rare, as is the case with good present-day transistors and diodes. Section 2 and Section 3 report on an

investigation of the second kind, related to excess noise in semiconductor devices.

Nearly every semiconductor device generates electrical noise in excess of thermal noise and shot noise.[1] Similar excess noise is also generated by vacuum tubes and many kinds of resistors, and even by single crystals of semiconductor. This excess noise is often called current noise because it is only generated when current flows; or it is called 1/f noise because of its peculiar 1/f spectral density. We include in the term excess noise all noise that is not thermal noise or shot noise.

Several characteristics of excess noise suggest a relationship to device failure: (1) Excess noise occurs most commonly in devices known to deteriorate, such as hot-cathode tubes and transistors. (2) In semiconductor devices most of the excess noise generally comes from the surface, and surface changes have previously been known to cause failures. (3) Excess noise, or part of it, may be generated by the deterioration process taking place in the device, since some electrochemical processes generate excess noise. (4) Measurements of excess noise from a large sample of devices are often widely scattered, and this may indicate lack of control[2] in the manufacturing process, and hence that devices in the sample may have other weak points.[3]

Our investigations indicate that there are two kinds of excess noise. One kind remains relatively the same in time, while the other kind is erratic. We call the first kind regular or <u>clean</u> current noise, and the second kind <u>burst</u>[4] noise. The burst noise appears to be correlated with parameter drift, and to come from a nonstationary random process.[5]

In the discussion to follow the theory for current noise is reviewed and extended. Most of this theory relates to regular or clean current

noise, since a comprehensive theory for burst noise has not yet been developed. Later, in Section 3, we employ some of the derivations of this section to interpret experimental results for both clean current noise and burst noise.

2-2. Excess Noise and Energy Conversion

Low-frequency excess noise results from an energy conversion process which changes d-c power from the biasing source into a fluctuating quantity. For example, in Fig. 2-1 (a), voltage v_1 has a time-varying component when bias current I_b flows through the noisy device R. For most devices, such as semiconductor junctions or carbon composition resistors, there is no evidence that the minute amounts of electrical energy stored in the device affects the low-frequency excess noise, thus we assume that the noise voltage results because the resistance R of the device fluctuates in time.

Assume that R varies according to

$$R(t) = R_o\, g(t) \tag{2-1}$$

where

$$0 \leq g(t) \leq \infty\,, \qquad g(0) = 1$$

If g(t) were a known function then $v_1(t)$ would be

$$v_1(t) = \frac{g(t)}{\frac{R_b}{R_o} + g(t)}\, V_b \tag{2-2}$$

Note that

$$0 \leq v_1(t) \leq V_b \tag{2-3}$$

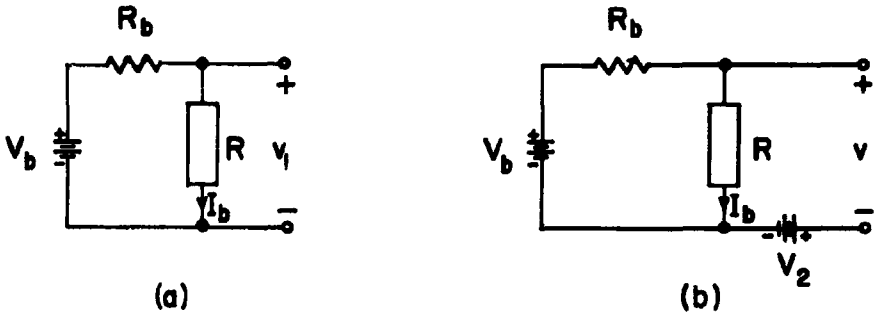

Fig. 2-1. Noisy device R in biasing circuits.

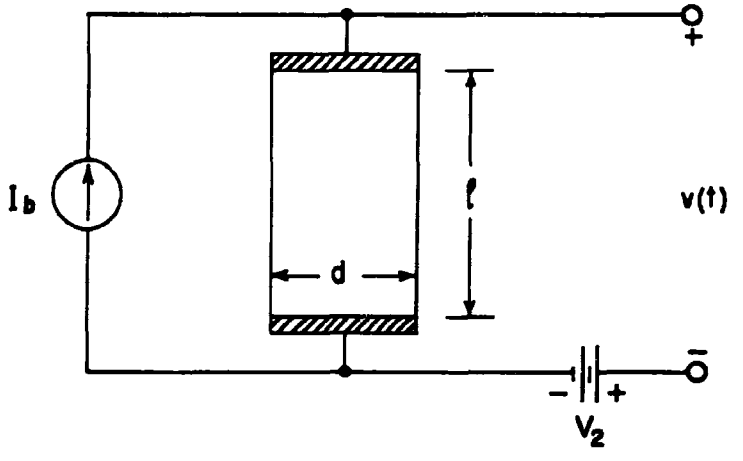

Fig. 2-2. Excess noise from a film resistor of thickness w. Voltage V_2 is chosen to make $\overline{v(t)} = 0$.

i.e., there is no possibility of infinite noise power or noise voltage. If g(t) is not known, however, and not a stationary random process few further conclusions are possible.

In many cases the resistance fluctuations are assumed to be governed by a stationary random process. Thus we can express R(t) by

$$R(t) = R_o\, h_o(t) = R_o[1 + h_1(t)] \tag{2-4}$$

where $h_o(t)$ and $h_1(t)$ are stationary random functions of time, and ensemble averages and time averages are equal.

For the stationary process, it is convenient to consider only the "a-c component." Thus in Fig. 2-1 (b) we chose V_2 so that the ensemble average of v(t) is zero

$$\overline{v(t)} = 0 \tag{2-5}$$

by making

$$V_2 = \overline{\left[\frac{R}{R + R_b}\, V_b\right]} \tag{2-6}$$

For small fluctuations

$$|h_1(t)| << \frac{R_b}{R_o} \tag{2-7}$$

this requires

$$V_2 = \frac{R_o}{R_o + R_b}\, V_b \tag{2-8}$$

For a stationary random process, an ideal true rms voltmeter (infinite bandwidth and infinite impedance) connected to read v(t) would have a time-average indication $\overline{[v(t)^2]}^{1/2}$. In noise work, however, it is often more

convenient to deal with $\overline{v(t)^2}$ which is proportional to the available noise power. For a nonstationary random process the short-term average used to approximate $\overline{v(t)^2}$ may change with time.

Up to now no mention has been made of the frequency characteristics of the noise. This will be treated later in Section 2-5.

2-3. Excess Noise and Geometry

If a device generates excess noise by virtue of a fluctuating resistance, then the noise magnitude will depend on the material, the geometry and the current. Here we present a functional form for this property, assuming that (1) the noise sources are distributed uniformly throughout the device, (2) correlation among noise sources extends over distances small compared with device dimensions, (3) the noise-induced current densities are small compared with bias current densities, and (4) the noise is a stationary random process. While some aspects of this functional form have been presented before[6] experimental verification can be inferred from the work published by others[7] who considered a less general functional form for the geometric noise dependence.

The discussion is presented in terms of bulk properties, but can easily be rephrased for surface properties. Experimental results on carbon film resistors, referred to below, indicate that the excess noise in these devices is a bulk or granular effect in the film, rather than a surface effect, at least for the thick films used commercially for resistors. On the other hand, for most semiconductor devices, the noise seems to originate in the surface.

Assume excess noise is generated in the device shown in Fig. 2-2 where the noiseless low-resistance end connections ensure uniform current density. We postulate that

$$\overline{v(t)^2} = \frac{\ell}{dw} \rho_m^2 \overline{h_1(t)^2} \mu_m(J) \qquad (2\text{-}9)$$

where $\overline{v(t)^2}$ = mean squared noise voltage

ρ_m = material resistivity (ohm meters)

$h_1(t)$ = stationary random function such that $\overline{h_1(t)} = 0$

J = average current density (amperes per square meter)

$\mu_m(J)$ = current density function.

ℓ, d, w = length, width, thickness (meters)

By assuming that the noise voltages generated by two resistors in series are uncorrelated, the linear dependence of $\overline{v^2}$ on ℓ indicated by Eq. (2-9) is plausible. Similarly, by considering two resistors in parallel, the dependence of $\overline{v(t)^2}$ on $1/(dw)$ is reasonable, provided the noise-induced currents are small compared with bias current; we have assumed this to be true.

If the resistivity were increased by a factor k, the noise voltage also would be increased by k provided $\overline{h_1(t)^2}$ and $\mu_m(J)$ were not changed. It follows that $\overline{v(t)^2}$ depends on ρ_m^2. This dependence can not be verified experimentally, since to change ρ_m requires a change of material, or at least a change of temperature, and μ_m and h_1 may also change.

One might at first expect that $\mu_m(J)$ should be proportional to J^α, with $\alpha = 2$. Experimentally, however, α is seldom exactly 2. An alternative form for Eq. (2-9) makes $\mu_m(J) = K J^2$ and lets $h_1(t)$ depend also on J. While this may be more physically correct, Eq. (2-9) is more convenient to use.

Experimental results by Kirby and Sibilia[7] on carbon film resistors essentially verify Eq. (2-9). The resistors used were made by firing carbon on to a ceramic rod, then cutting a spiral groove through the film to increase the resistance to the required value. If we neglect groove width and end effects, increasing the resistance by a factor k^2 is brought about, in effect, by increasing track length ℓ by k and decreasing track width d by k.

In all the experiments, the broad-band noise mean-square voltage was approximately

$$\overline{v(t)^2} = K I^{1.6} \tag{2-10}$$

Thus Eq. (2-9) becomes

$$\overline{v(t)^2} = \frac{\ell}{dw} \rho_m^2 \ \overline{h_1(t)^2} \ K J^{1.6} \tag{2-11}$$

Several experiments employed various spiralling lengths but constant track widths. With constant bias voltage, $\overline{v^2}$ varied as $\ell^{-0.6}$. This agrees with the results that can be predicted from Eq. (2-11), because J varied as $1/\ell$ in the test.

A second group of experiments, again at constant bias voltages, employed various spiral pitches and track lengths. The results presented are consistent with $\overline{v^2}$ varying with $\ell^{0.4}$, as predicted by Eq. (2-11). Further experiments at constant bias voltage in which the noise was measured before and after cutting the spiral groove, always showed a net increase in noise.

The results of several groups of experiments showed that the noise increased with increasing film resistance i.e., decreasing film thickness.

Equation (2-11) predicts that $\overline{[v(t)^2]}^{1/2}$ should vary as $R^{1/2}$ since R varies inversely with w, and the experimental results agree approximately with this prediction for values of film thickness used commercially. At high film resistances, (corresponding to thinner films), the noise was greater than predicted by Eq. (2-11) presumably because these films were subject to greater localized current concentrations.

Apparently, no equally comprehensive experimental results on other film and bulk materials have been published. Equation (2-9), however, should apply to other materials as well, provided the underlying assumptions are met.

2-4. Scattered Noise Measurements

It was not mentioned in the preceding section that the measurements referred to were the averages for samples of 10 or more devices. It turns out, in fact, that when the low-frequency noise is measured for a group of apparently similar devices the histogram of measurements shows a very wide scatter and is skewed toward large noise. Two interrelated explanations for this observation are (1) that the manufacturing process is not in "statistical control"[8] and (2) that some of the noise comes from a small number of discrete sources. This section discusses these explanations.

Several examples of skewed histograms have been published. Figure 2-3 (a) shows the results for 40 carbon film resistors[9] and Fig. 2-3 (b) shows the results for 99 tin oxide film resistors.[10] Even on a logarithmic scale, the measurements remain skewed toward higher values.[11] Figure 2-3 (c) shows on a logarithmic scale the distribution of measurements made on 4000 tin-oxide film resistors.[12]

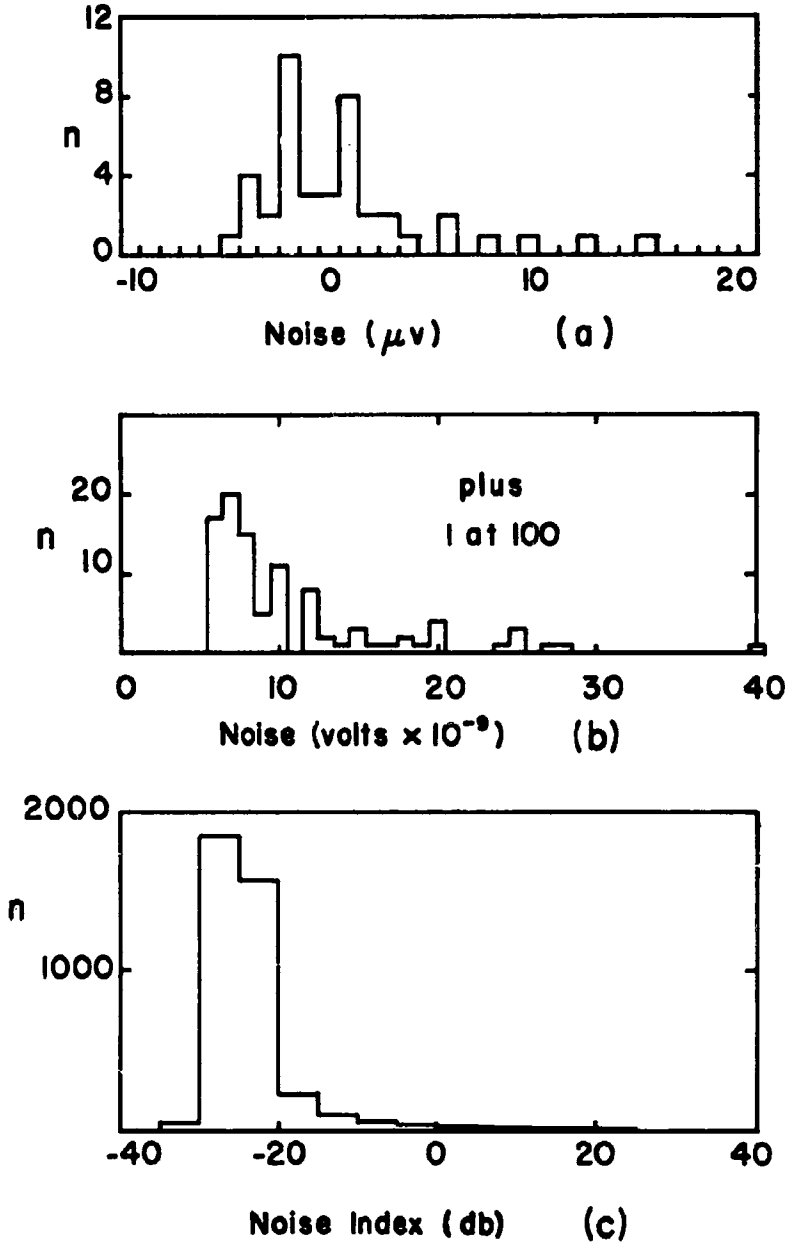

Fig. 2-3. Published histograms of noise measurements on (a) 40 carbon film resistors (b) 99 tin-oxide film resistors (c) 4000 tin-oxide film resistors.

When low-frequency noise measurements are used for statistical quality control, measurements are compared on large samples (25 or 100 or more) from several different lots or from several different manufacturers. A wide scatter in measurements in one sample as compared to another is said to imply lack of control in the manufacturing process in the widely scattered case, and hence a poorer reliability risk.[3]

We suggest that the scattered noise measurements generally observed may result from a small number (perhaps one or two in some cases) of large or high-level discrete noise sources in some devices. Careful investigations on tin-oxide film resistors[12] showed that cracks and short-circuiting chips and other gross defects made some devices very noisy. This observation justifies the use of statistical quality control techniques, and motivates the mathematical description presented next.

Assume that there are two components of excess noise, one at low level due to many small or low-level sources in all devices, and the second, at high level due to a small number of independent, usually large discrete high-level sources in the noisier devices. If the high-level sources are uniformly distributed throughout the material from which the devices are made, then $P(n)$, the probability of n high-level sources in any one of many devices of the same size, is given by a Poisson distribution.[13]

$$P(n) = \frac{\epsilon^{-N} N^n}{n!} \tag{2-12}$$

where

$$\sum_{n=0}^{\infty} P(n) = 1 \tag{2-13}$$

and N is the average number of high-level sources per device. The low-level noise may also result from a Poisson distribution of sources, which

becomes a Gaussian distribution for a large average number of sources per device. In Section 2-3 we tacitly assumed this was true.

While a Poisson distribution for the number of high-level sources seems reasonable, the probability density function for the strengths of the sources is unknown. For analysis, let us assume that all of the high-level sources belong to one kind and use $\overline{v^2}$ as a measure of source strength. We define the source probability density as $p_s(\overline{v^2})$; thus

$$\int_0^\infty p_s(\overline{v^2})\, d(\overline{v^2}) = 1 \qquad (2\text{-}14)$$

Among all the devices with exactly one high-level source, the probability density function is

$$p_1(\overline{v^2}) = p_s(\overline{v^2}) \qquad (2\text{-}15)$$

For those devices with two sources[14]

$$p_2(\overline{v^2}) = \int_0^{\overline{v^2}} p_s(x)\, p_s(\overline{v^2} - x)\, dx \qquad (2\text{-}16)$$

For those devices with k sources

$$p_k(\overline{v^2}) = \int_0^{\overline{v^2}} p_{k-1}(x)\, p_s(\overline{v^2} - x)\, dx \qquad (2\text{-}17)$$

When these definitions are combined, a general expression for all the devices is

$$p_d(\overline{v^2}) = P(0) \cdot 0 + P(1)\, p_1(\overline{v^2}) + \ldots$$

$$= \sum_{k=1}^{\infty} P(k)\, p_k(\overline{v^2}) \qquad (2\text{-}18)$$

Of course,

$$\int_0^{\infty} p_d(\overline{v^2})\, d(\overline{v^2}) = \int_0^{\infty} d(\overline{v^2}) \left\{ \sum_{k=1}^{\infty} P(k)\, p_k(\overline{v^2}) \right\}$$

$$= \sum_{k=1}^{\infty} P(k) \int_0^{\infty} p(\overline{v^2})\, d(\overline{v^2})$$

$$= \sum_{k=1}^{\infty} P(k) = 1 \qquad (2\text{-}19)$$

This probability density function $p_d(\overline{v^2})$ applies to the few high-level sources. It must be combined with the probability density function for the low-level noise to give the function to be compared with the histogram of measurements.

Alternative views are that there is only one kind of noise, or that there are more than two. These views would then employ different $p_s(\overline{v^2})$ functions to give equivalent results.

In order to illustrate the outcome of the analysis just presented consider the histogram shown in Fig. 2-3 (c). Estimate that 3500 out of 4000 devices have low-level noise only, hence,

$$P(0) = \epsilon^{-N} = 0.875$$

and

$$N \approx 0.13$$

Since no information is available on the probability density function for high-level sources, assume

$$p_s(\overline{v^2}) = ae^{-a\,\overline{v^2}} \qquad (2\text{-}20)$$

because it is easy to integrate. Here a is a scale factor. Following through with Eq. (2-18) for a = 1 gives the probability density curve in Fig. 2-4. There is a long tail on the function as required. We attribute lack of quantitative agreement to lack of knowledge of $p_s(\overline{v^2})$.

In this section we have shown that by assuming that some of the excess noise generated in devices comes from a few discrete sources we can account qualitatively for the widely scattered data generally obtained when one measures the noise from a number of apparently similar devices. We have not yet tried to determine if there is a correlation between measured burst noise, as discussed in Section 3, and the exceptionally noisy members of a large sample of devices.

2-5. Power Spectrum and Excess Noise

Up to now we have been dealing with $v(t)$ and $\overline{v(t)^2}$ neglecting any frequency-dependent properties of the noisy devices or measuring system. In this section we discuss the 1/f spectral density function associated

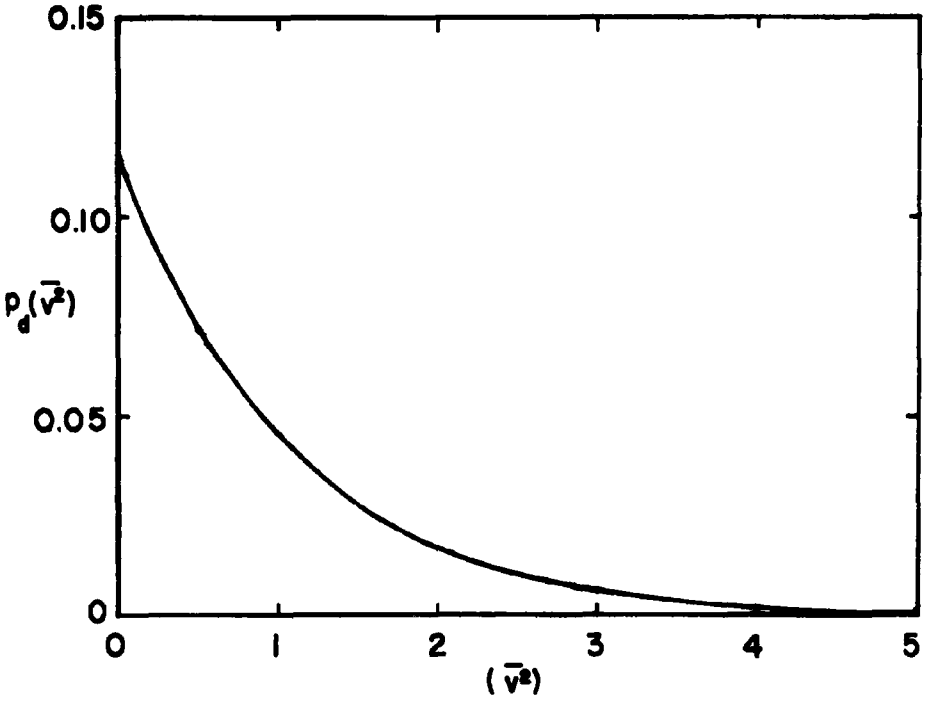

Fig. 2-4. Probability density function $p_d(\overline{v^2})$ for illustrative example.

with current noise, and mention its possible origins and limits.

Since the available excess noise power is limited by the source, as discussed in Section 2-2 no bandwidth limitations have been required in the discussion up to now. Many investigators, however, have connected wave analyzers to sources of current noise and found the power spectral density to vary nearly as 1/f in the entire range of measurement, of the order of eight decades. This outcome has been unsatisfying, since postulated physical mechanisms for 1/f noise behavior call for a lower limit to 1/f behavior, and moreover the integrated spectral density function does not converge.

To illustrate the convergence problem define a one-sided spectral density function w(f) such that

$$\overline{v(t)^2} = \int_{f_1}^{f_2} w(f)\, df \qquad (2\text{-}21)$$

Clearly, if

$$w(f) = \frac{K}{f} \qquad (2\text{-}22)$$

and we start with a finite bandwidth $f_2 - f_1 > 0$, then

$$\lim_{f_1 \to 0} \int_{f_1}^{f_2} \frac{K}{f}\, df = \lim_{f_1 \to 0} K \ln \frac{f_2}{f_1} \qquad (2\text{-}23)$$

does not exist.

It is interesting to estimate a low-frequency limit for the 1/f spectral density using the discussion of Section 2-2. From Fig. 2-1 (b) the maximum $\overline{v(t)^2}$ results when R acts as a switch. If over the measurement

interval T the switch is open half the time, and if $V_2 = V_b/2$, then

$$\overline{v(t)^2} = \frac{V_b^2}{4} \tag{2-24}$$

and

$$\int_{f_1}^{f_2} \frac{K}{f}\, df \leq \frac{V_b^2}{4} \tag{2-25}$$

Now take as a numerical example the results of noise measurements on the collector junction of a 2N1021 transistor with $V_b = 12$ volts and a bandwidth approximately 1.0 cps to 10 KC. This device gave excess noise of about 10^{-4} volts rms. From Eqs. (2-21) and (2-22),

$$K = \frac{10^{-8}}{\ell n\ 10^4} \tag{2-26}$$

Using this value of K in Eq. (2-25), and assuming f_2 remains the same while f_1 is lowered until a departure from 1/f behavior is observed, we find that

$$f_1 \geq 10^4\ \epsilon^{-36 \times 10^8\ \ell n\ 10^4} \tag{2-27}$$

This is of the order of one cycle per century. Thus there is no reason to expect a measurable lower limit to 1/f behavior unless it comes from the physical mechanism postulated to account for the noise.

Postulated physical mechanisms for a <u>stationary random process</u> to explain 1/f behavior require long time constants, associated, for example with surface quantum states,[15] and these time constants must be insensitive to temperature. An alternative explanation in terms of a nonstationary process, linked to irreversible chemical processes such as surface changes would link excess noise to deterioration. However no such theory has

been discovered in the literature and our own work is incomplete.

As an example of how a process which is not necessarily stationary can give indications of a $1/f^2$ spectral density (but unfortunately not a 1/f spectrum), assume that the noisy device comprises many independent sources. During a measuring interval T some elements generate a step voltage

$$v_i(t) = V_i\, u(t - t_i) \qquad (2\text{-}28)$$

$$0 < t_i < T$$

Analysis then shows that each such element, and hence the whole device would give

$$w(f) = \frac{K}{f^2} \qquad (2\text{-}29)$$

The noise properties of such a device would be analyzed by means of a so-called comb filter, or else by recording the noise for $0 < t < T$ and repeatedly playing it back into a wave analyzer such as is discussed in Section 3-5. No problem arises through lack of convergence of Eq. (2-29), since the lowest measurable frequency must be greater than the reciprocal of the measuring interval T.

This example is interesting as well since it shows that 1/f noise cannot be generated by elementary independent steps; if elementary steps are involved they must be correlated perhaps partially with near neighbors. If

$$v_i(t) = V_i(t - t_i)^{1/2}\ \ u(t - t_i) \qquad (2\text{-}30)$$

a 1/f spectrum would be observed, but few common physical processes give such a voltage.

2-6. Spectral Density and Autocorrelation Function

Even very noisy devices give so little noise power that high-gain amplifiers are generally employed. Consequently, even if the input noise has a 1/f spectrum for $0 < f < \infty$, the amplifier output has a limited spectrum. In this section the bandwidth limits are discussed and a typical autocorrelation function calculated in order to provide background theory for correlation function measurements reported in Section 3-5.

Most measurements of current noise are made with a-c amplifiers that span the audio frequency and low radio frequency range. For low impedance sources, the upper limit is set by the cross-over between current noise and amplifier noise. For high impedance sources, amplifier input capacitance sets the upper frequency limit. Typical limits are 10 KC - 500 KC. The low-frequency limit is set by coupling capacitor problems; d-c amplifiers are generally not feasible because of the high gain required and the high d-c bias across the noisy device which would have to be balanced out.

Figure 2-5 relates amplifier input and output spectral density when the amplifier pass band is determined by one high-frequency and one low-frequency time constant. We assume here that the input noise is a stationary random process with 1/f behavior over all frequencies for which the amplifier gives measurable response.

The input 1/f noise spectral density is conveniently expressed by

$$W_1(f) = W_1(\omega) = \frac{\omega_o}{\omega} W_1(\omega_o) \qquad (2\text{-}31)$$

so that if the amplifier has a transfer function

$$H(j\omega) = \frac{V_2(j\omega)}{V_1(j\omega)} = \frac{A\ j\omega\ T_1}{(j\omega\ T_1+1)(j\omega\ T_2+1)} \qquad (2\text{-}32)$$

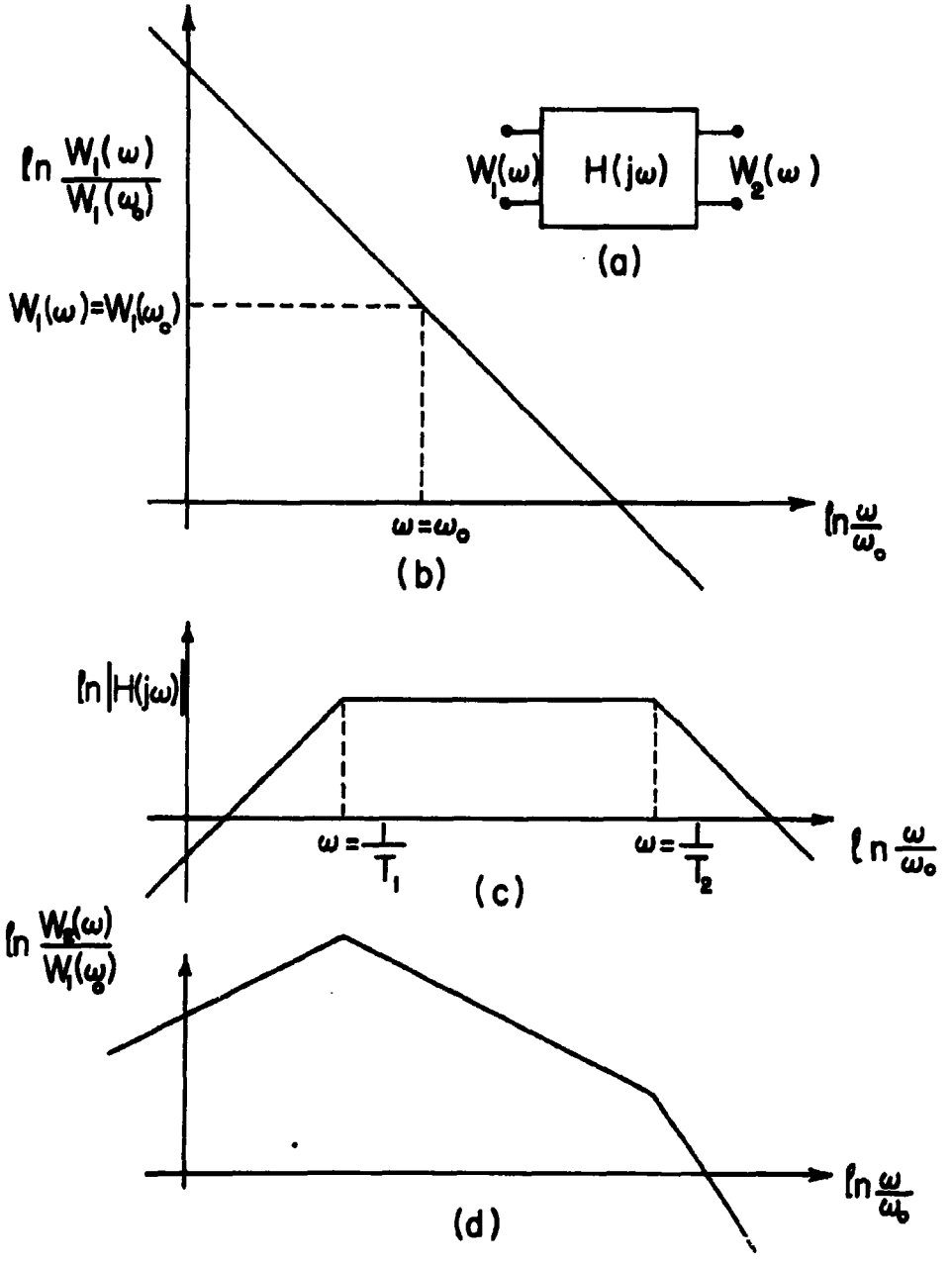

Fig. 2-5. An amplifier (a) with pass band (c) acts on 1/f noise input (b) to give an output (d). Asymtotes only are shown.

$$T_1 >> T_2$$

then the output spectral density is

$$W_2(\omega) = |H(j\omega)^2| \; W_1(\omega) \tag{2-33}$$

$$= \frac{A\,\omega\,\omega_o\,T_1^{\,2}\,W_1(\omega_o)}{(\omega^2 T_1^{\,2} + 1)(\omega^2 T_2^{\,2} + 1)} \tag{2-34}$$

We note that the problem of lack of convergence has disappeared, because now

$$\overline{v_2(t)^2} = \int_0^\infty W_2(\omega)\, d\omega \tag{2-35}$$

exists.

For a broad class of stationary random processes, the spectral density function and the autocorrelation function comprise a Fourier transform pair.[16] Thus, the (time average) autocorrelation function

$$R(\tau) = \lim_{T \to \infty} \int_0^T v(t)\, v(t + \tau)\, dt \tag{2-36}$$

is related to the one-sided spectral density by the pair of equations

$$R(\tau) = \int_0^\infty w(f) \cos \omega\tau \, df \tag{2-37}$$

$$w(f) = 4 \int_0^\infty R(\tau) \cos \omega\tau \, d\tau \tag{2-38}$$

where $\omega = 2\pi f$

Using Eq. (2-34) in Eq. (2-37) gives the autocorrelation function $R_2(\tau)$ for the output of the amplifier

$$R_2(\tau) = \int_0^\infty \frac{A\,\omega\,\omega_o\,T_1^2\,W_1(\omega_o)}{(\omega^2 T_1^2 + 1)(\omega^2 T_2^2 + 1)} \cos \omega\tau \, df \qquad (2\text{-}39)$$

$$= \frac{A\,\omega_o\,W_1(\omega_o)}{2\pi} \frac{T_1^2}{T_1^2 - T_2^2} \left\{ \int_0^\infty \frac{\omega \cos \omega\tau \, d\omega}{\omega^2 + \frac{1}{T_1^2}} - \int_0^\infty \frac{\omega \cos \omega\tau}{\omega^2 + \frac{1}{T_2^2}} d\omega \right\} \qquad (2\text{-}40)$$

This can be integrated[17] to yield

$$R_2(\tau) = \frac{A\,\omega_o\,W_1(\omega_o)}{2\pi} \cdot \frac{T_1^2}{T_1^2 - T_2^2} \left\{ -\frac{1}{2}\left[e^{-\frac{\tau}{T_1}} \overline{Ei}\left(\frac{\tau}{T_1}\right) + e^{\frac{\tau}{T_1}} Ei\left(-\frac{\tau}{T_1}\right)\right] + \frac{1}{2}\left[e^{-\frac{\tau}{T_2}} \overline{Ei}\left(\frac{\tau}{T_2}\right) + e^{\frac{\tau}{T_2}} Ei\left(-\frac{\tau}{T_2}\right)\right] \right\} \qquad (2\text{-}41)$$

where $\overline{Ei}\,(x)$ and $Ei\,(-x)$ are tabulated exponential integral functions.[18]

Notice that the amplifier sets the limits for the 1/f range in the derivation just presented. If the limits are set by the model for the physical mechanism, for example Van der Ziel's model,[19] then a different autocorrelation will result.[20]

SECTION 3

EXPERIMENTAL STUDIES OF CURRENT AND BURST NOISE

3-1. Noise Measurements

In addition to the analytical work reported in Section 2 we have been using several kinds of systems to measure the noise and other properties of a variety of devices. The purposes of these investigations were (1) to determine how each noise measuring system responded to both clean current noise and burst noise[1,2] with a view to the development of a detector of burst noise, (2) to determine the noise properties of several different devices, and (3) to begin attempts to determine whether either clean noise or burst noise is related to deterioration or other anomalous behavior in devices.

The results reported in this section show that the measured spectral density and the measured autocorrelation functions for clean current noise and burst noise do not differ appreciably. On the other hand, the amplitude distribution function for burst noise is nongaussian, while that for clean noise apparently is gaussian. Also, the broad-band rectified noise level fluctuates more for burst noise than for clean noise. While our measurements are not yet complete, preliminary conclusions are (1) that noise from chemical processes is burst noise so that burst noise indicates the possibility that chemical processes may be taking place, and (2) burst noise comes from a statistically nonstationary random process.

3-2. System for Measuring Broad-Band Noise

Figure 3-1 shows the system we use most often for measuring broad-band noise. Here the noise voltage is amplified, rectified, filtered, and then

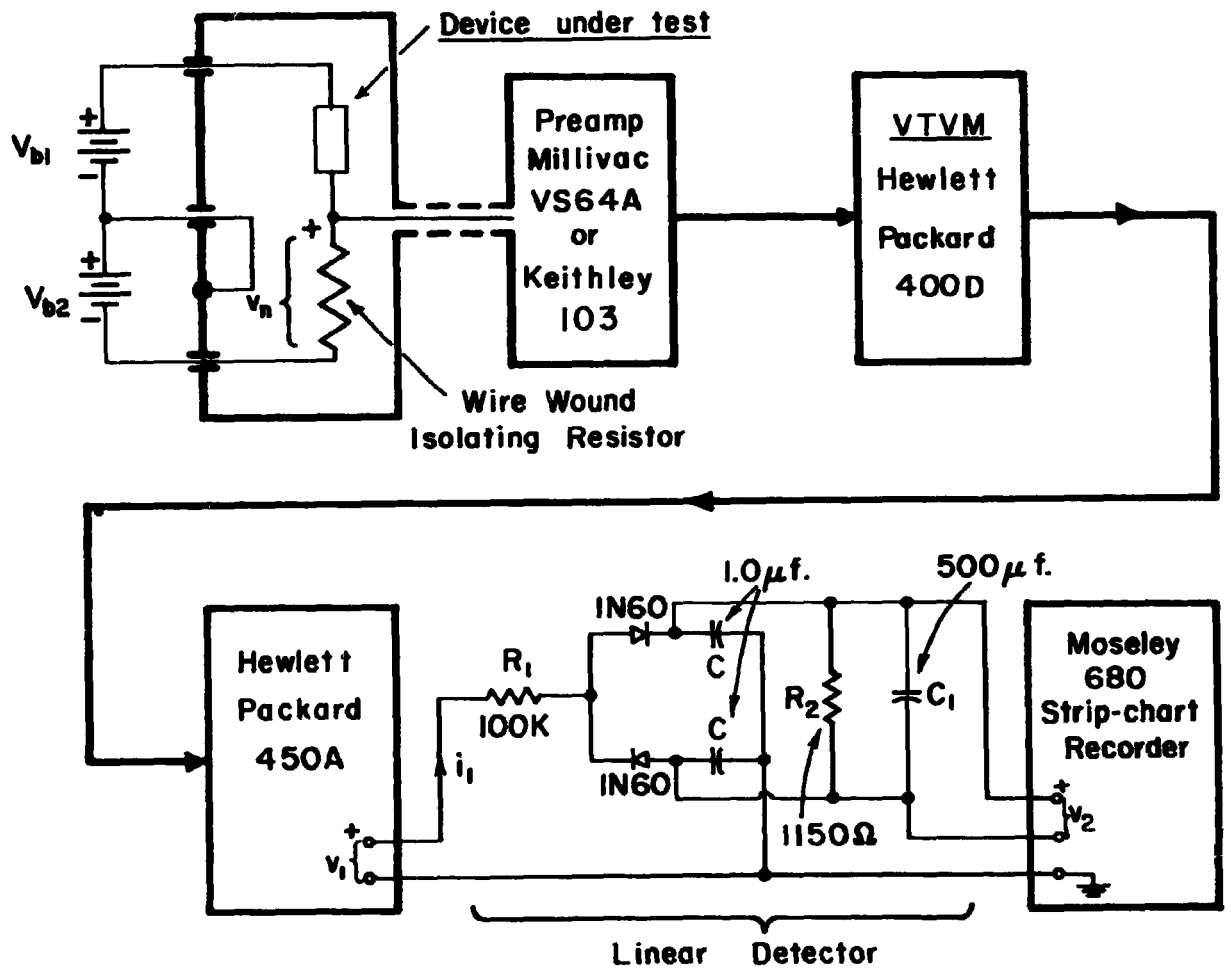

Fig. 3-1. Broad-band noise measuring system.

fed to a strip-chart recorder. Typically, several minutes of chart record is averaged to provide the noise reading, and this average can be made as accurate as desired by counting squares or using a planimeter. Employment of the strip-chart recorder thus eliminates the difficulty of estimating the average deflection of a fluctuating indicator over a long period of time. More important, as will be shown in Section 3-4, the strip-chart records for burst noise differ from those for regular current noise. This section discusses the measuring system and shows how the average recorder deflection is related to the input noise.

Usually the two-battery bias circuit shown in Fig. 3-1 is employed for measurements of resistor noise in order to balance out most of the d-c voltage across the isolating resistor before the preamplifier is connected. Adjusting bias voltage to provide balance to within $\pm$ 1.0 volts adequately protects the preamplifier input. Transistor junctions give such low currents that a one-battery bias circuit (i.e., $V_{b2} = 0$) is usually satisfactory.

Either of two commercial preamplifiers is employed. For low impedance sources we use a battery-powered Millivac VS64A (hushed) transistor amplifier, typically with nominal bandwidth 2.0 cps to 14 kc, and 40 to 80 db gain. Very noisy devices saturate this amplifier on the 50 to 80 db gain settings. For high impedance sources a Keithly 103 is employed, typically with 1.0 cps to 10 kc bandwidth and gain of 1000. Either rectifier power supply or batteries are employed. Noise from the amplifiers generally limits the sensitivity of measurements.

The rectifier circuit shown in Fig. 3-1 operates as a full-wave linear detector[3] followed by an RC low-pass filter. If we assume that the diodes

are ideal, that the recorder input impedance is large compared with R_2, and that $i_1(t)$ is a current-source drive, then analysis shows that

$$V_2(s) = \frac{R_2}{2} \frac{1}{1 + R_2 \left[C_1 + \frac{C}{2}\right] s} \cdot \mathcal{L}\left[|i_1(t)|\right] \qquad (3\text{-}1)$$

For the frequency range of interest here, R_1 is sufficiently large compared with the other impedance magnitudes so that, approximately, $i_1(t)$ is a current source

$$i_1(t) = \frac{v_1(t)}{R_1} \qquad (3\text{-}2)$$

Noting also that $C_1 >> C/2$, Eq. (3-1) becomes

$$V_2(s) = \frac{R_2}{2R_1} \frac{1}{1 + R_2 C_1 s} \mathcal{L}\left[|v_1(t)|\right] \qquad (3\text{-}3)$$

Most of the post-detector filtering is provided by C_1 which with R_2, gives about a 0.5-second time constant.

Ideally, for any stationary input, such as a stationary random noise, the d-c output voltage depends on the amplitude probability density function of the input voltage. Thus, if $v_1(t)$ has a gaussian distribution of amplitudes

$$p(v_1) = \frac{1}{\sigma \sqrt{2\pi}} \epsilon^{-\frac{v_1^2}{2\sigma^2}} \qquad (3\text{-}4)$$

with rms value

$$\overline{[v_1(t)^2]}^{1/2} = \sigma \qquad (3\text{-}5)$$

then it can be shown[4] that

$$\overline{|v_1(t)|} = 2\int_0^\infty v_1 p(v_1)\, dv_1 \tag{3-6}$$

$$= \sqrt{\frac{2}{\pi}}\ \sigma \tag{3-7}$$

Using this result in the d-c limit of Eq. (3-3) gives

$$V_{d\text{-}c} = \overline{v_2(t)} = \frac{R_2}{2R_1}\sqrt{\frac{2}{\pi}}\ \sigma \tag{3-8}$$

$$= \frac{R_2}{\sqrt{2\pi}\ R_1}\sqrt{\overline{v_1(t)^2}} \tag{3-9}$$

Consequently, if the voltage gain from v_n to v_1 is K then

$$\overline{v_n(t)^2} = \frac{2\pi R_1^2}{K^2 R_2^2}\ [\overline{v_2(t)}]^2 \tag{3-10}$$

$$= \frac{2\pi R_1^2}{K^2 R_2^2}\ V_{d\text{-}c}^2$$

Because C_1 does not provide "complete" filtering, the recorder indication will have a fluctuation superimposed on the average deflection. Section 3-3 discusses this. For a nonstationary input, or an input with nongaussian amplitudes, such as burst noise, not all of the preceding analysis applies.

The amplifier-rectifier system shown in Fig. 3-1 gives full scale on the recorder 50 mv range without overloading appreciably; however, for a gaussian amplitude function peaks above 3.7 standard deviations are clipped.

3-3. Output Fluctuations from a Broad-Band Noise Measuring System

In this section we show how the fluctuations of the recorder indication may be calculated for a restricted class of stationary random functions. This calculation is used in Section 3-4 to interpret experimental results.

First, consider a time-independent full-wave rectifier characteristic

$$v_a = b\,|\,v_1\,| \tag{3-11}$$

From the d-c limit of Eq. (3-3), we know that for the system in Fig. 3-1

$$b = \frac{R_2}{2R_1} \tag{3-12}$$

Second, for convenience, use a two-sided spectral density function

$$S(f) = \frac{1}{2}\,w(f) \qquad f > 0 \tag{3-13}$$

$$S(-f) = S(f) \tag{3-14}$$

where

$$\overline{v(t)^2} = \int_{-\infty}^{\infty} S(f)\,df \quad (\text{volts}^2) \tag{3-15}$$

Third, assume that the noise has not only a gaussian distribution of amplitudes (as assumed in Section 3-2) but is further restricted to be a gaussian random process.[5]

With these assumptions, a straightforward extension of the analysis for a half-wave linear detector[6] to the full-wave case gives for the spectral density of the output (with no post-detector filter)

$$S_a(f) = \frac{2}{\pi}\,b^2\,\sigma_1^{\,2}\,\delta(f) + \frac{b^2}{\pi\sigma_1^{\,2}} \int_{-\infty}^{\infty} S_1(x)\,S_1(f-x)\,dx \tag{3-16}$$

The d-c output voltage

$$V_{d\text{-}c} = \left[\frac{2}{\pi}\ b^2\ \sigma_1^2\right]^{1/2} \qquad (3\text{-}17)$$

predicted by Eq. (3-16) agrees, of course, with $V_{d\text{-}c}$ predicted by Eq. (3-8) and (3-12). The second term in Eq. (3-16) gives the spectral density of the ripple in the output before the post-detector filtering.

For example, if $S_1(f)$ were the ideal band-limited flat-spectrum noise shown in Fig. 3-2(a) with mean-square value E^2 volts^2, then the d-c output would be $[2b^2\ E^2/\pi]^{1/2}$ and the ripple spectrum would be as shown in (b). Furthermore, if the rectifier is followed by an ideal low-pass filter, as shown in (c), then (d) shows $S_2(f)$, the restricted spectrum of the output. Using the rectangular approximation indicated by the broken lines in (d) gives an approximate rms ripple voltage at the indicator (strip-chart recorder) of

$$V_{a\text{-}c} = \left[\frac{b^2E^2}{2\pi f_1}\ 2f_c\right]^{1/2} \qquad (3\text{-}18)$$

$$= b\ E\ \left[\frac{f_c}{\pi\ f_1}\right]^{1/2} \qquad (3\text{-}19)$$

For the present discussion, the interesting relation is the ratio of rms ripple to the d-c output, i.e.,

$$\alpha = \frac{V_{a\text{-}c}}{V_{d\text{-}c}} = \frac{b\ E\ \left[\frac{f_c}{\pi\ f_1}\right]^{1/2}}{b\ E\ \left[\frac{2}{\pi}\right]^{1/2}} = \left[\frac{f_c}{2f_1}\right]^{1/2} \qquad (3\text{-}20)$$

The ratio $V_{a\text{-}c}/V_{d\text{-}c}$ can be computed by the above method for any spectral density function from a gaussian random process. Consider, as a further example, white noise and 1/f noise both filtered by a bandpass amplifier with transfer function

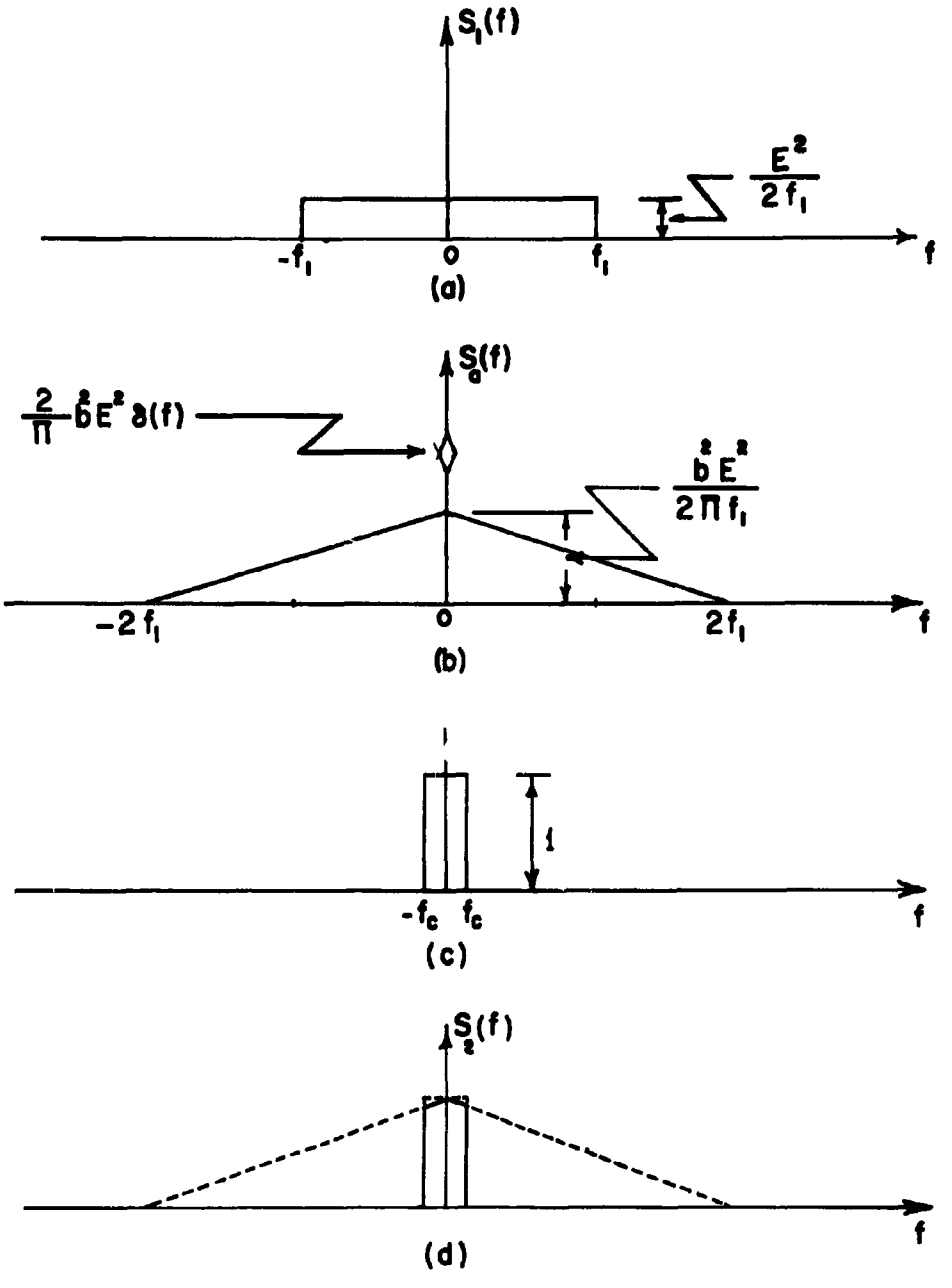

Fig. 3-2. Behavior of full-wave linear detector and low-pass filter for high-frequency-limited white noise.

$$H(j\omega) = \frac{j\omega T_1}{(j\omega T_1 + 1)(j\omega T_2 + 1)} \qquad (3\text{-}21)$$

$$T_1 >> T_2$$

Assuming also that $1/T_2 >> f_c$, fairly tedious analysis shows that for white noise input

$$\alpha_1 = \frac{V_{a\text{-}c}}{V_{d\text{-}c}} \approx \sqrt{f_c T_2} \qquad (3\text{-}22)$$

and for 1/f noise input

$$\alpha_2 = \frac{V_{a\text{-}c}}{V_{d\text{-}c}} \approx \pi \frac{[T_1 f_c]^{1/2}}{\ell n \left(\frac{T_1}{T_2}\right)^2} \qquad (3\text{-}23)$$

As a numerical example, assume that the amplifier has a transfer function given by Eq. (3-21) with $T_1 = 1/(10\pi)$ and $T_2 = 1/(2\pi \times 10^4)$. With $f_c = 1/\pi$ cps, calculation shows $\alpha_1 = 0.00225$ and $\alpha_2 = 0.0382$. An interesting parameter

$$\gamma = \frac{\alpha_2}{\alpha_1} = \frac{\pi}{\ell n \left(\frac{T_1}{T_2}\right)^2} \sqrt{\frac{T_1}{T_2}} \qquad (3\text{-}24)$$

gives the ratio of ripple for 1/f noise to the ripple for white noise if the gains are set to give the same d-c output. For the present example $\gamma = 17$.

In principle the ratio $V_{a\text{-}c}/V_{d\text{-}c}$ can be calculated for any input which is a gaussian random process, and any amplifier transfer function. For small such ratios, the fluctuation about the mean deflection will

have a gaussian distribution of amplitudes. Thus, tolerance lines can be drawn on the strip chart, and a calculable fraction of the record, on the average, should fall within the tolerances. For example, lines drawn at $V_{d-c} \pm 2\ V_{a-c}$ should contain 95 percent of the record.

Strictly speaking, failure of the calculated percent of the record to fall within the tolerances only means that the noise does not come from a gaussian random process. From the charts and waveforms presented in Section 3-4 it appears that in these cases the noise is also nonstationary. Thus we assume that an out-of-tolerance strip chart implies a nonstationary noise, which, as mentioned in the next section, is classed with burst noise.

3-4. Burst Noise and Broad-Band Noise Measurements

This section reports results of broad-band noise measurements made on a number of devices, mostly using the system of Fig. 3-1. We relate these strip chart records to the time waveforms observed with an oscilloscope, and also to the discussion of Section 3-3.

The excess noise from some devices shows spikes, steps, skewed amplitude distribution functions, or changing noise levels. Other devices have none of these anomalies. We say that those devices with the anomalous behavior have burst noise.

Figure 3-3 shows the strip-chart records for the collector junctions of two 2N1021A transistors in (a) and (b), and nearly-white noise in (c) for comparison. (In fact, a magnetic tape of the noise was also made, as is discussed in Section 3-5.) Although the gain and bandwidth were the same for both transistor tests, the two charts are different, with (a) showing greater fluctuations than (b). Very roughly, (b) has fluctuations about 10 or 20 times as large as those in (c) as predicted by Eq. (3-24) and we assume (b) has clean current noise. Because the fluctuations in (a)

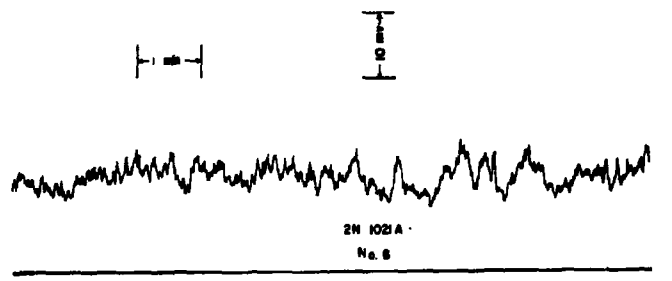

(a)

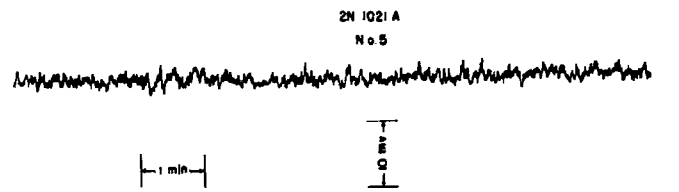

(b)

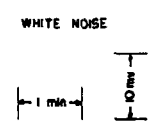

(c)

Fig. 3-3 (a), (b) Broad-band excess noise from transistor collector junctions with 12 volts bias. (c) Thermal and amplifier noise.

are larger and the noise level appears to fluctuate we infer that (a) has burst noise.

For a second example, Fig. 3-4 shows results for two 200K carbon composition resistors, (that is, with one substituted for the wire-wound isolating resistor normally employed in Fig. 3-1). In Fig. 3-4 (a) the segments are labelled for the battery voltage across the two resistors. The discrete step in the 202.5-volt segment, and the several spikes in the 225-volt segment are typical of the strip-chart records generally obtained with carbon composition resistors. In (b) the nongaussian amplitude distribution function lasted for several minutes; similar waves lasting a few seconds are often observed but are exceedingly difficult to photograph. Evidence such as this indicates that the noise from carbon composition resistors (also called contact noise) is nonstationary.

For an example of noise with exceedingly large burst content, linked to a chemical process, Fig. 3-5(a) shows results from a deteriorated 45-volt dry cell battery, supplying current to a 5000-ohm wire-wound resistor; (b) shows a sample of the waveform. Spikes and steps in the time waveform predominate in battery noise.

Figure 3-6 shows results at several voltages from a 220K carbon film resistor. At low voltage the oscilloscope pattern and strip-chart record were regular, indicating few if any bursts. For 135 volts and above, bursts appeared in the oscilloscope pattern and the strip chart became more erratic.

By contrast with the results from carbon film resistors, Fig. 3-7 shows the relatively regular noise recorded from a Kodak EKTRON lead sulphide photoconductor cell. We assume this is clean current noise.

As a final example of broad-band noise measurements, Fig. 3-8 shows results from a silicon resistor designed for sensing temperature

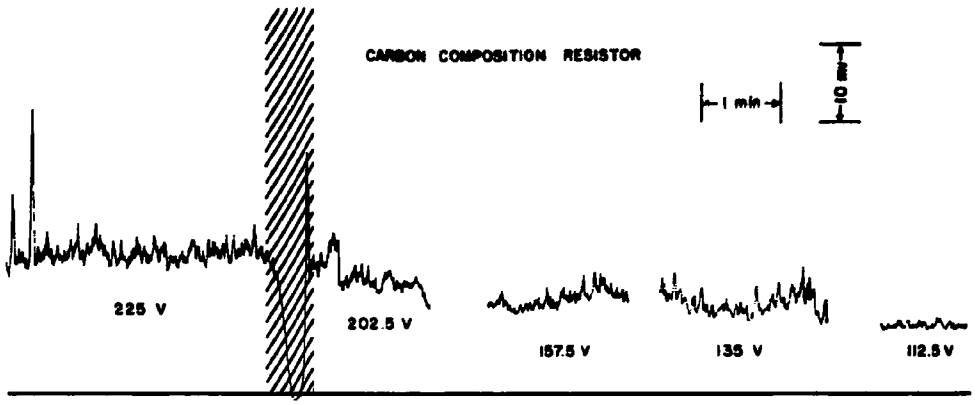

(a)

(b)

Fig. 3-4. (a) Excess noise from carbon composition resistors.

(b) Waveform with 5 milliseconds per division.

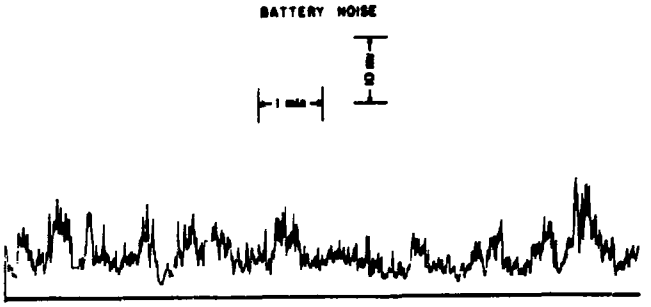

(a)

(b)

Fig. 3-5. (a) Noise from a deteriorated dry-cell battery
(b) Waveforms with 5 milliseconds per division.

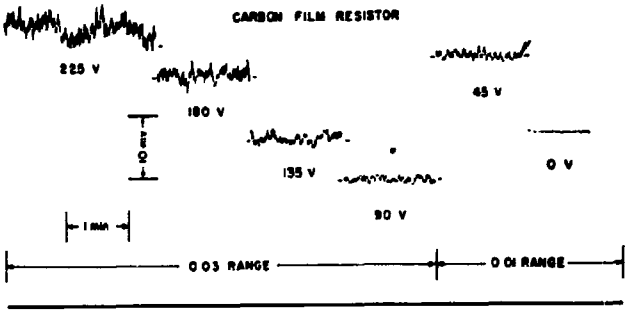

Fig. 3-6. Noise from a 220K carbon film resistor at various voltages.

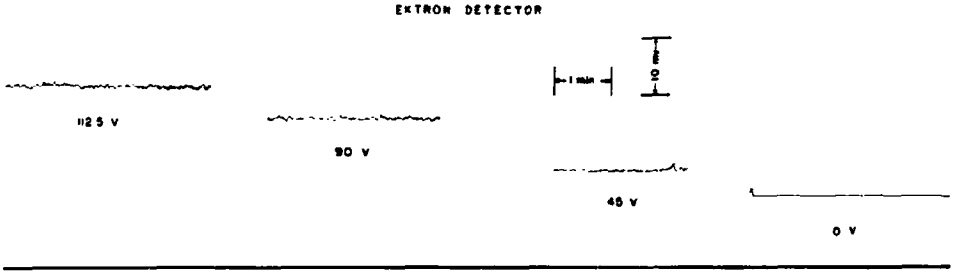

Fig. 3-7. Noise from lead-sulphide photoconductive cell.

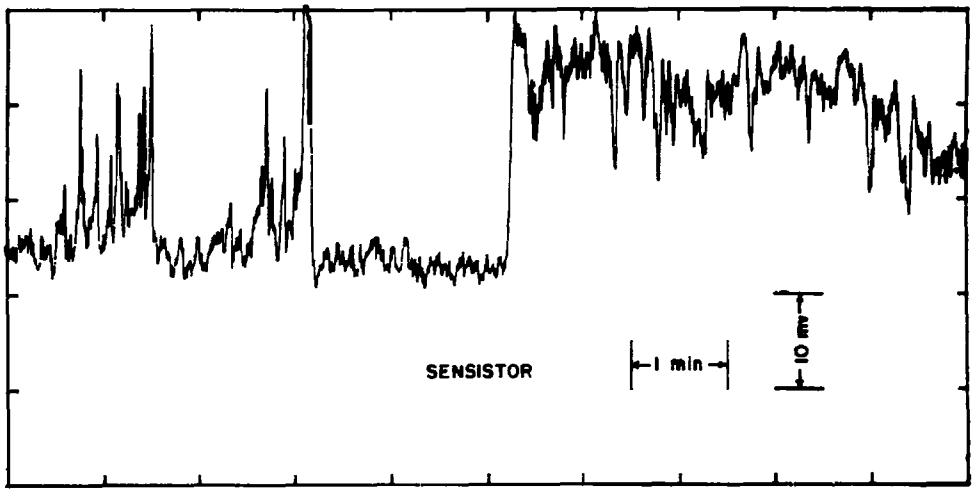

Fig. 3-8. Noise from a 2K silicon temperature-sensing resistor at rated dissipation and room ambient.

(SENSISTOR). Here the noise changes from intervals of very bursty behavior to intervals of almost clean current noise.

We have observed and measured the excess noise from many other devices as well. As judged by the occurence of steps and spikes in the oscilloscope pattern some of the devices had burst noise and others did not. Those devices with a lot of steps and spikes gave excessive fluctuations to the strip-chart record. Thus the broad-band noise measuring system provides a nonsubjective but, unfortunately, fairly insensitive indicator of burst noise. More selective instruments for distinguishing burst noise would be useful.

3-5. Autocorrelation Function and Spectral Density Measurements

One characteristic of low-frequency excess noise that continually attracts the attention of researchers is the power spectral density function which varies closely as reciprocal frequency. Occasionally, reported results have shown considerable scattering of the experimental points. Moreover, we wondered if the very erratic broad-band noise records for burst noise, such as are reported in the preceding section would give rise to any anomalies in the spectral density function, thus accounting for scattering of measured points. This section reports studies of this sort made with a wave analyzer to give spectral density directly. In addition, we report measurements made with a special autocorrelation function computer to determine the Fourier transform of the spectral density. Our results indicate that both burst noise and clean current noise give close to a 1/f spectrum. We have no definite evidence that burst noise contributes anomalies to either the spectral density curve or the autocorrelation function curve.

In order to make measurements which are of value even for a nonstationary process, we record the noise to be analyzed on a special-purpose magnetic tape recorder. By repeatedly rewinding the tape we can get each measured point from exactly the same sample of noise.

Figure 3-9 shows the noise recording system. Part of the system is the same as in Fig. 3-1. By recording on the magnetic tape and strip chart simultaneously, we can determine if any relation exists between broad-band noise and spectral properties. The same recording system was employed for the spectral analysis and autocorrelation function measurements reported in this section and also for the amplitude distribution function measurements reported in Section 3-6.

The Mnemotron "extended frequency range" modulator-demodulator and tape-recorder system employed here has nominal frequency range 0-800 cps, but a calibration curve was necessary to compensate for the non-flat frequency response. With the calibration curve, however, useful results 0-1000 cps were obtained.

For spectral analysis measurements, the system shown in Fig. 3-10 was employed. The voltage-to-frequency converter nominally generates pulses at a rate directly proportional to the amplitude indication on the wave analyzer. By totalizing these pulses over the measurement interval T (as timed with a stop watch) an average very close to the theoretically best can be obtained.

We can compute the required measurement interval T for any desired accuracy.[7] For example, provided the bandwidth of the analyzer is much less than the center frequency, of the pass band, we can be 95 percent sure that the error is less than P percent if

$$T = \frac{4 \times 10^4}{P^2 \Delta f} \text{ (seconds)} \qquad (3\text{-}25)$$

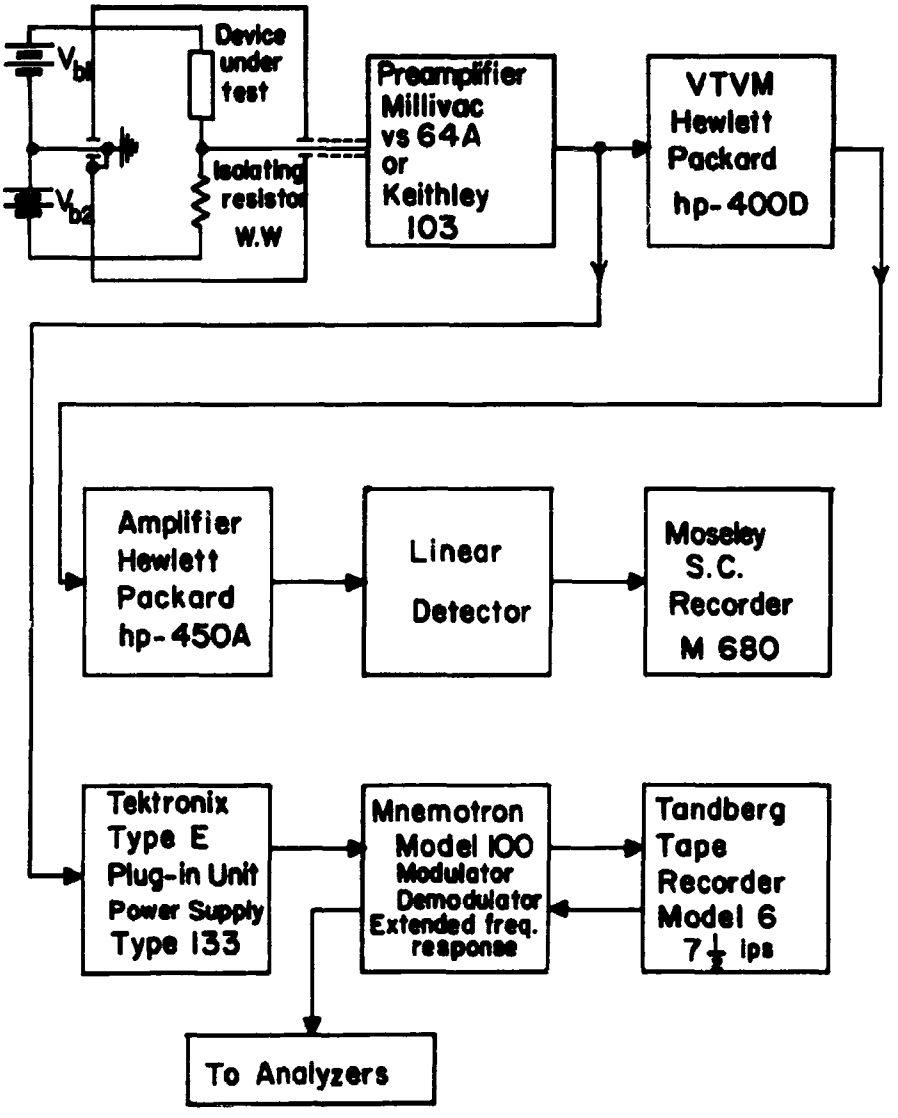

Fig. 3-9. System for recording low-frequency noise.

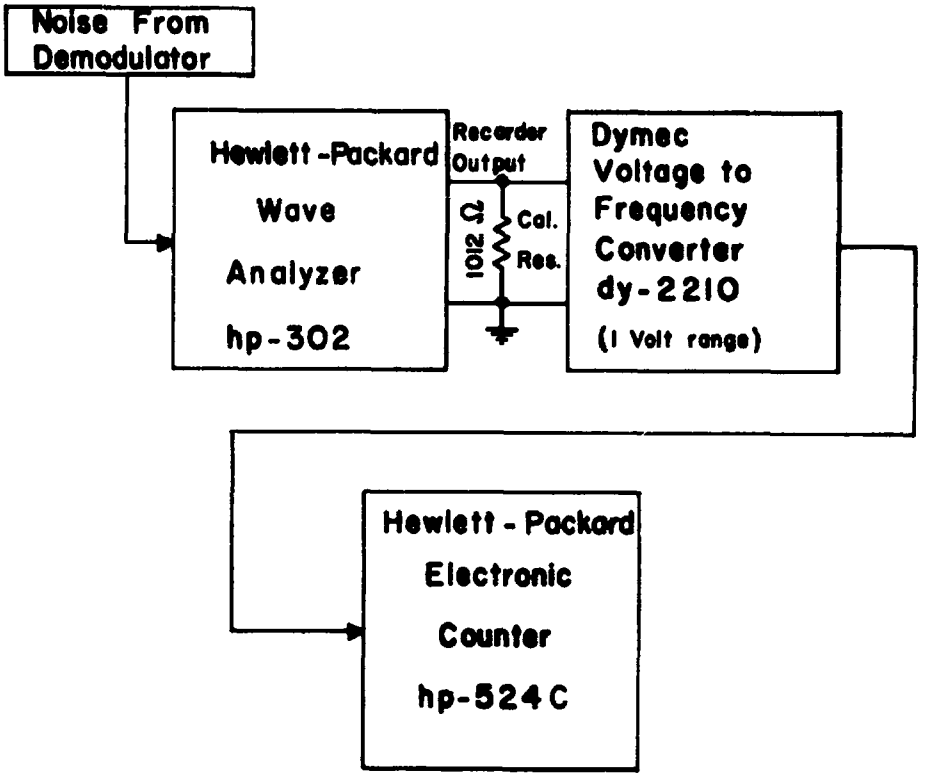

Fig. 3-10. Spectrum analysis system.

For Δf = 7 cps and P = 5 percent T is about 4 minutes. Thus even for this modest accuracy, averaging the reading of a fluctuating indicator by eye is not likely to be satisfactory.

Typical results for spectral analysis are shown in Fig. 3-11 and Fig. 3-12. Two 3-minute samples marked A and B on the strip chart record shown in Fig. 3-11 were analyzed, and the results are shown in Fig. 3-12. Both samples gave smooth spectra and both are nearly 1/f. The curve for sample A may be slightly steeper; however, other similar experiments on both clean current noise and moderately burst noise gave no clear evidence of large departures from 1/f behavior. Measurements made on germanium whiskers, transistors, batteries, and carbon-film resistors showed nearly 1/f noise in every case.

For autocorrelation function measurements we employed a special sampling correlator which is discussed elsewhere[8] in the system shown in Fig. 3-13. Autocorrelation functions, shown in Fig. 3-14, were measured for the two samples of noise shown in Fig. 3-3. The slight differences, aside from amplitude, between these two results can be attributed to inaccuracies in the computer. Moreover, they both agree in form with calculated curves using Eq. (2-41). (Direct comparison with Eq. (2-41) is not valid since in that equation low-frequency response depended on only one time constant.)

We conclude from these results that neither spectral density nor autocorrelation function measurements provide sensitive means for distinguishing burst noise from clean current noise.

It was mentioned that the recorder system permits useful measurements for even a nonstationary process. To illustrate this consider a stationary 1/f noise source which is turned off at some time not too close to the beginning of the measurement interval T. The input is now nonstationary.

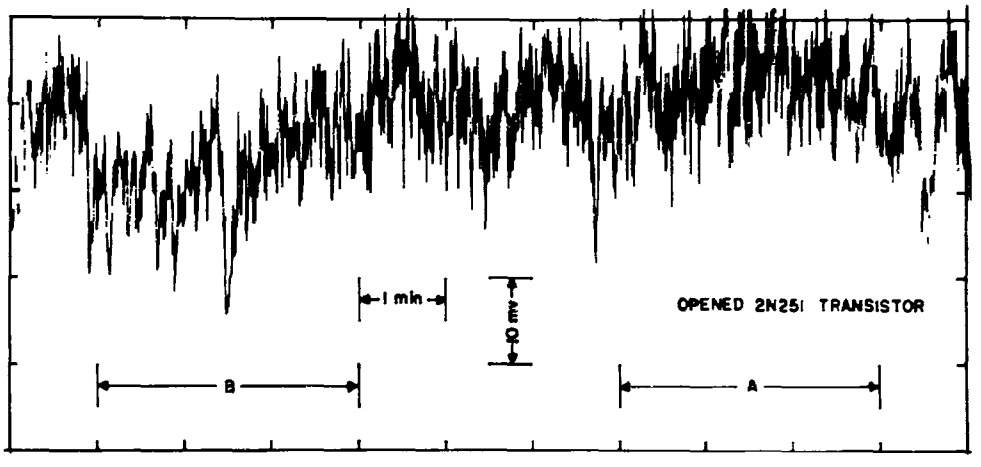

Fig. 3-11. Strip chart records of noise from an opened 2N251 transistor. The labels show the two samples that were analyzed.

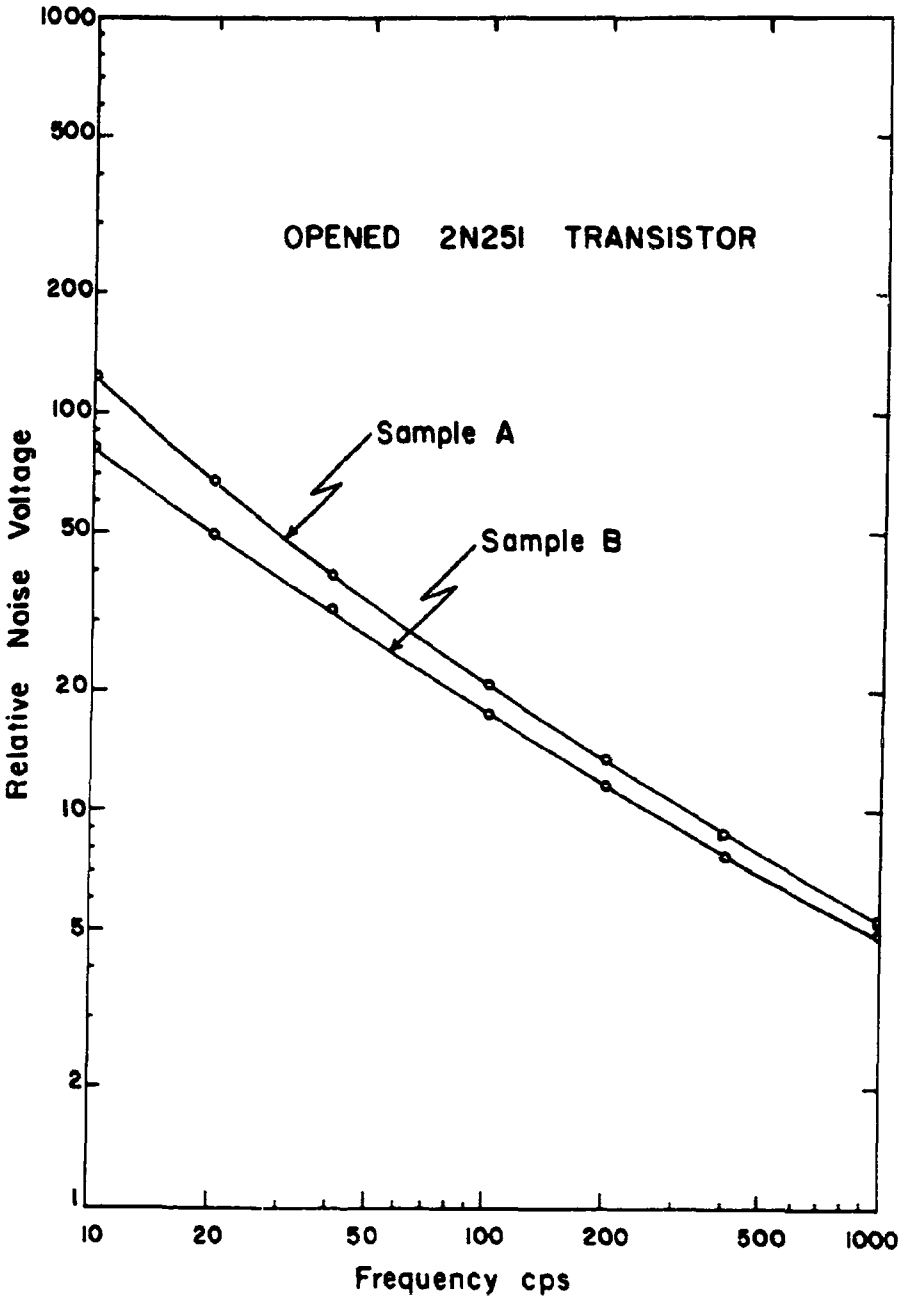

Fig. 3-12. Measured spectral density for burst noise.

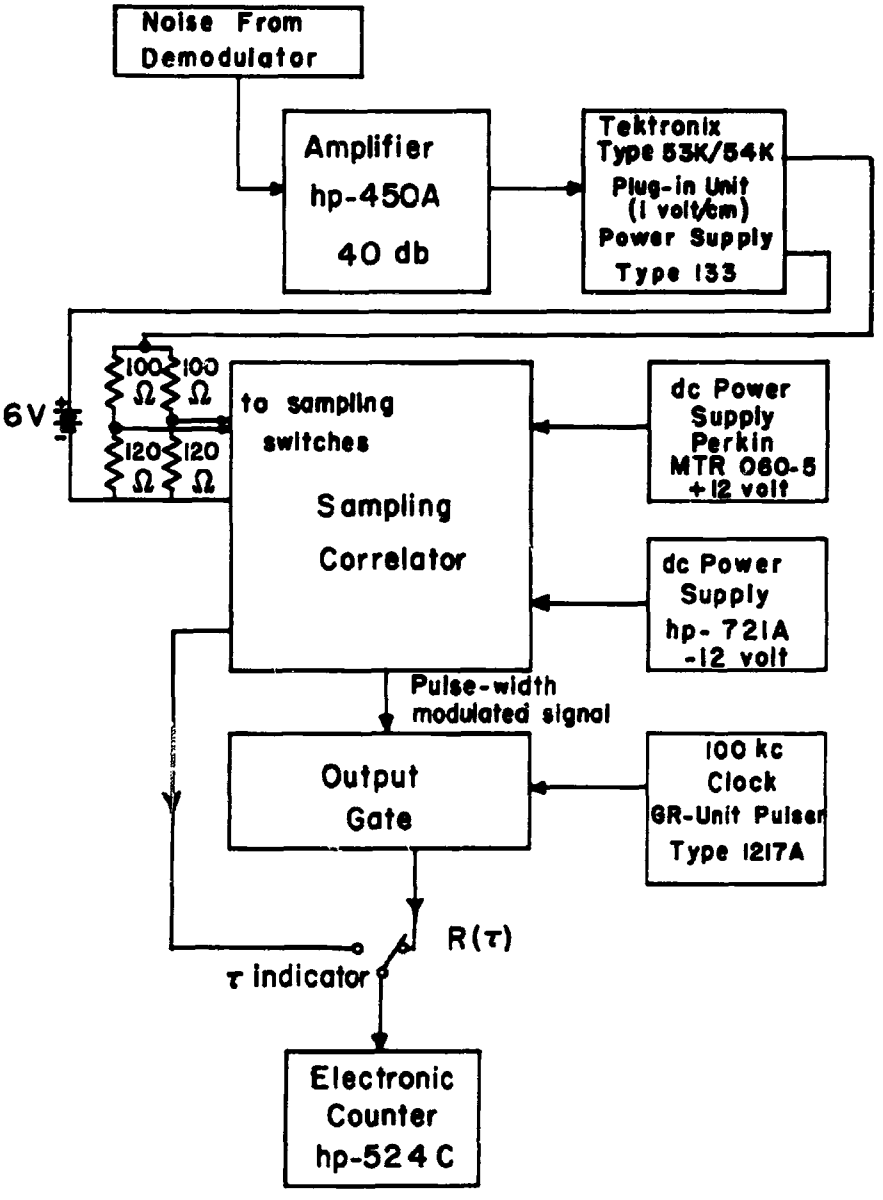

Fig. 3-13. System for measuring autocorrelation function of excess noise. The electronic counter is used as a τ indicator, and also to measure $R(\tau)$.

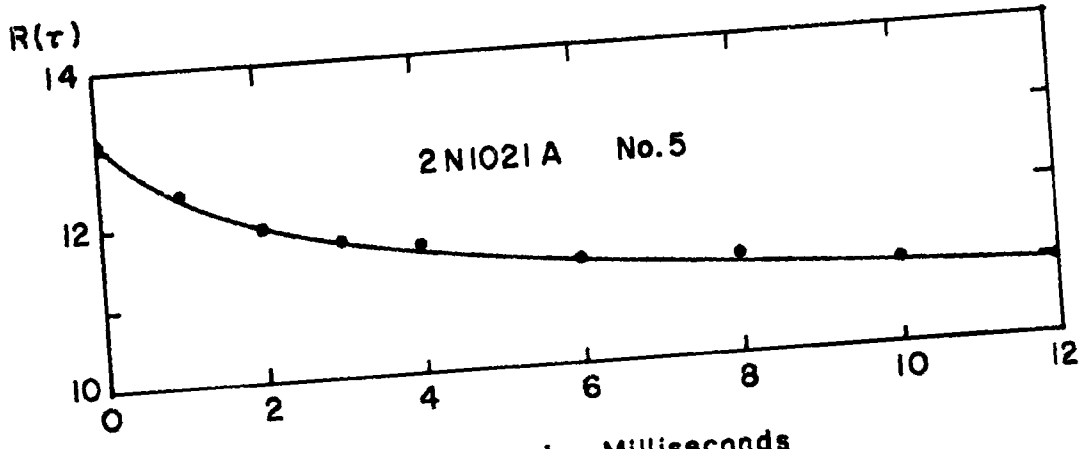

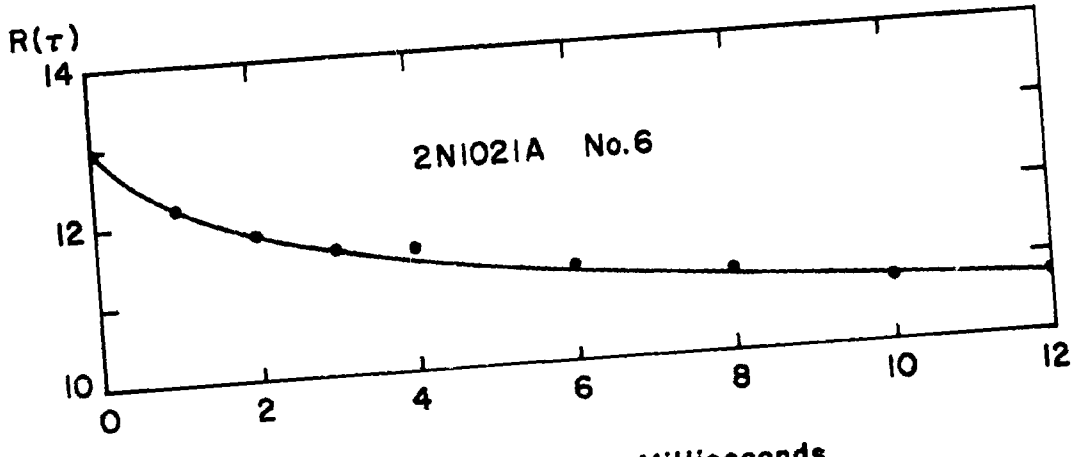

Fig. 3-14. Measured autocorrelation functions from tape-recorded noise corresponding to the strip-chart records of Fig. 3-3 (a) and (b).

A spectrum analysis carried out with the recorder and wave analyzer system employed here would still show very closely a 1/f spectrum, at least within the range of valid measurements for which the center frequency is much greater than 1/T. The measurement thus gives little indication of anything except 1/f behavior.

In the same manner, we interpret some erratic strip chart records as resulting from changes in noise level. In view of the example just discussed we expect our measurements to indicate 1/f behavior, as they do.

3-6. Measurements of Amplitude Distribution Function

Measurements show that clean current noise has a gaussian amplitude distribution function, whereas burst noise has a distorted distribution. This section shows how these measurements were made and reports typical results.

The recording system of Fig. 3-9 was used to supply noise to the amplitude distribution function analyzer* employed in the system shown in Fig. 3-15. Once again the recording system permits all measurements to be made from the same sample, and the electronic counter permits accurate averaging.

Typical experimental results are plotted on probability coordinates in Fig. 3-16. These coordinates give straight lines for inputs having gaussian amplitude distributions.

Measurements were made on the first three minutes of each of the noise samples shown in Fig. 3-3, and the data are plotted in Fig. 3-16. Curvature at the extreme ends may have resulted from amplifier distortion. Also plotted are measurements of battery burst noise; it is clearly nongaussian.

*A Quan-Tech model 317 Amplitude Distribution Analyzer was loaned to us by the Robert F. Lamb Company, Inc., Syracuse, N.Y., by arrangement with Mr. William Lawrow.

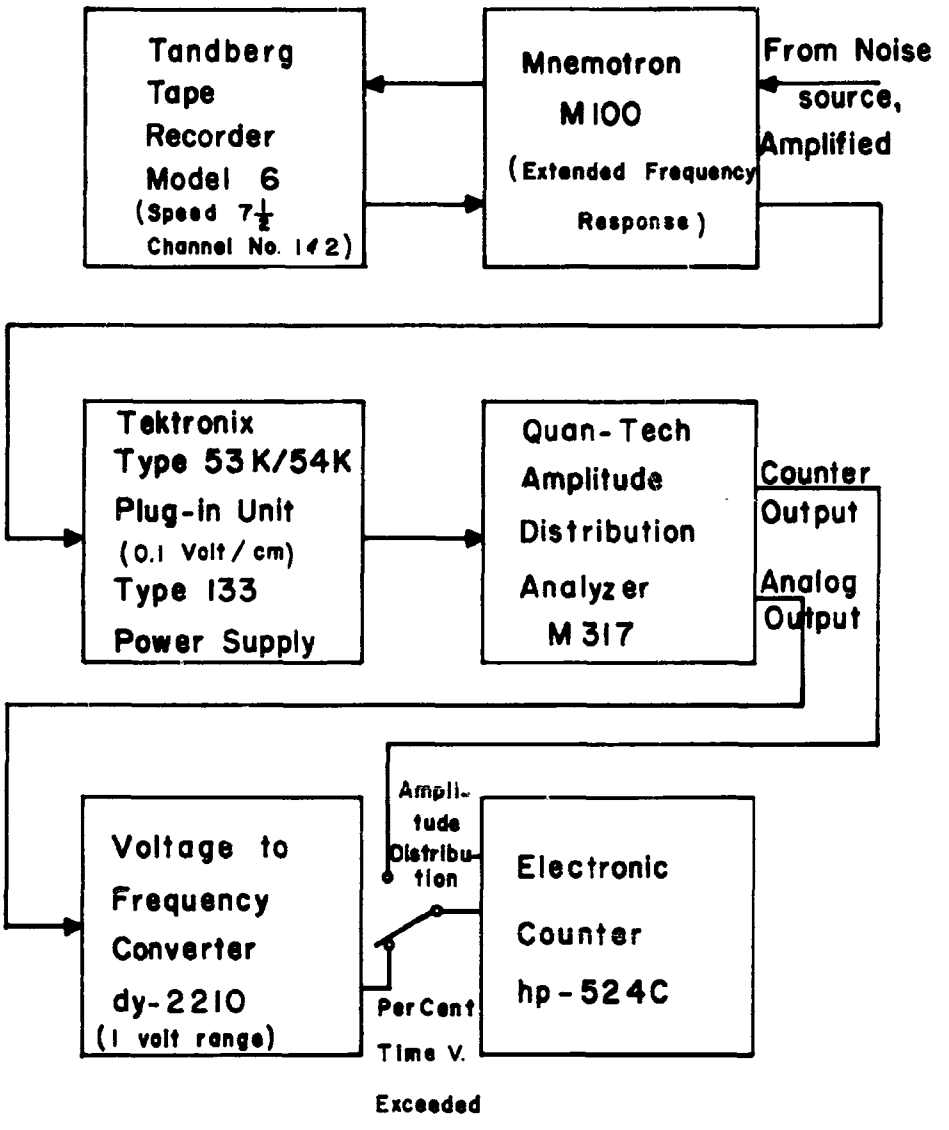

Fig. 3-15. System for measuring amplitude distribution.

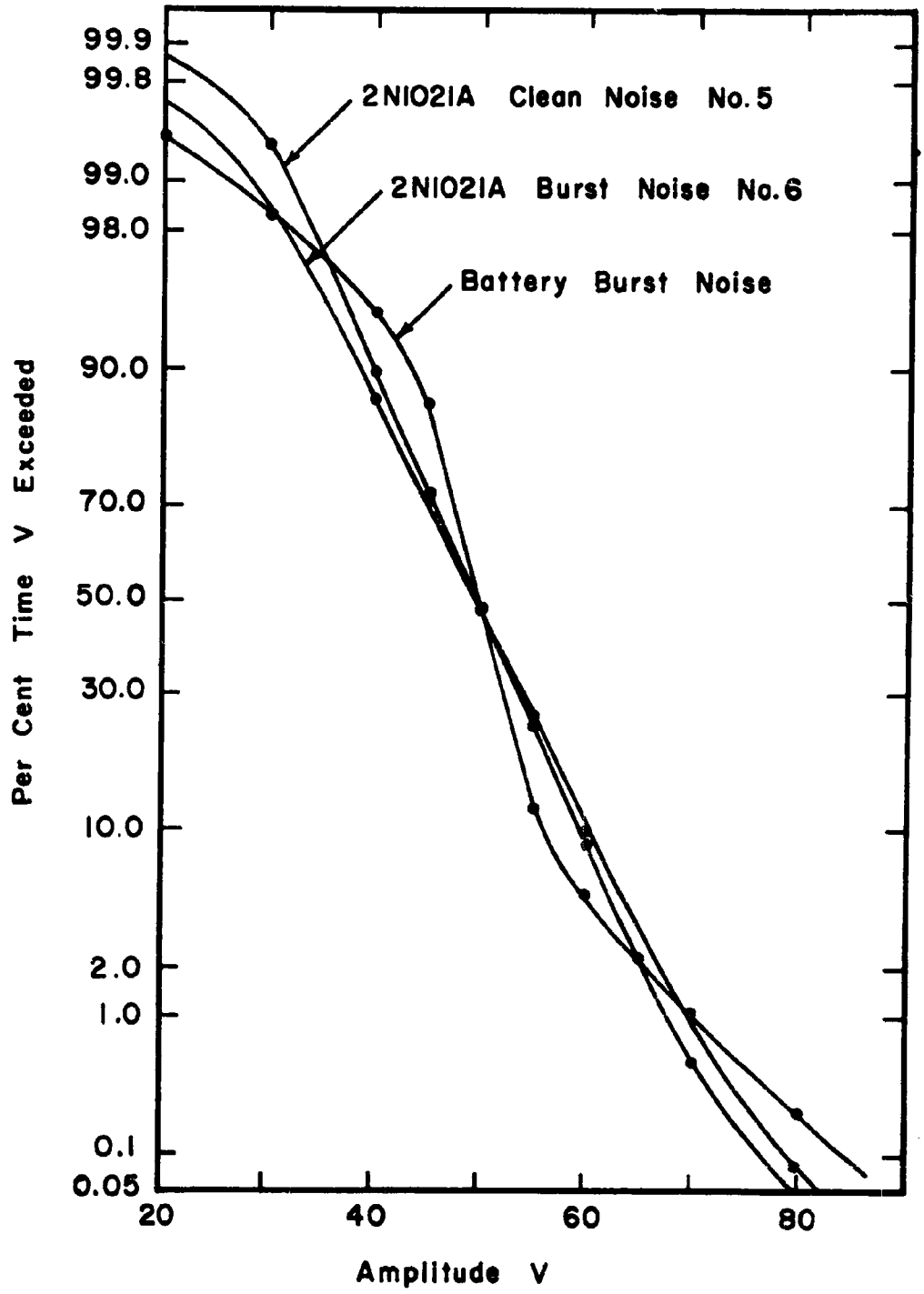

Fig. 3-16. Measured amplitude distribution functions.

We conclude that measurements of amplitude distribution functions can distinguish devices with burst noise from those without. Because of the similarity of the two results for transistors, however, this appears not to be a sensitive test. In view of the central limit theorem[9] one would not expect great differences from a gaussian distribution except possibly at the extremes where measurements are very difficult to make anyway.

3-7. Excess Noise and Drift

Changes in transistor-junction reverse current indicate long-term instability, and a large increase in this current manifests failure. If excess noise is linked to this mode of deterioration, then we expect a correlation between drift and some parameter of this noise. This section reports on very preliminary searches for such a correlation. The results are not yet conclusive.

Figure 3-17 shows data from measurements of noise and drift for 13 transistors. Each point represents one device. Narrow-band noise voltages at 1000 cps were measured first with a Quan-Tech M310 transistor noise analyzer and used as abscissa. Maximum fractional changes in collector-junction reverse current at from 12 to 60 volts bias during 1200 hours of continuous bias at room temperature are used as ordinates. These measurements, comparing total excess noise with drift do not show much correlation, but the sample sizes are too small to provide firm conclusions.

In another experiment broad-band noise was measured at the end of a drift test. The collector junctions of nine type 2N251 and one type 2N1021A

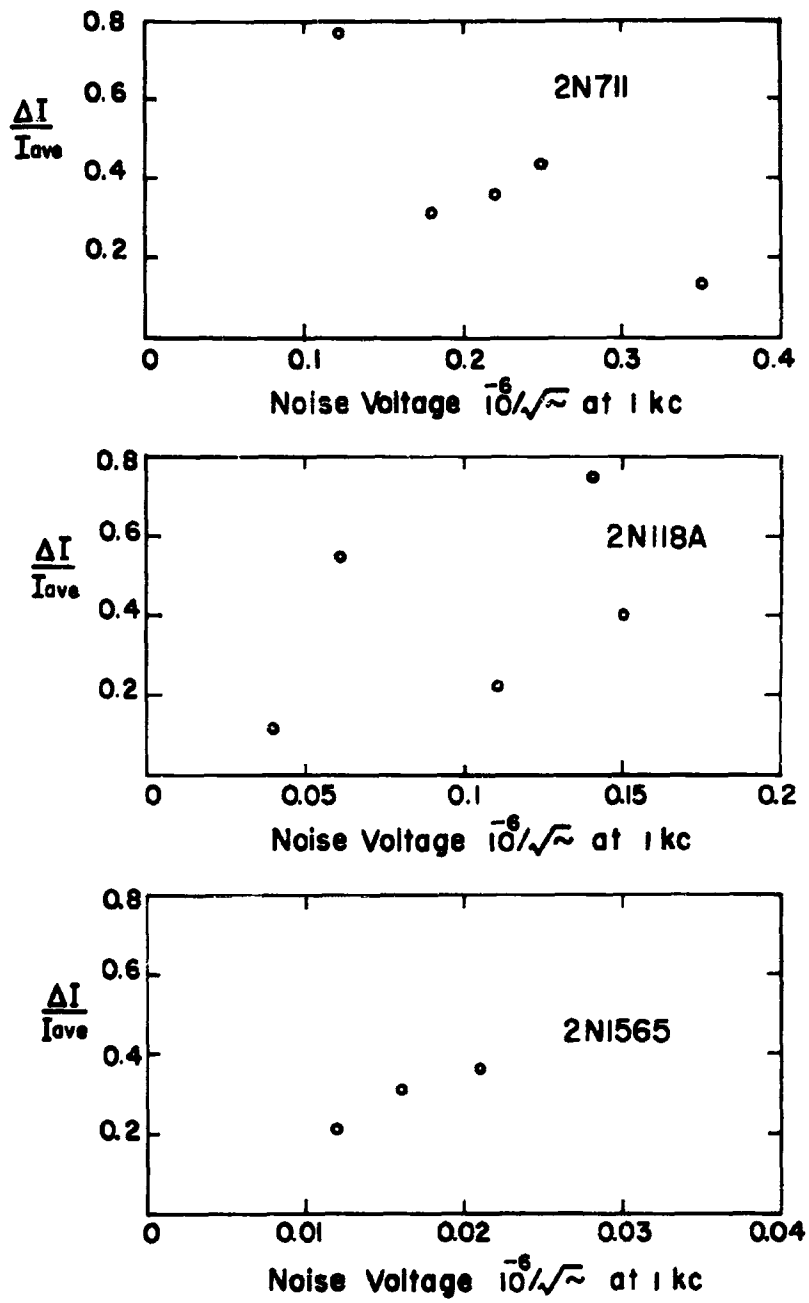

Fig. 3-17. Fractional drift versus noise for transistors.

transistors were reverse biased at 60 volts for 1250 hours. Broad-band noise was measured using the system of Fig. 3-1. As a rough measure of burst noise we used the peak-to-peak fluctuation in a 7-minute strip chart, divided by the average level, (compare with Eq. (3-23)). The results plotted in Fig. 3-18, with one point per device, show little correlation. It was apparent, however, that each device had burst noise and each device was subject to appreciable drift.

Future experiments are intended to determine what parameter of burst noise, if any, is correlated with particular drift modes. For example, in the results just reported, no distinction was made between increasing or decreasing current, and no distinction was made between many small bursts and a few large ones.

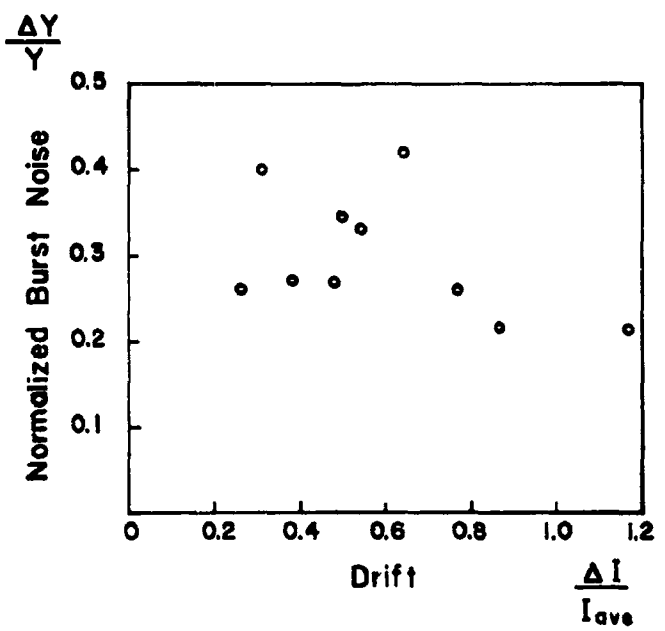

Fig. 3-18. Drift and burst noise for transistors.

SECTION 4

INFLUENCE OF INJECTION CURRENT ON DEGRADATION OF GALLIUM ARSENIDE TUNNEL DIODES

4-1. Introduction

The usual failure mode is associated with high forward bias and is manifested by an increase in valley current (I_v) and a decrease in peak current (I_p) with time.[1,2,3] Although in a given junction, the rate of degradation is a monotonic function of forward current (I_f), few quantitative generalizations have been made. Gold and Weisberg[3] have reported an "activation energy" for failure of about 0.5 volts. This corresponds to a doubling of the rate of failure with an increase of temperature of about 10°C. They also report a decrease of capacitance with failure.

To explain their results they postulated:

A. The injected electrons recombined with holes through the aid of a "deep level" located about the middle of the gap.

B. The energy released by recombination was given to a substitutional impurity atom and the atom was moved to an intersticial site (Frenkel defect). Such an intersticial atom has a charge (when on the p-side of the junction) and is therefore in reality, an ion.

C. The intersticial atom (ion) diffuses to the junction where it forms ion-pairs with the p-type dopant and thus:

1. The doping is neutralized in part and thus the junction becomes wider and the peak current decreases.

2. The valley current decreases because of this same effect. However, there is, in addition, an accumulation of these ions on the edges of the transition region which creates band-gap states which increase tunneling

in the valley region and consequently an increased current results. Either of these two effects may predominate.

Little quantitative work has been published which tests this hypothesis. One of the difficulties is that the injection current has not been identified in GaAs tunnel diodes. The injection current is expected to vary as $e^{qV/KT}$, but at sufficiently high bias where injection current is expected to predominate, the I R drop masks the voltage dependence of the current. (This $e^{qV/KT}$ dependence has been observed, however, in Ge tunnel diodes[4]).

By measuring infra-red emission from forward biased tunnel diodes,[5] we have shown that injection current does exist and follows the theoretical $e^{qV/KT}$ relation. We have attempted to relate deterioration rate to injection current. Although we do not have sufficient data to be certain, the results to date strongly indicate that deterioration rate is indeed directly proportional to injection current. Further, we can explain the Gold-Weisberg "Activation Energy" from our results.

4-2. Radiation from GaAs Tunnel Diodes

Infra-red emission has been reported from GaAs diffused diodes and such devices have been used as solid-state lasers. At room temperature the radiation spectrum has a sharp peak at 1.35 ev and another broad peak near 1.0 ev. It is the peak at 1.35 ev which predominates at high currents and is responsible for laser action.

We measured the radiation intensity (relative number of photons emitted per second) on GaAs tunnel diodes obtained from three manufacturers and on units made in our laboratory. A silicon photo duo-diode was used as a

detector. By placing a monochrometer between tunnel diode and detector, it was found that the detector measured only the radiation at the 1.35 ev peak. All subsequent tests were made without the use of a monochrometer.

The radiation intensity (ρ) was measured as a function of voltage at room temperature. Figure 4-1 shows a plot of the (ℓn I)-V_a and (ℓn ρ)-V_a characteristics of a representative tunnel diode. The radiation can be empirically expressed as

$$\rho = \rho_o \, e^{qV/KT} \qquad (4\text{-}1)$$

where V is the applied barrier voltage, i.e. the applied voltage (V_a) minus the I R drop in the series ohmic resistance. Equation (4-1) agrees with Fig. 4-1 for a value of R = 0.4 ohms. The temperature dependence of ρ_o can be obtained from a measurement of the radiation as a function of temperature at constant voltage. Figure 4-2 shows a plot of (ℓn ρ)-$10^3/T$ characteristics for the diode of Figure 4-1. Since the curve is a straight line, the term ρ_o in Eq. (4-1) can be written:

$$\rho_o = A \, e^{-q\phi/KT} \qquad (4\text{-}2)$$

where A is a constant and ϕ is 1.69 volts. From Eq. (4-1) and Eq. (4-2) we obtain for the radiation

$$\rho = A \, e^{-q(\phi - V)/KT} \qquad (4\text{-}3)$$

In any consideration of carrier transport in the vicinity of a barrier, an injection current, due to carriers flowing over the barriers, is expected to exist in addition to (and reasonably independent of) the recombination

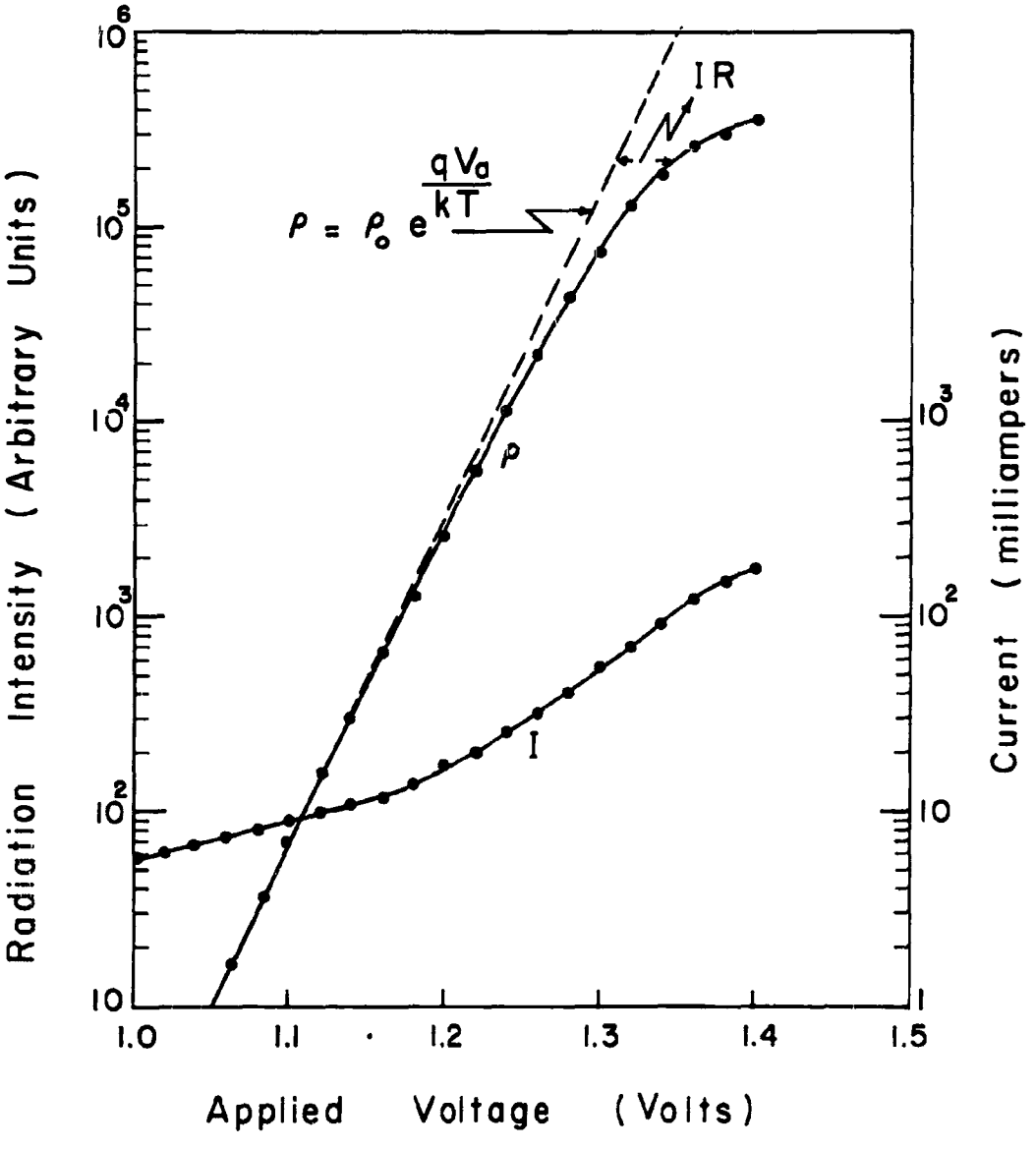

Fig. 4-1. Measured I-V and ρ-V characteristics of a tunnel diode.

The radiation follows the form

$$\rho = \rho_o \exp \frac{q(V_a - I R)}{KT}$$

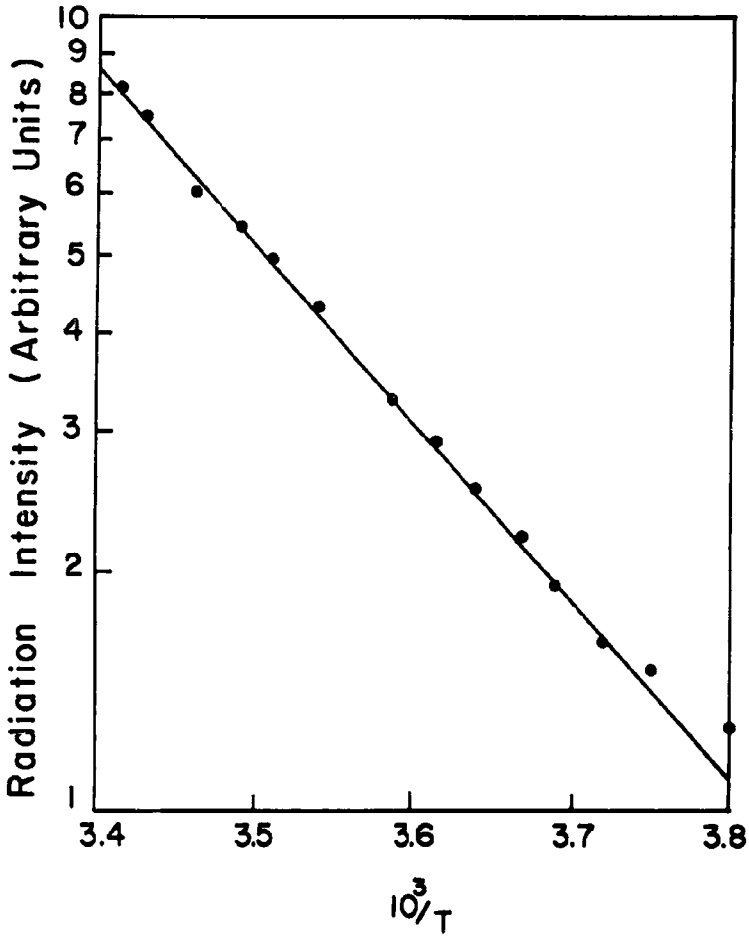

Fig. 4-2. Plot of $\ell n\ \rho$ - $10^3/T$ at constant applied voltage (V_a = 1.25V) for the diode of Fig. 4-1.

current and other anomalous currents which predominate. The forward current then can be expressed

$$I = I_E(0)\, e^{qV/\eta KT} + B\, e^{-q(V_D-V)/KT} \qquad (4\text{-}4)$$

where the first term is an empirical relation which describes the excess current. Both $I_E(0)$ and η generally vary with voltage and temperature. The second term in Eq. (4-4) represents the injection current. This is small compared to the excess current except at very high forward bias for GaAs junctions. The coefficient B is independent of voltage and is only a weak function of temperature. The term V_D represents the built-in voltage.

Comparing Eq. (4-3) with the last term in Eq. (4-4), we can conclude that the radiation is proportional to the injection current and is independent of the excess current, provided we can relate ϕ to V_D. Writing $V_D = V_D(0) + \beta T$ where β is the temperature coefficient of V_D, from the experimental results (Fig. 4-2) we can identify ϕ with $V_D(0)$. However, in tunnel diodes, the material is degenerate on either side of the junction and so the Fermi level should be reasonably fixed with respect to the band edges and consequently we expect β to be small. The values obtained experimentally for ϕ in tunnel diodes are about 1.7V. This is approximately the value expected in such a junction.

4-3. Experimental Procedure for Measurement of Deterioration

A four-section wafer switch with 12 contacts per section was mounted on a 1 rpm motor shaft; the peak current,* valley current,* and the forward

*Although we refer to peak currents and valley currents, what we measure are the currents at specified voltages. Because biasing at the peak or valley often caused the circuit to break into (class-C) oscillation, bias was slightly on the positive resistance side of the extrema. (See Fig. 4-3) Although the terms peak current and valley current have no meaning when the negative resistance region vanishes, we will use these terms as defined above.

current was monitored once each minute. To assure constant temperature, the diode was immersed in a circulating oil bath.

A typical run has the following cycle:

1st 10 sec.	measure I_P
2nd 10 sec.	measure I_V
Next X sec.	inject at perscribed voltage ($\pm$ 2 mv) ($x \leq 40$)
Next (40-X) sec.	no voltage applied.

The cycle is then repeated. The monitored currents are plotted on a strip-chart recorder.

To compare the deterioration rate under different conditions, the voltage, temperature, or duration of injection (X) is varied during the test on a particular diode or on subsequent diodes.

A portion of a strip chart record showing forward current, I_f, peak current, I_P, valley current, I_V and the zero reference is shown in Figure 4-3.

4-4. Experimental Results

The strip chart record of Fig. 4-3b is somewhat typical of our results. We can see that the peak current decays with time. The rate of change is dependent on the applied voltage. On the left of the chart, the data are erratic. This is caused by a "bad contact" in the diode. This "break" is common and appears after a considerable degradation. It often occurs after I_P and I_V have reached steady state values. Unfortunately the diode of Fig. 4-3 did not produce much quantitative data since the forward current varied with time (see below) at a given bias voltage and because the diode "opened" before a steady state in the peak and valley currents was reached.

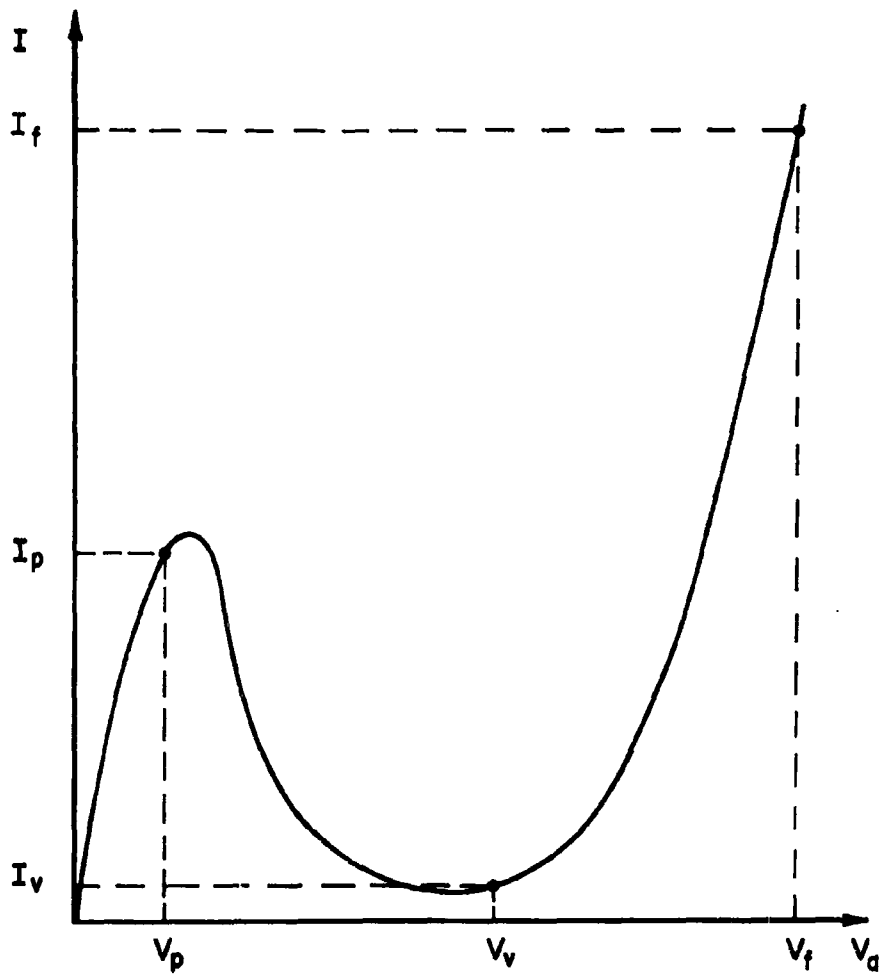

Fig. 4-3a. I-V characteristic of tunnel diode and definition of symbols.

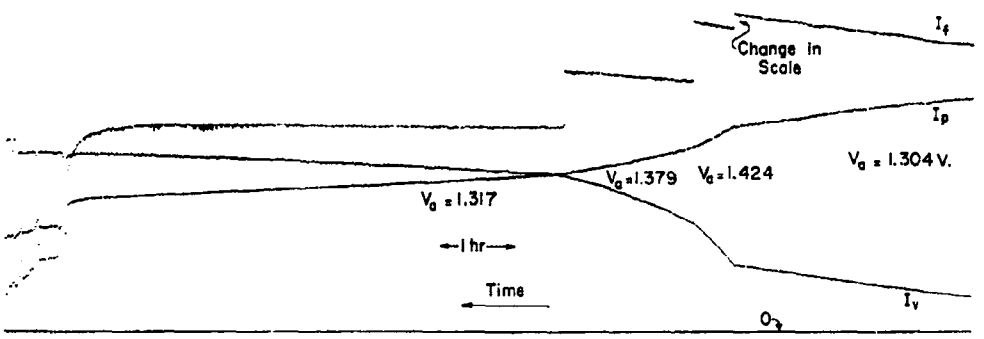

Fig. 4-3b. Strip chart recording of peak current (I_p), valley current (I_v) and forward current (I_f) with time, at prescribed bias voltages. The scale for forward current is different from that for peak and valley currents.

Failure data for a more typical GaAs tunnel diode are plotted in Fig. 4-4. Here $(I_P(t) - I_P(\infty)$ and $(I_V(\infty) - I_V(t))$ are plotted against time for a run at constant temperature, constant injection voltage, and constant injection time (25 sec.) per cycle. The values of $I_P(\infty)$ and $I_V(\infty)$ were the steady state or final values of peak and valley current respectively and were obtained from the data.

We can see from Fig. 4-4 that I_P and I_V are both constant initially and then approach their final values exponentially with time. The time constants for peak current and for valley current degradation are approximately equal. The initial constant portion is of longer duration for the peak current than for the valley current. In Germanium units and in GaAs diodes with larger series resistances, the time constant appears to decrease with time. This is presumably a result of an increase (with time) of excess current in the injection region causing an increased I R drop and consequently a reduced barrier voltage and reduced injection current, and thus a reduced failure rate.

For diodes with sufficiently small series resistance then, we can write

$$I_P(t) = I_P(\infty) + [I_P(t_o) - I_P(\infty)]\, e^{\frac{-(t-t_o)}{\tau}}$$

$$I_V(t) = I_V(\infty) - [I_V(\infty) - I_V(t_o)]\, e^{\frac{-(t-t_o)}{\tau}}$$

If we define the failure rate as

$$\frac{-\frac{d\, I_V(t)}{dt}}{[I_V(t) - I_V(\infty)]} = \frac{\frac{d\, I_P(t)}{dt}}{[I_P(t) - I_P(\infty)]} = \frac{1}{\tau} \qquad (4\text{-}5)$$

our postulate that degradation is proportional to injection current then is equivalent to

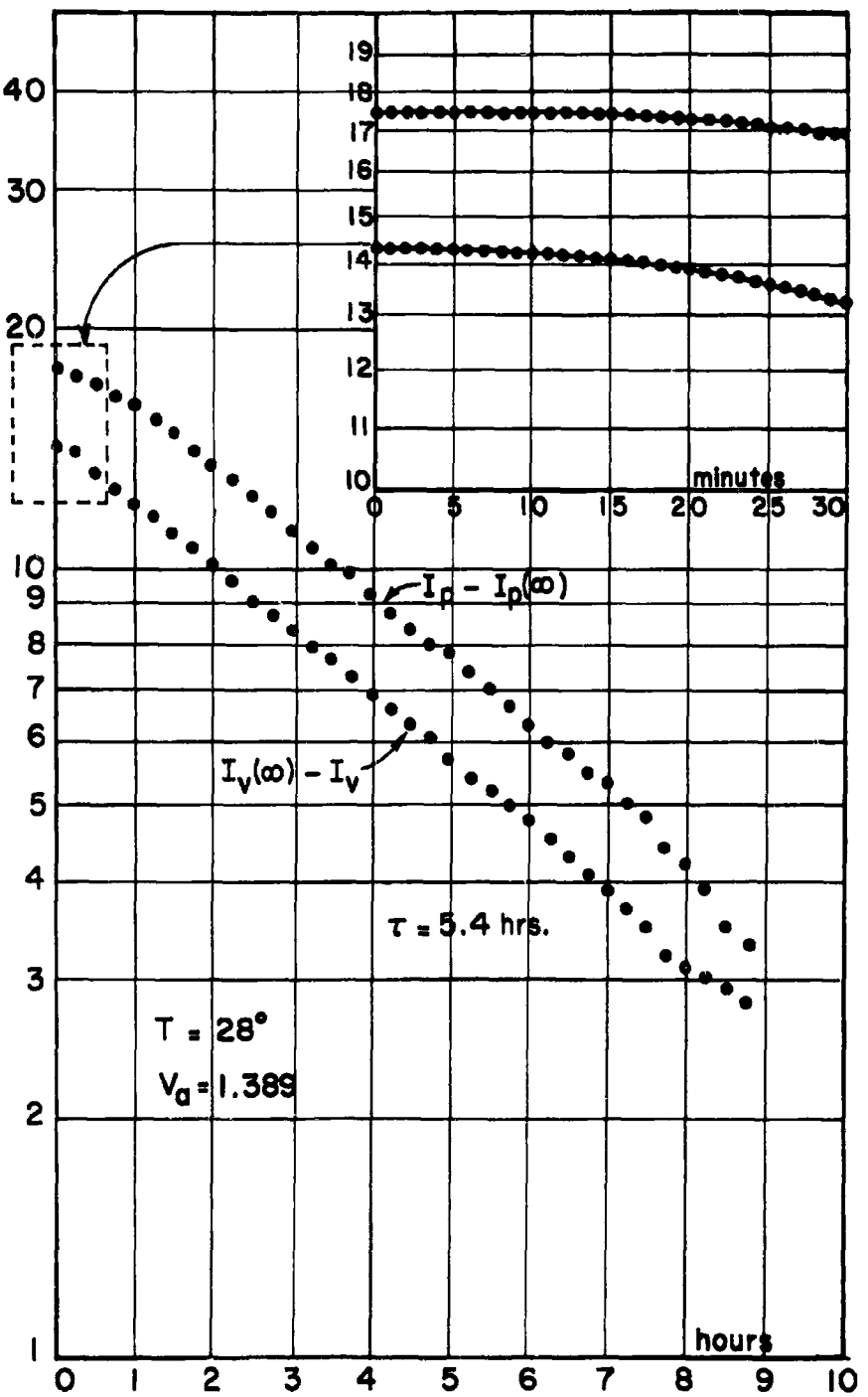

Fig. 4-4. Plots of $(I_p - I_p(\infty))$ and $I_v(\infty) - I_v$ for a diode biased at a fixed voltage. The variation is exponential with time.

$$\tau = C\, e^{-qV/KT} \qquad (4\text{-}6)$$

In Fig. 4-5 is shown a plot of τ vs. V. V is the applied voltage minus the I R drop. This data was taken from a single run where the injection bias was varied. We can see that the time constant for failure as deduced from peak current can be described by Eq. (4-6) quite well except for large t where the time constant increases. The variation of time constant with voltage as determined from valley current measurements do not fit the theory quite as well.

Since the slope is close to that predicted by Eq. (4-6), we can tentatively say that the failure rate is indeed proportional to injection current.

A difficulty with the above procedure is that as the steady state value is approached, the denominator of Eq. (4-5) is difficult to determine. However, if the bias is changed from V_a' to V_a'' at t_o, and the failure rates are compared just before and just after t_o, we get from Eqs. (4-5) and (4-6)

$$\frac{\partial I_V'/\partial t}{\partial I_V''/\partial t} = \frac{\partial I_P'/\partial t}{\partial I_P''/\partial t} = \exp \frac{q}{KT}\left[(V_a' - V_a'') - R(I_f' - I_f'')\right] \qquad (4\text{-}7)$$

we can then solve for R.

$$R = \frac{(V_a' - V_a'') - \frac{KT}{q}\ell n \frac{\partial I_V'/\partial t}{\partial I_V''/\partial t}}{I_f' - I_f''} \qquad (4\text{-}8a)$$

$$R = \frac{(V_a' - V_a'') - \frac{KT}{q}\ell n \frac{\partial I_P'/\partial t}{\partial I_P''/\partial t}}{I_f' - I_f''} \qquad (4\text{-}8b)$$

Below is a table of R as obtained from Eq. (4-8a) and Eq. (4-8b) and using data on a single unit on which the bias voltage was changed 6 times. For comparison, R was obtained in the same manner but the time constant for failure (Eq. 4-6) was assumed to vary as $e^{qV/2KT}$.

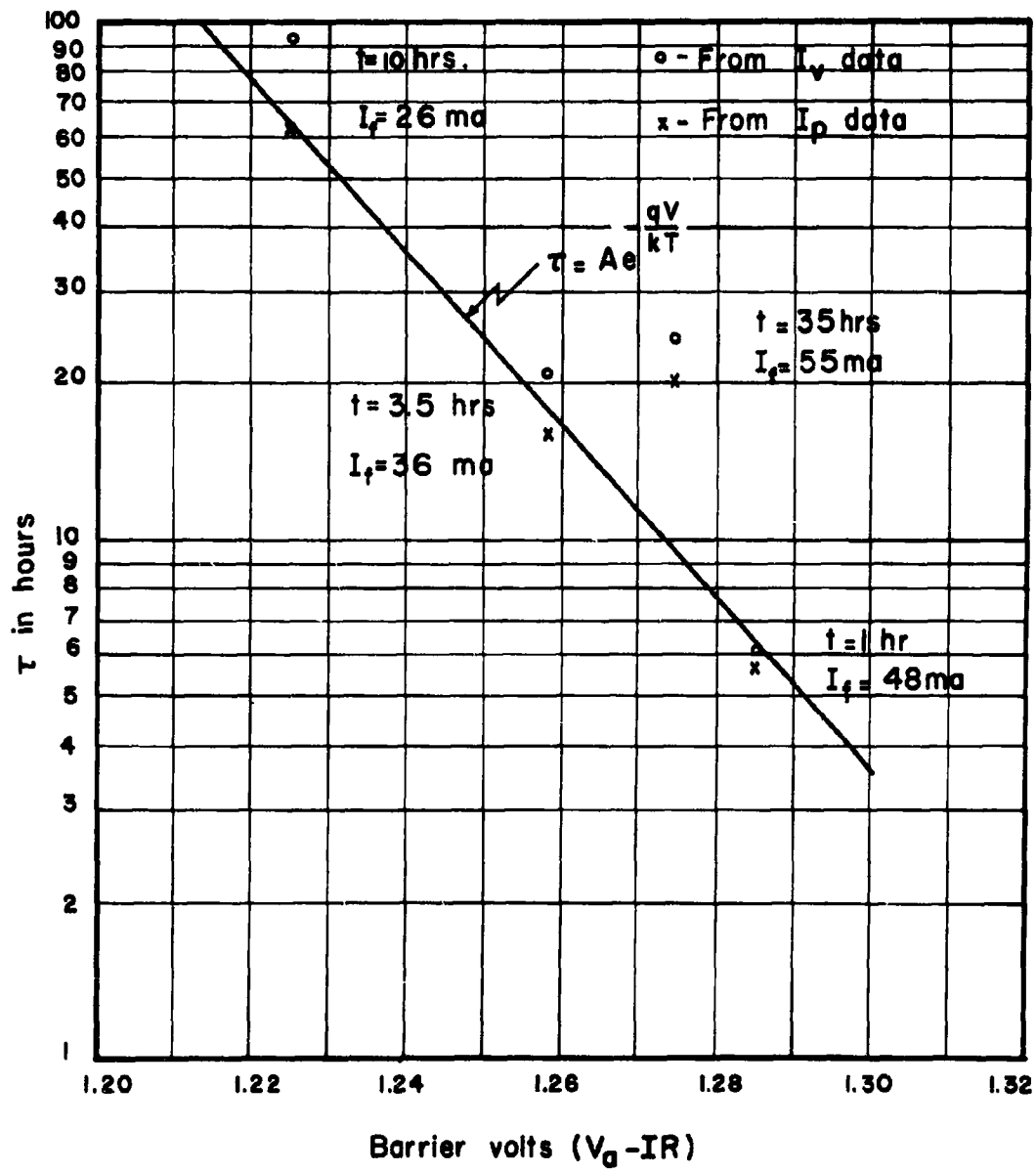

Fig. 4-5. Plot of failure time constant (τ) against barrier voltage (V_a - IR) in a single diode. The failure rate appears to depend exponentially on the barrier voltage or directly on the true injection current.

SERIES RESISTANCE R (OHMS)

	Assuming $\tau = C\, e^{-qV/KT}$		Assuming $\tau = C\, e^{-qV/2KT}$	
t_o(hrs)	From I_P Data	From I_V Data	From I_P Data	From I_V Data
2	2.5	2.4	0.0	-0.7
5	2.8	2.3	-1.3	-2.5
19	3.5	4.0	1.7	3.2
27	2.4	2.4	1.6	1.5
44	2.5	2.2	2.1	1.4
51	2.4	2.4	1.3	1.3

Table 1. Series resistance as deduced from failure studies. The measured value using pulse techniques (at a forward current of one ampere) is R = 2.4 ohms.

We can see from Table 1 that the data are consistent with the hypothesis that the failure rate is proportional to injection current. Not only are the values deduced for R reasonably consistent but agree well with a measured value of R = 2.4 ohms. On the other hand, the assumption that failure rate is proportional to $e^{qV/2KT}$ gives unreasonable values for R.

In the above analysis, we assume that both R and the steady state values are reasonably independent of bias. This seems to be true from the data.

Although all our data indicates that the failure rate is proportional to injection current, we have not tested a sufficient number of units to positively reach this conclusion. If failure rate is indeed proportional to injection current we can rewrite Eq. (4-6)

$$\tau = C\, e^{\frac{q}{KT}(V_D - V)} \qquad (4\text{-}9)$$

and correlate the failure rate with temperature. We have done little work on this. However, Gold and Weisberg have reported failure rate having an "Activation Energy" of about 0.5 volts. This would mean that

$$\tau = C\, e^{q(0.5)/KT}$$

If V_D = 1.7 volts, and V = 1.2 volts, this result would be expected. It is not known at what voltage the diodes reported on were biased, but it is almost certainly very near this value, (see Fig. 4-5).

The initial constant portion of the degradation curve is of interest. If the cycle is interrupted for a time, (say one day) and then resumed, the values of I_p and I_V do not change in this interval but again the slope is zero for a short time before decay commences once again.

4-5. Discussion of Results

We have shown from the voltage dependence of degradation, that failure is proportional to true injection current and quite likely caused by it. It is reasonable to believe that recombining carriers impart their energy to the lattice and thus cause Frenkel defects. We see no evidence of a deep level acting as a recombination center. When the intersticial atom and vacancy are in close proximity, no forbidden-region states are created and there is no immediate effect on the I-V characteristics. As the more mobile half of the Frenkel defect (probably the intersticial atom) diffuses away, the interband states are formed and the valley current increases because of tunneling to (or from) these states due to the high electric field in the transition region. These intersticial atoms accumulate at the edge of the transition region on the p-type side (or the vacancies congregate on the n side if they are more mobile.) The doping is partially neutralized and the peak current begins to decrease. This requires a somewhat longer delay than that needed merely for the creation of interband states.

The time delay in degradation after an interruption is thought to result from a "healing" of the Frenkel defects which are present. This healing might be expected to cause a small recovery in the I-V characteristics. This is sometimes observed but it is always very small in magnitude. The "breaking" of the tunnel diode after considerable degradation is thought to be caused by mechanical failure due to the Frenkel defects. We have not microsectioned these junctions as yet to determine where the break is.

SECTION 5

TUNNEL DIODE FAILURE STUDIES

5-1. Introduction

The problem of rapid failure of Gallium Arsenide tunnel diodes under conditions of high forward bias raised serious questions about the extensive use of III-V compound semiconductor materials in general. Studies of Gallium Arsenide tunnel diodes and their possible mechanisms of failure were undertaken as part of the work of the previous contract and a tentative explanation of tunnel diode failure was given in Chapter 6 of the final report. Part of the objective of this work was to extrapolate some of the results and some of the understanding of GaAs tunnel diode failure to an explanation of failure mechanisms in other devices involving other compound semiconductors or other highly doped p-n junctions.

Subsequent experimental and theoretical studies in addition to the radiation studies discussed in Section 4 have extended and modified the conclusions of the previous report.

5-2. Modes of Failure in Tunnel Diodes

A number of observations of modes of failure in Gallium Arsenide tunnel diodes have been made. Some of these observations were made and reported on in the previous contract, however most of them were made during the current contract. These results may be discussed conveniently with reference to Fig. 5-1 showing the static characteristic of a typical tunnel diode. The arrows indicate the direction of change with failure, with their lengths approximately proportioned to the proportion of tunnel diodes tested which exhibited the indicated change. The results are summarized as follows:

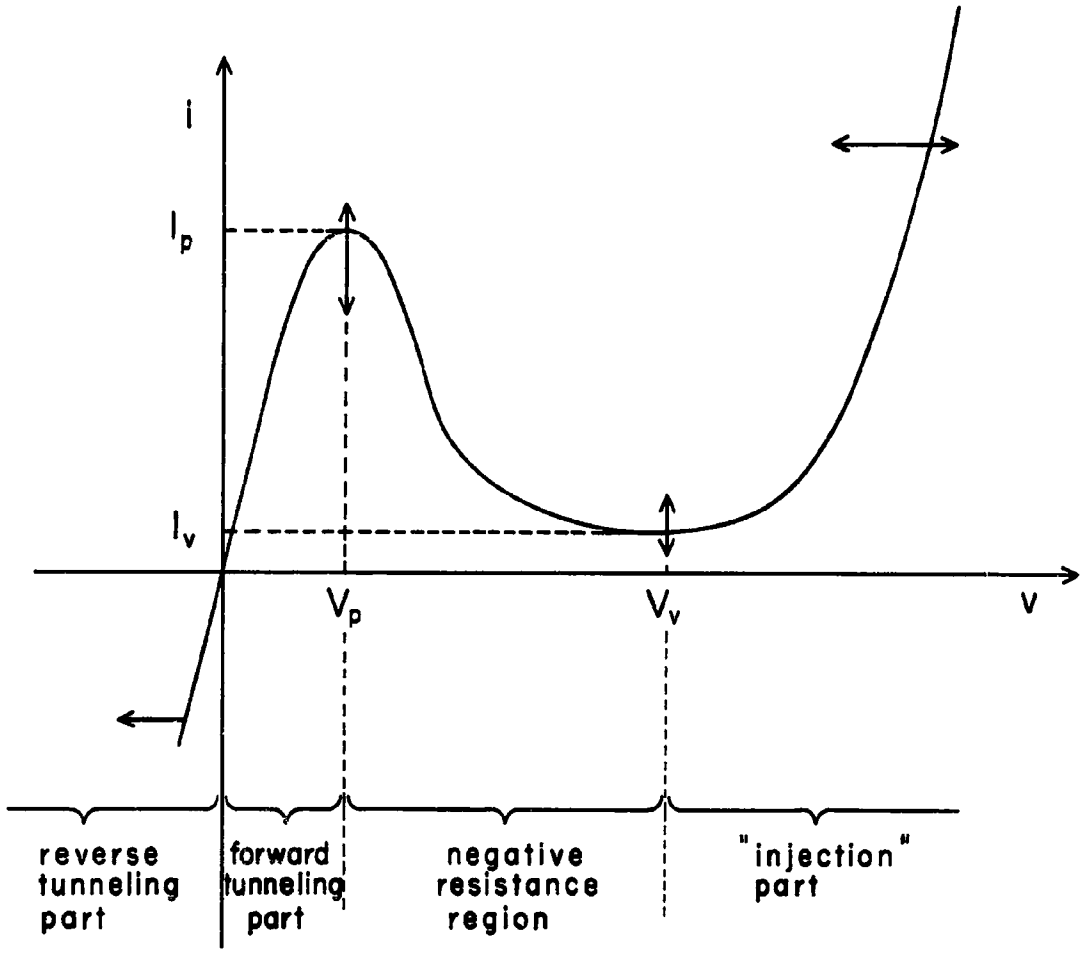

Fig. 5-1. Static characteristics of the tunnel diode.

(1) When forward biased in the so-called injection region, the rate of deterioration increased with increased forward bias. This agrees with the results obtained independently described in Section 4.

(2) When voltage-biased in the reverse tunneling direction the current does not change even when biased to the point of the same power dissipation which caused forward-biased diodes to fail.

(3) No tunnel diodes with no applied source showed degradation even when stored at elevated temperature, (unless they had previously been subjected to large forward bias).

(4) In a specific test, two similar tunnel diodes were biased at a high forward voltage bias corresponding to twice the peak current, one at room temperature and one at liquid nitrogen temperature. In a 24-hour period the peak almost disappeared in the one at room temperature while the one at liquid nitrogen temperature showed no noticeable change.

(5) In all tunnel diodes measured (about 10), junction capacitance decreased monotonically as deterioration progressed for voltages above the valley voltage.

(6) In the majority of tunnel diodes (13 out of 15) the valley current as well as the current at higher forward voltages increased with time. In the others, the current decreased with time. (These independent observations agree essentially with those of Section 4 where the injection component of forward current was separately identified and found to be identified with deterioration rate.)

(7) The more heavily doped tunnel diodes (and hence the higher current density units) deteriorated at a faster rate than the more lightly doped ones. For example, for GaAs diodes made from materials doped to approximately 9×10^{19}/cc the peak was reduced by 50 percent in a few minutes; those doped

to 7.5 x 10^{19}/cc gave similar deterioration in a matter of hours; and those doped to 5 x 10^{19}/cc similarly deteriorated in approximately a 24-hour period.

(8) GaAs tunnel diodes biased at a fixed current level in the injection region showed an exponential decrease (with time) of their peak current and reverse tunneling current. Again, these observations agree with the more quantitative measurements discussed in Section 4.

5-3. A Proposed Theory of Failure for Tunnel Diodes

The following discussion proposes and shows the plausibility of a theory of failure for tunnel diodes. This theory is based specifically on the experiments outlined in Section 5-2 above, as well as upon the studies reported in Section 4 and the observations of other workers in the field.*

The following two conditions are proposed as sufficient to cause failure of tunnel diodes:

(1) A sufficient source of energy must be available within the device to create crystal defects by removing host and/or impurity atoms from their normal lattice sites. (These will then exist as charged ions.)

(2) The electric field intensity in the transition region must be high enough to move these atoms across the transition region.

In addition, we assume there is a deterioration threshold below which self-healing of defects proceeds faster than defect generation.

Let us now focus our attention on GaAs tunnel diodes which failed rapidly and see if the above two-part hypothesis can explain the observed modes of deterioration.

First, radiation measurements[2-7] show that photons with 1.35ev energy are generated within the device. It would seem that a sufficient number of

*See references for both Section 4 and Section 5.

such photons could create crystal defects and thus account for Part 1 of the hypothesis. In order to test this possibility, a detailed examination was made of the characteristics of GaAs tunnel diodes at voltages in the vicinity of the radiation threshold, i.e., in the vicinity of the threshold of detectable radiation as determined by the noise and sensitivity of the silicon detector used. Thus, Fig. 5-2 shows the current vs. voltage and the radiation vs. voltage characteristics for a typical GaAs tunnel diode; the radiation threshold was in the vicinity of 1.12 volts.

Measurements on a number of diodes showed a correlation between radiation and deterioration. Three tunnel diodes were biased respectively at 40, 60, and 100 mv above the radiation threshold; they all deteriorated within 48 hours. Two diodes biased 40 mv below the radiation threshold showed no deterioration after several days. Similarly, other diodes reverse biased at comparable power levels showed no deterioration. These results are all consistent if the radiation causes the defects which are assumed to occur during deterioration. Moreover, the radiation threshold and deterioration threshold may occur at nearly the same bias voltage.

It was also observed that GaAs tunnel diodes made by alloying substantially longer than normally did not deteriorate when biased at a voltage corresponding to twice the peak current in the forward direction.[8] This voltage turned out to be well below the radiation threshold. However when the temperature was raised to 160°C, the same current point was beyond the radiation threshold and the diodes showed deterioration. These observations provide added evidence that voltage rather than current is the critical failure-related parameter.

Furthermore, it is known that at a given current level, the deterioration rate is an increasing function of doping level. This observation is

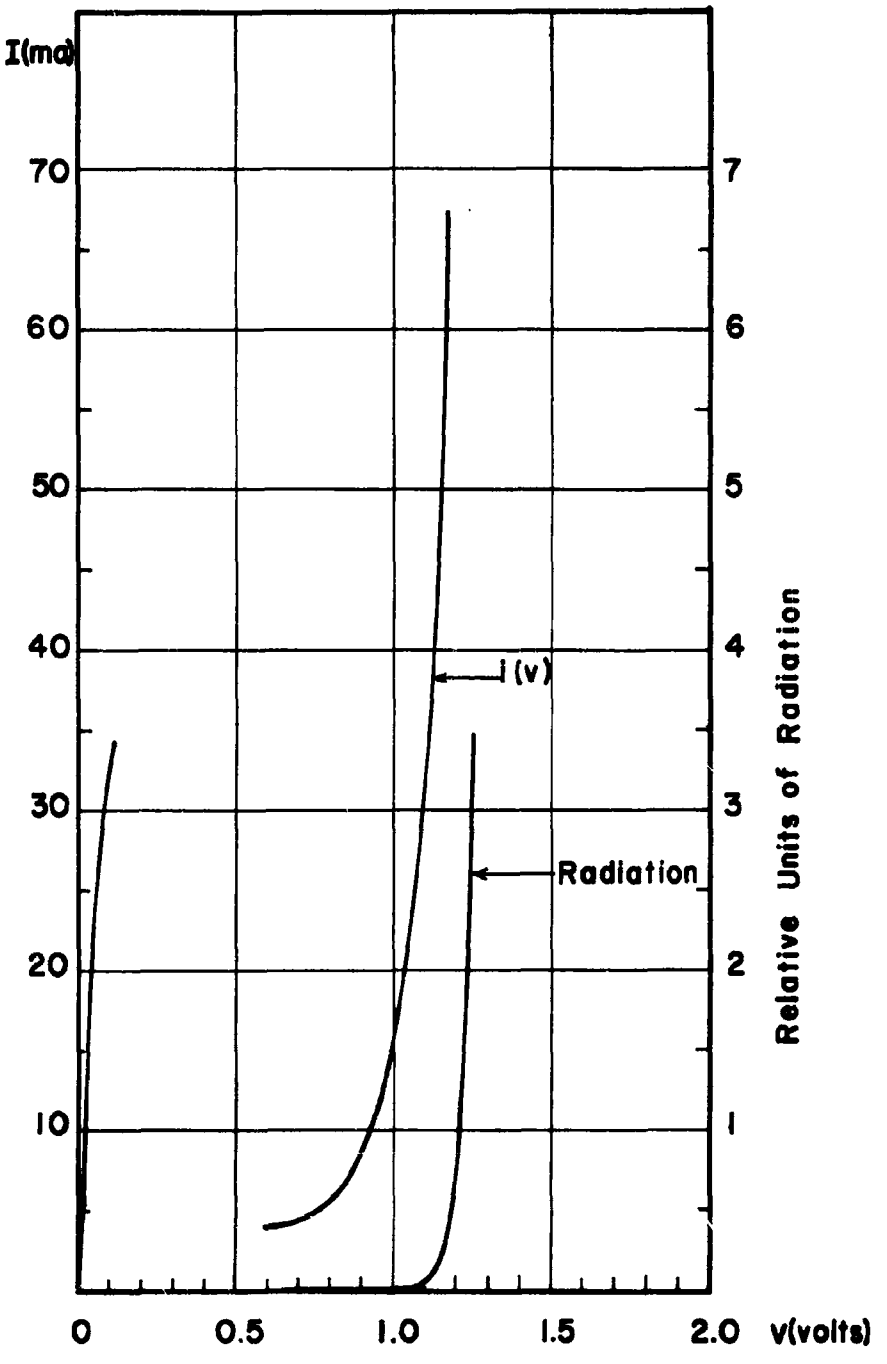

Fig. 5-2. Current and radiation as a function of voltage.

consistent with the hypothesis of deterioration, because more highly doped devices have higher voltage for the same current, and consequently more radiation for the same current, since the radiation vs. voltage curve changes little with doping level. The greater radiation would presumably result in a higher rate of defect generation in the highly doped devices.

The above observations show that deterioration is voltage sensitive; they make plausible the hypothesis that radiation provide the energy to generate lattice defects, as called for in Part 1 of the hypothesis. We now turn to Part 2.

Because all tunnel diodes are made from highly doped materials on both sides of the metallurgical junction, there is a relatively high electric field intensity in the transition region. Any atom which has been removed from a normal lattice site is ionized and hence can move across the junction in the high field. Of course in the more heavily doped diode (at the same current level) the field will be higher; and hence, not only can defects be more readily created as described above but, once removed, they will move through the transition region at a higher rate, thus satisfying simultaneously both of our stated conditions.

We have referred to the higher electric field as a function of doping with specific reference to the large forward biased situation which we have been describing. It should be pointed out that high fields are present in the transition region even under low or zero bias conditions, with the fields actually being higher at low biases. This suggests that if the proposed mechanism of failure is valid, that once the crystal defects have been created, the failure process will continue even when the external bias is removed. This has been shown to be true as illustrated in Fig. 5-3. This figure shows a tunnel diode which has been biased in the injection region

(a) Original

(b) After 2 hours of bias at $< I_p$

(c) 25 min.

(d) 1 hour

(e) 16 hours

Fig. 5-3. Deterioration of tunnel diode (Gallium Arsenide) after bias was removed.

for two hours. When the bias was removed, no change was immediately apparent in the static characteristic. However after 30 minutes with no bias the static characteristic was again plotted and it was found that the peak current was lower and within one hour it was reduced by 25 percent. After sixteen hours, no further deterioration was evident, suggesting that most of the crystal defects which had been created were removed from the high field region in the first hour or so.

If, as postulated, the motion of host and/or impurity atoms is responsible for deterioration, the rate of such motion and hence deterioration should be quite sensitive to temperature. Tunnel diodes forward biased at twice peak current showed no deterioration at liquid nitrogen temperature.

5-4. General Discussion of GaAs Tunnel Diode Failure Processes

Up to this point it has been postulated that in the majority of cases failure in Gallium Arsenide tunnel diodes is a two-step process (1) removal of atoms from normal lattice sites and (2) movement across the junction in the high field of the transition region. Various measurements have been made which tend to support such a theory with the distinct possibility that radiation is a cause of such failures. We shall now consider in somewhat greater detail what the effects of such movements through the crystal would be. At least two distinctly different effects might be produced.

First the net charge density in the transition region would be reduced and the transition region would be broadened. Such a mechanism is illustrated by Fig. 5-4. This statement is supported by capacitance measurements at and beyond the valley voltage, which indicate that degradation is associated with a decrease in this capacitance (see Appendix II). A conclusion can be reached that the tunneling barrier width should increase with degradation thus resulting in a lowering of the tunneling probability.

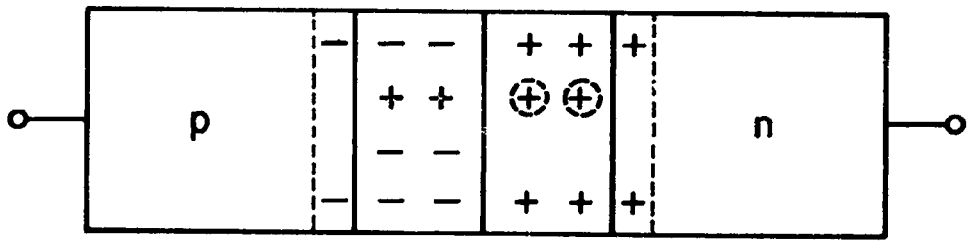

Fig. 5-4. A mechanism leading to the broadening of transition region.

Second, the motion of ions can lead to the production of additional crystal defects. The moving atoms may end up interstitially, they may form a cluster of like atoms, or they may leave vacancies. All such defects lead to additional band-gap states which tend to increase that part of the tunneling current which tunnels into band-gap states. It is by now fairly well understood that band-edge tailing and broadening of impurity bands produce band-gap states in a degenerate semiconductor. Thus current tunneling into band-gap states would increase.

The two effects outlined above lead to opposite effects as far as the tunneling current into band-gap states is concerned. This can help explain the experimental observations that the valley current may decrease or increase while a tunnel diode is deteriorating. Moreover the valley current and the excess current in the "injection" region change in the same direction with deterioration in any one diode, apparently for the same reason, i.e., depending on the relative importance of the two components of tunneling current into band-gap states.

Since carriers tunneling into or out of the main bands account for most of the current for low forward and reverse voltages, both should decrease with transition region widening. All experimental results agree with this prediction.

With constant current bias the current peak of some diodes did not disappear entirely. One possible explanation is that with deterioration, the bias voltage (for the constant current) decreased below the degradation threshold in some devices.

One final consequence of the proposed deterioration mechanism is of interest because from it, the prediction can be made that tunnel diodes

made from direct wide band-gap material will fail faster than those made from indirect material such as germanium. (A material is direct or indirect depending on whether or not the lowest conduction band valley is at the same value of crystal momentum $\hbar k_c$ as the highest valence band maximum.) In GaAs, the observed radiation is primarily due to direct recombination which need involve only photons. In Germanium the recombination process for forward-biased diodes must of necessity involve a much more complicated mechanism because both momentum and energy must be considered. Thus, in addition to photons, phonons or impurity scattering or some other scattering process must be involved. Because Germanium has a band gap of only 0.7 ev the recombination process necessarily involves multi-particle collision with rather low probabilities. Probably at least three photons must interact simultaneously with a host or impurity atom, thus we must conclude that while germanium tunnel diodes will deteriorate under extreme conditions they would be expected to do so at a much slower rate.

5-5. Excess Current in Tunnel Diodes

Tunnel diodes generally have currents greater than predicted. Several mechanisms that account for the loss of energy experienced by a tunneling electron when the bands are "uncrossed" have been considered by Kane,[9] and found to contribute only a small fraction of the experimentally observed excess current. Yajima and Esaki,[8] have suggested instead that excess current comes from carriers that tunnel only part way through the barrier, making use of local band-gap states due to imperfections; the two-step transition, only one of which is energy conserving tunneling, is shown in Fig. 5-5.

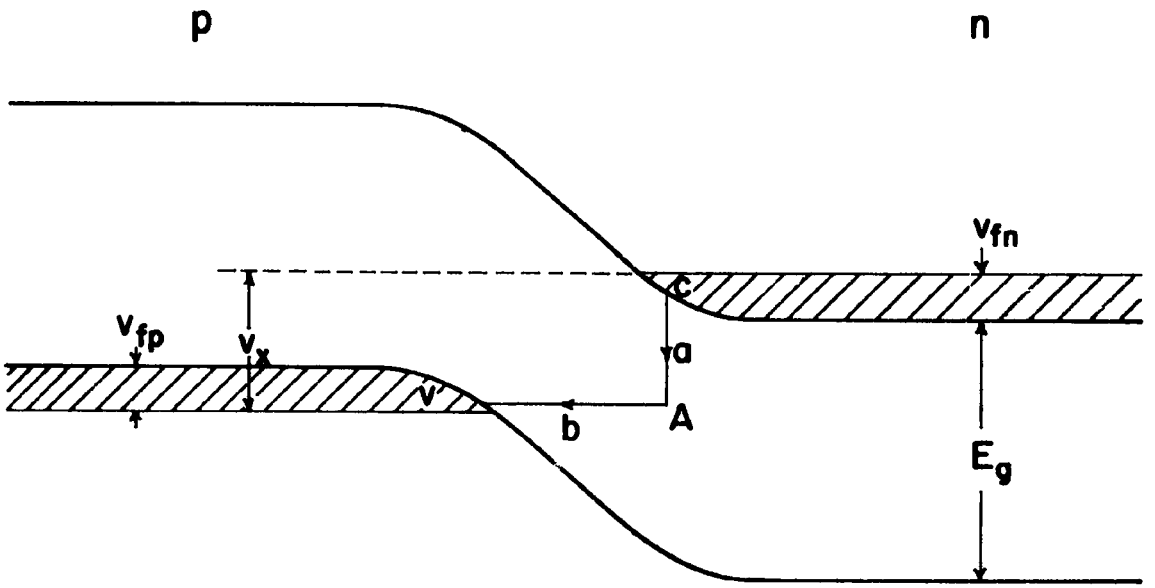

Fig. 5-3. A simple model for excess current.

Several simplifying assumptions permit analysis of the Yajima and Esaki model, and lead to useful predictions. Local band-gap states such as A in Fig. 5-5 are assumed to be continuously distributed throughout the band gap. If only transition 2 is rate controlling then a simple formulation leads to an expression for excess current in GaAs tunnel diodes. Others[10] have used the model to predict excess current in silicon diodes. By assuming that the band gap is the only parameter that varies significantly with temperature, we can predict the temperature dependence of excess current observed experimentally.

Analysis of the mechanism shown in Fig. 5-5 leads to the following expression for excess current

$$I_x = C\, N_x\, P_x \qquad (5\text{-}1)$$

where

C = constant

N_x = density of occupied band-gap states (e.g., at A) above the top of the valence band.

P_x = tunneling probability for electrons from states N_x to valence band.

The tunneling probability P_x is given by[11]

$$P_x = \epsilon^{\frac{-\alpha_x E_x^{3/2}}{\mathcal{E}}} \qquad (5\text{-}2)$$

where

$$\alpha_x = \frac{4(2m_x)^{1/2}}{3\, q\, \hbar}\, \theta \qquad (5\text{-}3)$$

m_x = reduced electron effective mass

θ = numerical factor $\sim$ unity

q = electronic charge

$\mathcal{E}$ = electric field in junction transition region.

In Eq. (5-2) E_x is the partial energy gap for tunneling along transition 2 in Fig. 5-5, and is given by

$$E_x = E_g - qv_x + q(v_{fn} + v_{fp})$$

The field $\mathcal{E}$ is assumed constant and given by the maximum field

$$\mathcal{E} = \mathcal{E}_{max} = \frac{2(v_b - v_x)^{1/2}}{w_1} = \frac{2}{w_1}\left[\frac{E_g}{q} + v_{fn} + v_{fp} - v_x\right]^{1/2} \qquad (5\text{-}4)$$

where

v_b = built-in voltage

v_x = externally applied voltage

w_1 = transition region width at $v_b - v_x = 1.0$ volt

v_{fn}, v_{fp} = voltages corresponding to the Fermi energies on the n and p sides.

Equations (5-1), (5-2) and (5-4) can be combined to give

$$I_x = CN_x \exp\left\{-\frac{(\alpha_x w_1 q^{1/2})}{2}[E_g - qv_x + q(v_{fn} + v_{fp})]\right\} \qquad (5\text{-}5)$$

For temperatures within a restricted range the band gap varies linearly with temperature

$$E_g(T) = E_g(0) - \beta_g T \qquad (5\text{-}6)$$

so that Eq. (5-5) becomes

$$I_x = CN_x \exp\left\{-\left(\frac{\alpha_x w_1 q^{1/2}}{2}\right)[E_g(0) - \beta_g T - qv_x + q(v_{fn} + v_{fp})]\right\} \qquad (5\text{-}7)$$

In Eq. (5-7) the factor $\alpha_x W_1$ involves the effective mass of the electron and varies with temperature. Cardona[12] reports that in GaAs this dependence is very weak for wide temperature ranges. Consequently Eq. (5-7) predicts a simple temperature dependence for I_x proportional to exp ($\beta_g T$). By contrast injection current varies as exp (qv/kT). Thus, if Eq. (5-7) applies a plot of $\ell n\ I_x$ vs. T for fixed voltage should be a straight line.

Experimental results confirm these predictions. Figure 5-6 shows the nearly straight lines for two GaAs tunnel diodes. Figure 5-7 shows results on a third diode up to 103°C, which gives β_g = 0.0013 ev/deg K. Other results give values for β_g within 15 percent of 0.0013. This value is about twice the value for nondegenerate gallium arsenide.

Equation (5-7) also predicts that $\ell n\ I_x$ varies linearly with voltage (for fixed temperature). Figure 5-8 shows experimental results verifying this prediction with coefficient 4.9 $(\text{volts})^{-1}$.

Experiments such as these are difficult to carry out because of device deterioration. In Eq. (5-7) N_x depends on the density of band-gap states, which should increase with deterioration. Experimental results show a monotonic increase of I_x as expected.

In GaAs tunnel diodes the experimental results show that excess current predominates to several times the peak current. Thus for the usual operating voltages the injection current component is negligibly small by comparison.

Plots of $\ell n\ I_x$ vs. T give single straight lines for voltages between 0.65 and 0.95 volts, and temperatures 77°K to 405°K. For fixed voltages greater than 1.0 volt, however, the results show several straight-line segments. The upper voltage limit for one straight line depends on the maximum temperature. These results are not yet fully understood.

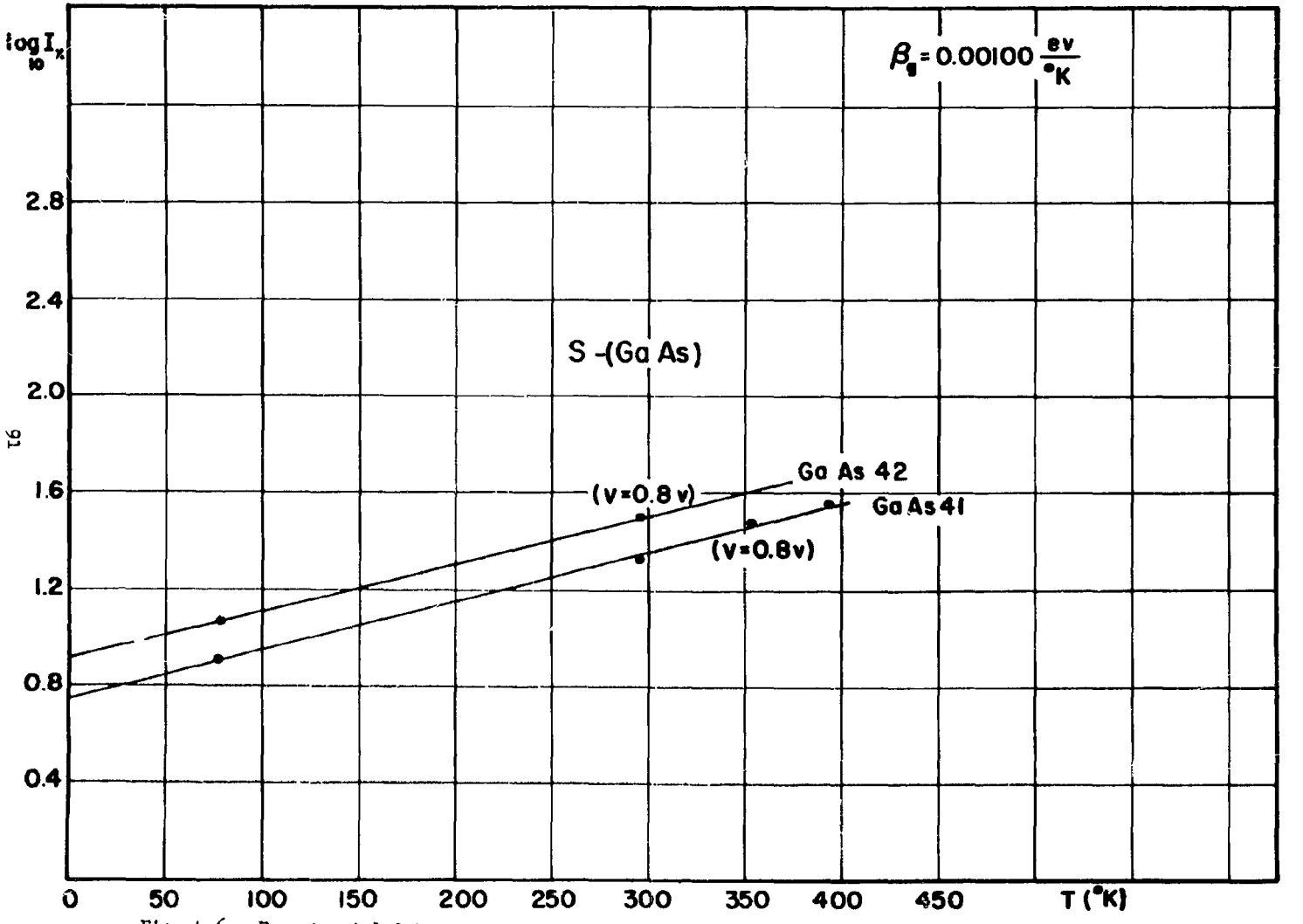

Fig. 4-6. Experimental data on GaAs tunnel diodes--excess current versus temperature.

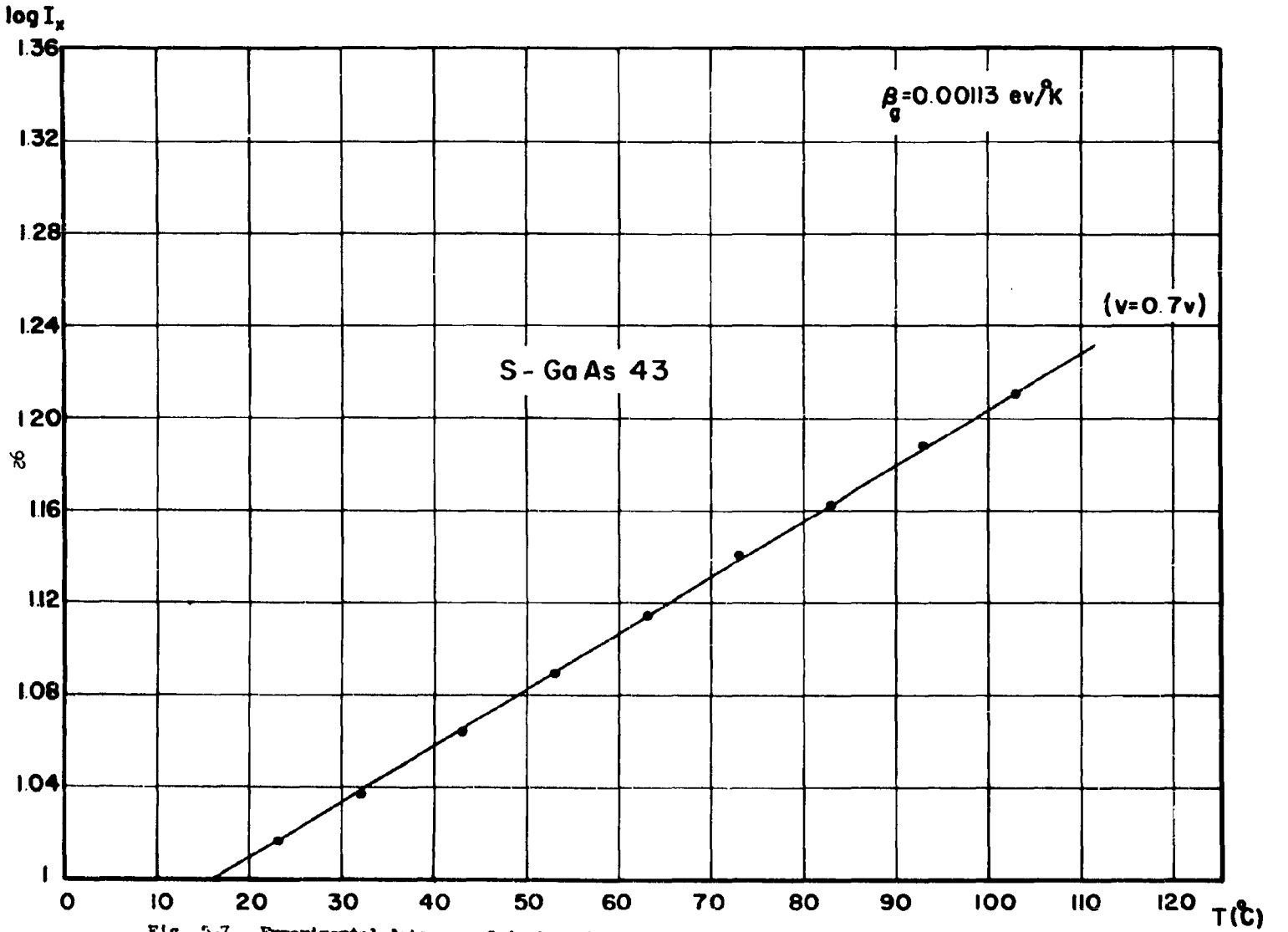

Fig. 5-7. Experimental data on a GaAs tunnel diode--excess current versus temperature.

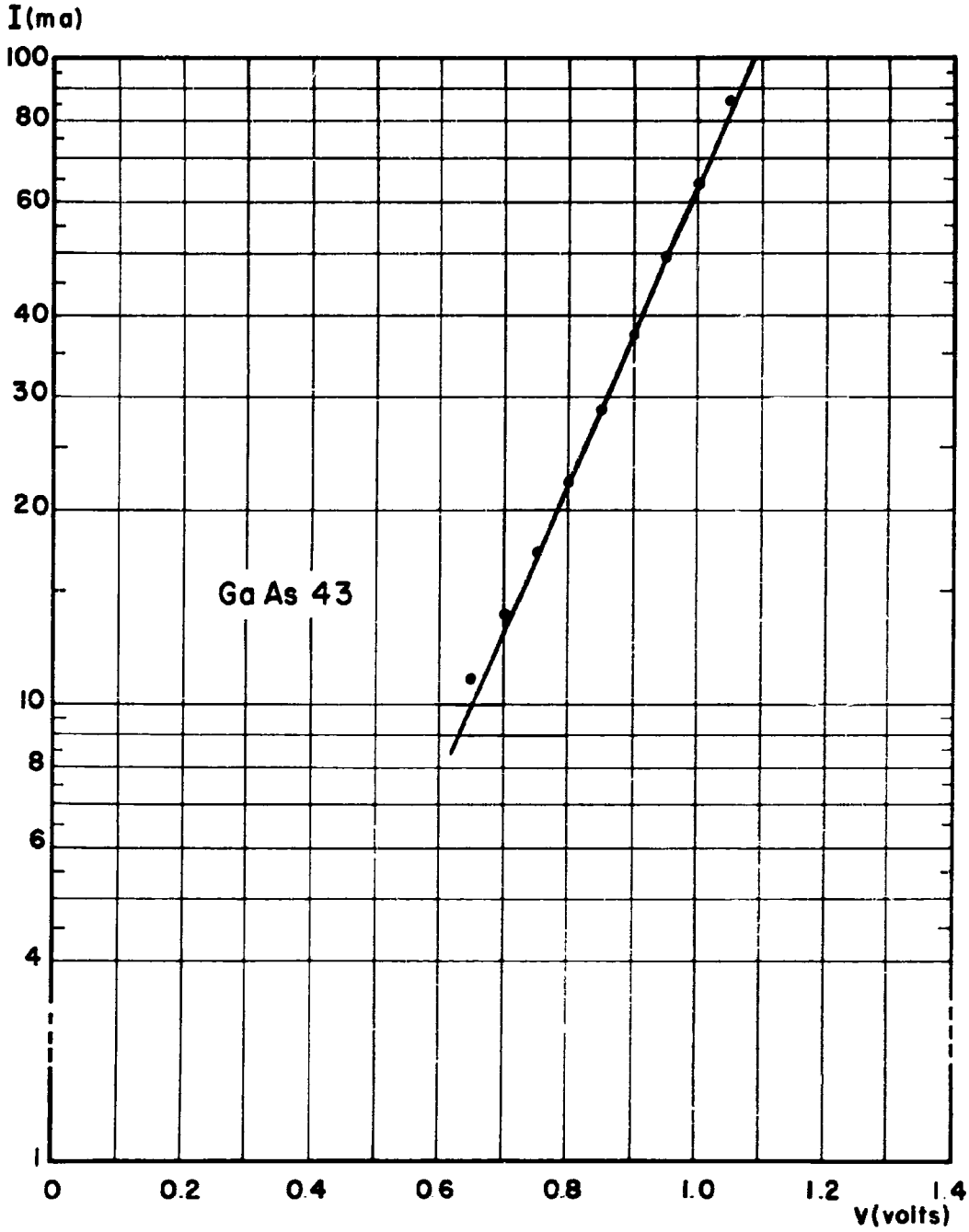

Fig. 5-8. Experimental data on a GaAs tunnel diode--excess current versus voltage.

5-6. Miscellaneous Experimental Results

This section reports further experimental results which are either incomplete or not fully understood.

Figure 5-9 shows the long-term decay of peak current, and of reverse tunneling current in a tunnel diode. After the initial period both current magnitudes decayed exponentially with 95-hour time constants.

Figure 5-10 shows the capacitance vs. voltage and conductance g vs. voltage curve for a tunnel diode whose static characteristics has a "bump" which was clearly observable only at liquid nitrogen temperature as seen in Fig. 5-11. The two straight-line segments of the $1/C_j^2$ characteristic for $v > 0.2$ volt is typical in tunnel diodes having a "bump." Figure 5-10 shows how the capacitance characteristics change after some degradation. Figure 5-12 shows a somewhat unusual characteristic of capacitance obtained on another GaAs tunnel diode with a bump. These characteristics are as yet not fully understood.

Other interesting experimental results are presented in the sequence of oscilloscope pictures shown in Fig. 5-13 where a GaAs tunnel diode was biased in the "injection" region where it would be expected to deteriorate at room temperature. This diode, however, was in liquid nitrogen while under bias. The reduction of reverse tunneling current with time is quite noticeable. This current continued to decrease for a time after the bias was removed. After a while the reverse tunneling current started to recover. The recovery stopped half way while the diode was maintained in liquid nitrogen. When the tunnel diode was brought to room temperature the recovery was almost complete. This experiment suggests that there are two mechanisms at work, one which leads to degradation and other which restores the device to its original state. Other results show that beyond a certain

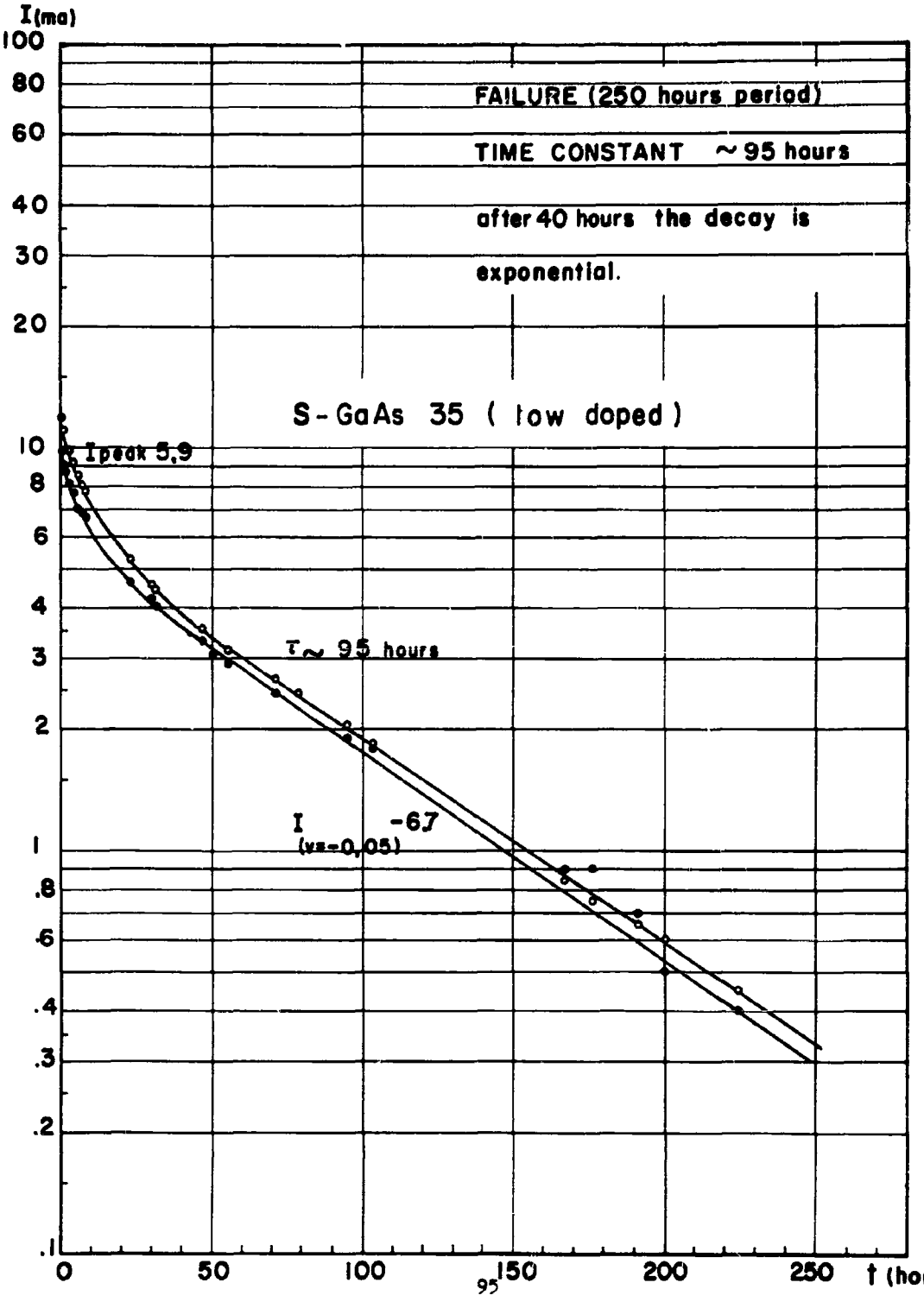

Fig. 5-9. Long term decay of peak and reverse tunneling currents in a GaAs tunnel diode.

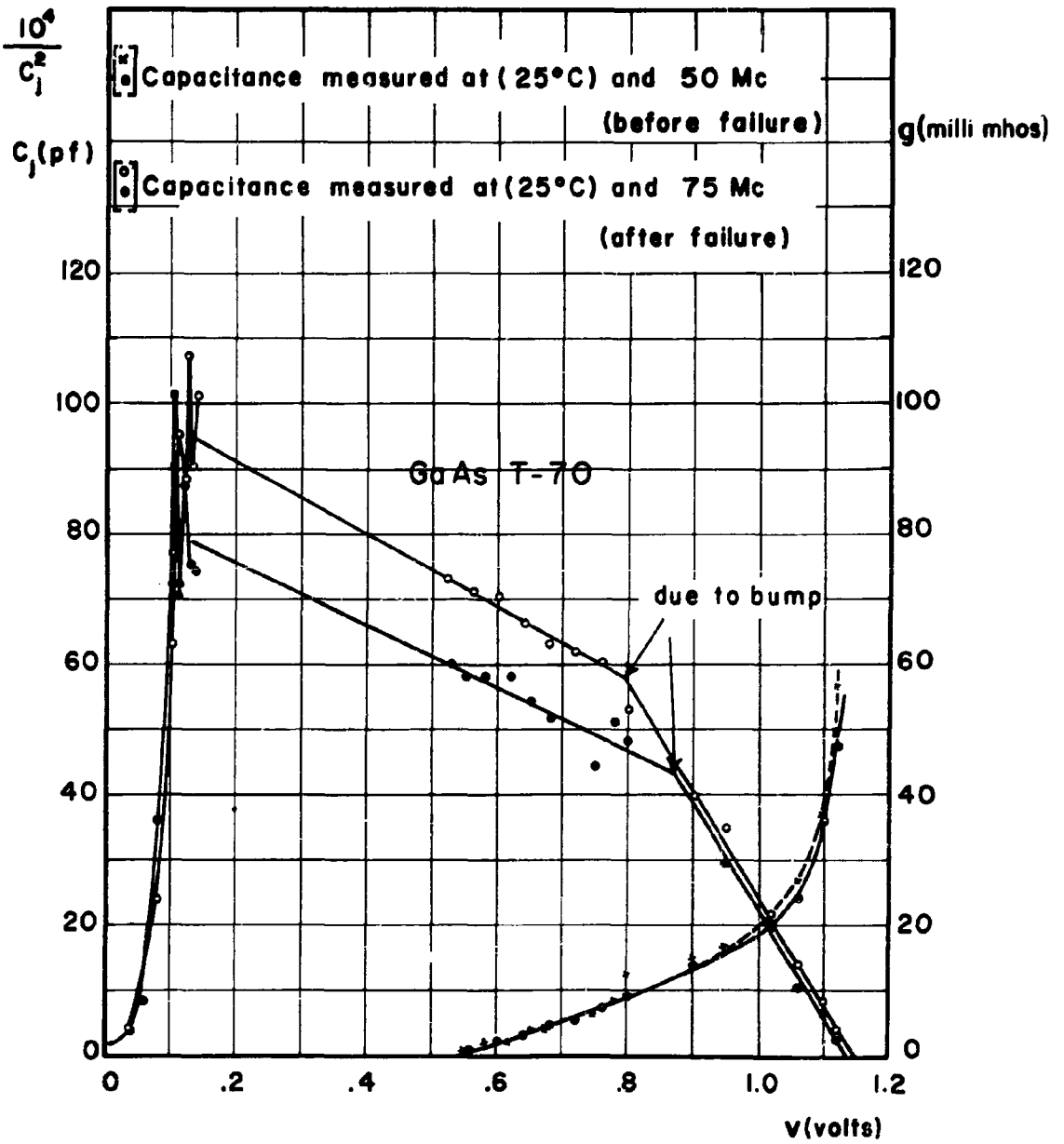

Fig. 5-10. Capacitance versus voltage curves before and after degradation.

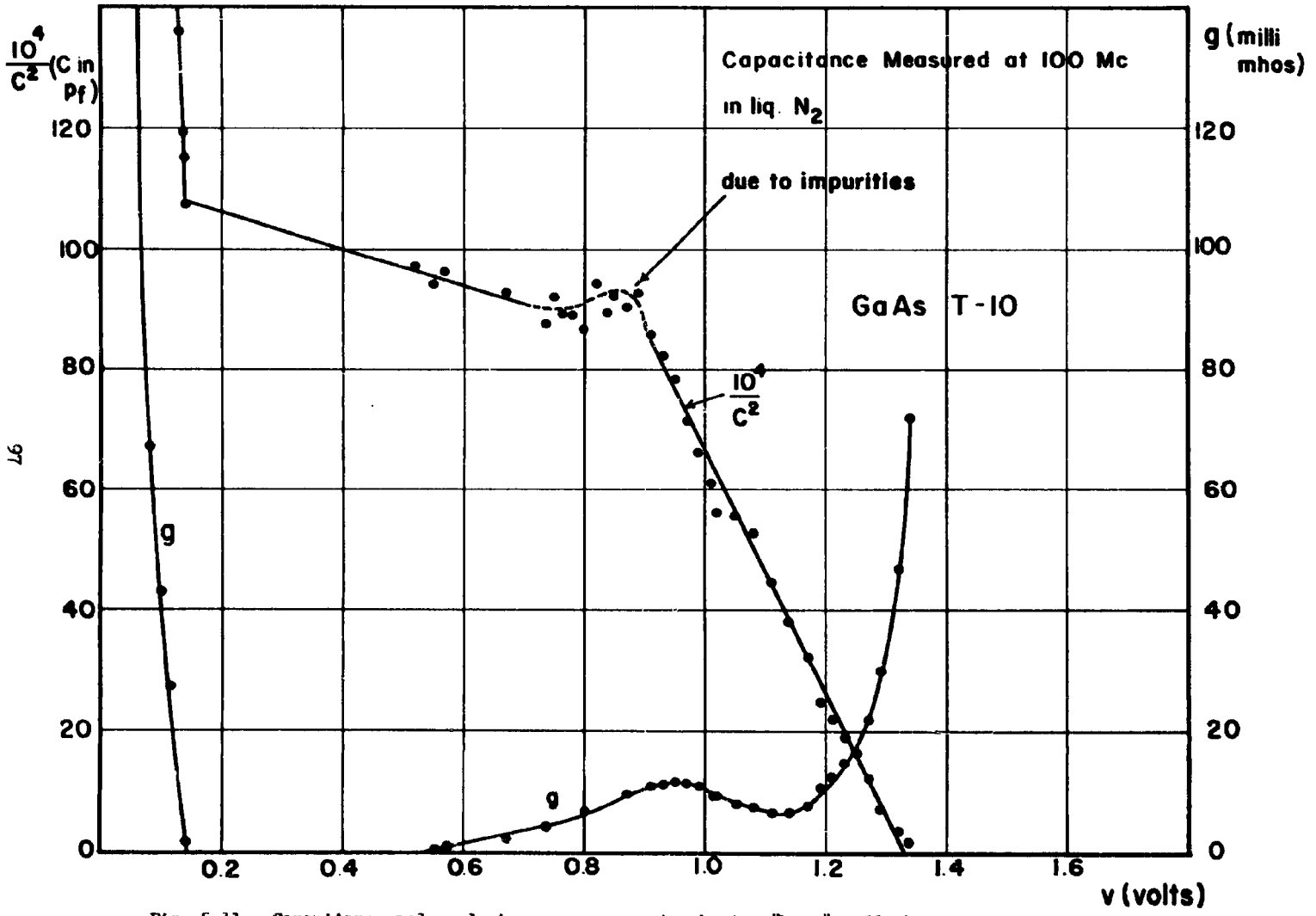

Fig. 5-11. Capacitance and conductance measurements showing "bump" effect.

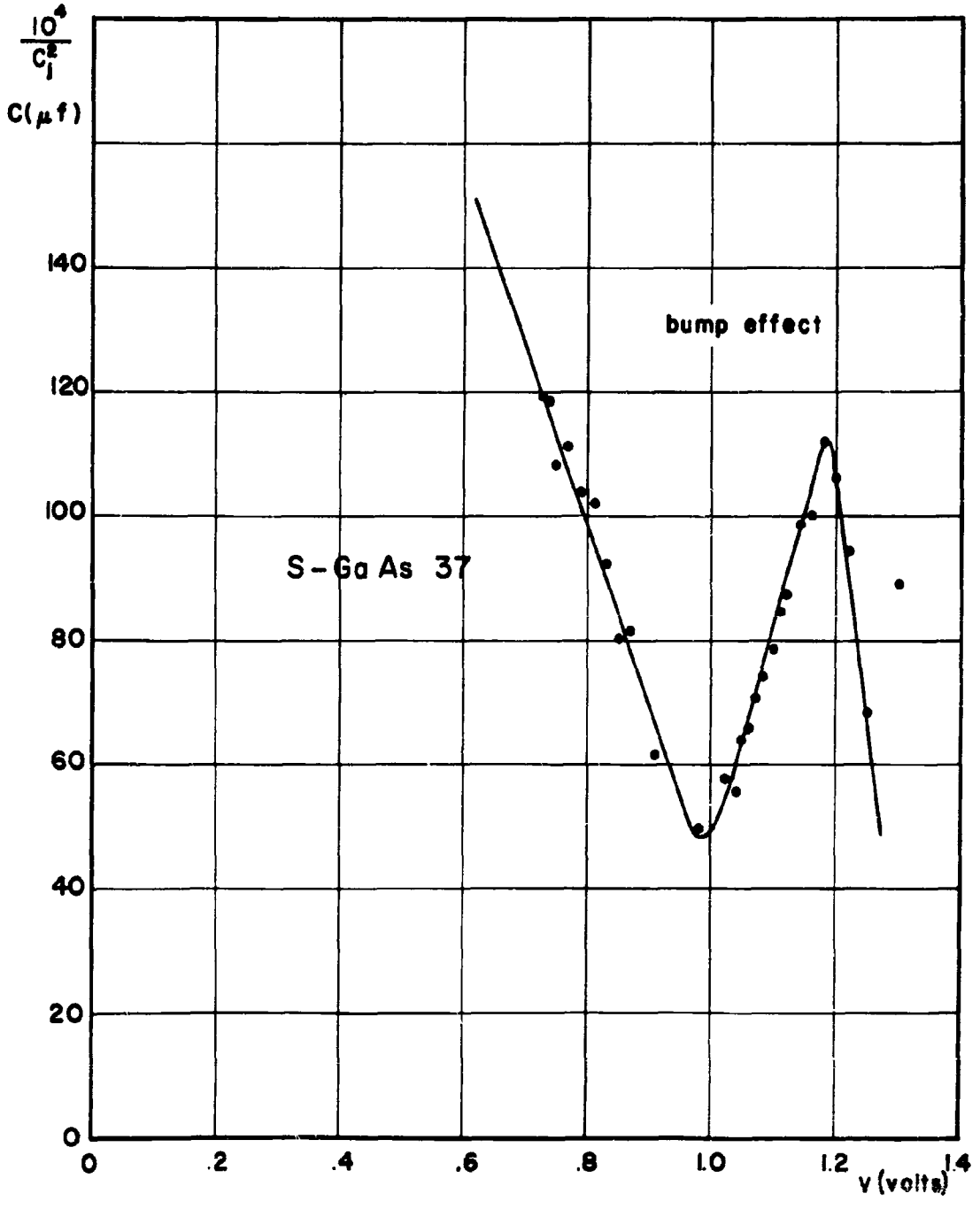

Fig. 5-12. Capacitance data showing an unusual "bump" characteristic.

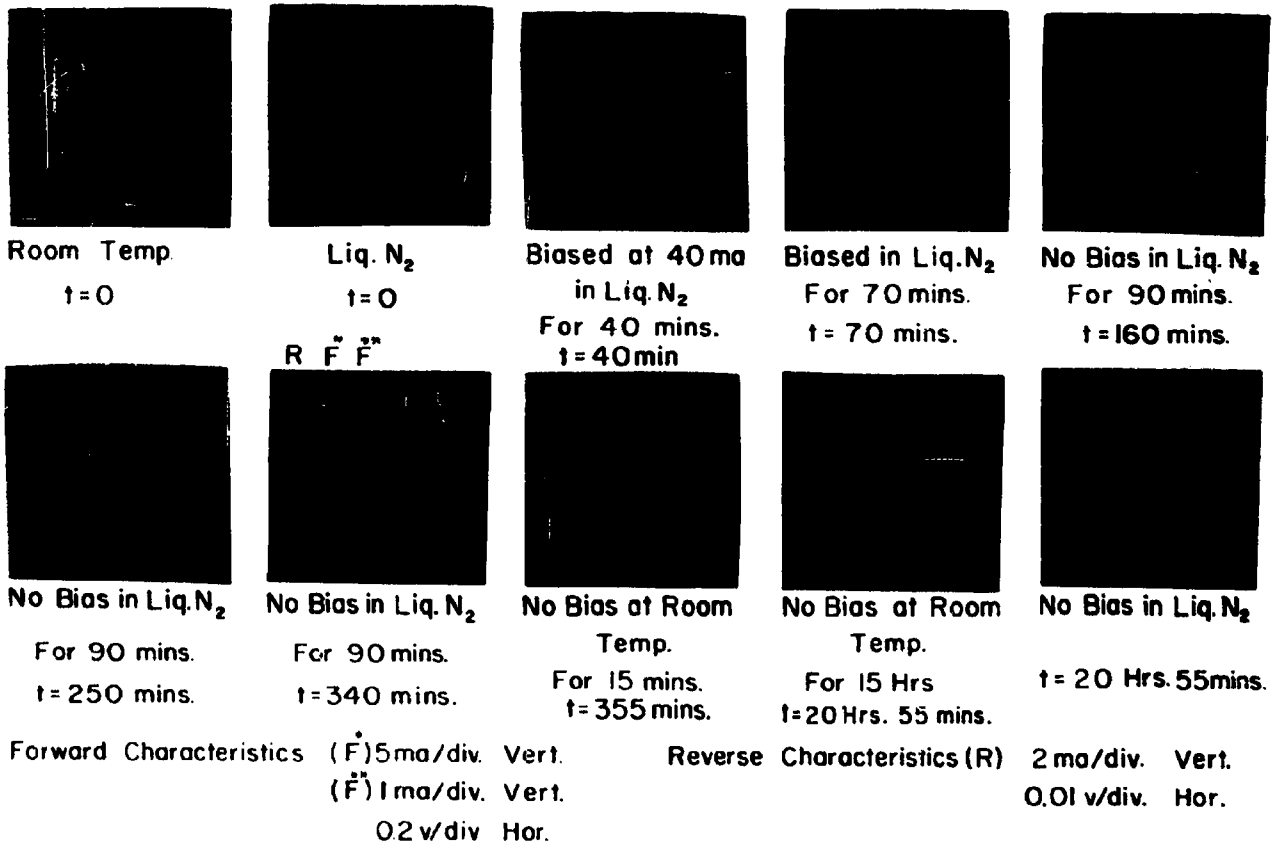

Fig. 5-13. Experimental data on a Gallium Arsenide tunnel diode showing a reversible deterioration pattern.

amount of degradation full recovery is impossible. Apparently temperature plays a key role in determining the equilibrium point between the two opposing tendencies. This experiment provides further evidence of the deterioration threshold discussed in Section 5-3.

5-7. Summary

A simple theory for tunnel diode deterioration has been presented. The predictions of the theory are consistent with the experimental observations on GaAs tunnel diodes. To check the theory further additional experiments must be performed on GaAs and other tunnel diodes.

If the proposed theory is correct then the following are undesirable characteristics of material for tunnel diodes: (1) direct, (2) wide band gap, (3) high diffusivity of moving ions in the crystal, and (4) high doping levels. On this basis GaSb and InP tunnel diodes should also deteriorate. All these predictions need further checking.

It may be mentioned that the discovery of a capacitance minimum in the vicinity of the peak current in the GaAs tunnel diode and its extreme sensitivity to deterioration may provide an early indicator of degradation in tunnel diodes (see Appendix II). Similar studies in other tunnel diodes are also contemplated.

APPENDIX I

INVESTIGATIONS OF GERMANIUM-GALLIUM ARSENIDE TUNNEL HETERODIODES*

Introduction

When two dissimilar semiconductors exist on either side of a junction, the junction is called a "heterojunction" in contrast to "homojunction" where only one semiconductor with different doping levels is involved. Semiconductors with similar lattice structures such as Ge and GaAs permit epitaxial contact with each other. The periodicity of the lattice is not disturbed at the junction and so the properties at the junction can be expected to be those of the bulk. When degenerate Ge is despoited epitaxially on degenerate GaAs, the heterojunction formed is a tunneling junction. Since the materials on either side of the junction are different, the energy band diagram of such a junction is expected to have discontinuities in the bands at the junction. Figure I-1 shows the energy band diagram proposed for a (n - Ge) - (p - GaAs) tunnel heterodiode. The I-V characteristics of such a tunnel heterodiode are shown in Fig. I-2.

Due to the existence of discontinuities in band edges at the junction, the analysis of transmission coefficient and the tunneling current is very difficult. However, if Ge is more lightly doped than GaAs, the relative voltage** supported in the Ge is much higher than that in the GaAs. If this is the case, the characteristics of the junctions are dependent on germanium

*In this appendix R. L. Anderson summarizes the Electrical Engineering master's thesis by Keiske Yawata.

**The relative voltages supported in Ge and GaAs are approximately

$$V_{D1} - V_1 / V_{D2} - V_2 = N_{A2}\epsilon_2 / N_{D1}\epsilon_1$$

where $(V_{D1} - V_1)$ and $(V_{D2} - V_2)$ are the total of built-in and applied voltages for Ge and GaAs respectively, N_{D1} and N_{A2} are the donor and acceptor concentrations in Ge and GaAs respectively and ϵ_1 and ϵ_2 are the permittivity of Ge and GaAs which are $16\epsilon_o$ and $11.1\epsilon_o$ respectively.

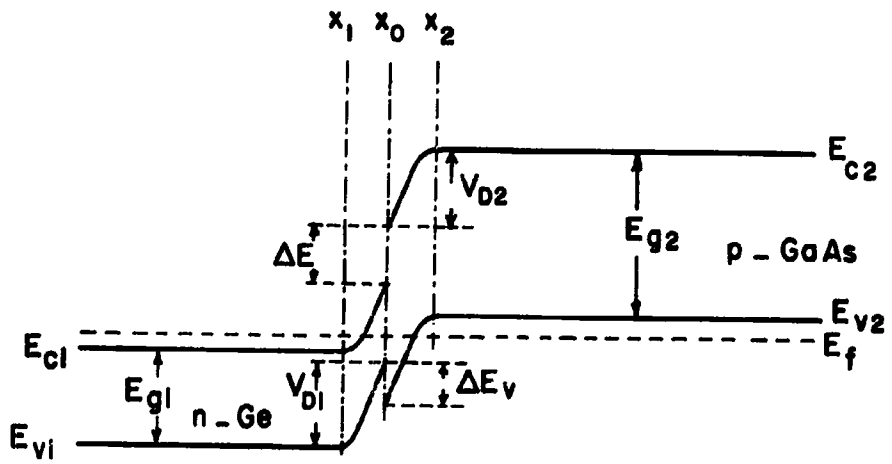

Fig. I-1. Equilibrium energy band diagram for Ge-GaAs n-p heterodiode showing discontinuities at the interface x_o.

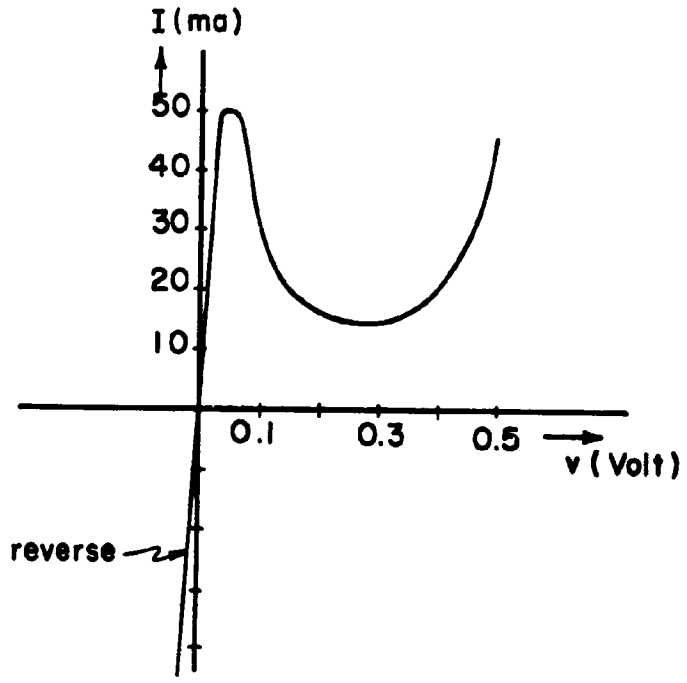

Fig. I-2. Typical I-V characteristics of a tunnel heterodiode.

properties, and if the opposite is true, i.e., if GaAs is more lightly doped, the characteristics of the junctions are expected to depend on the GaAs.

Fabrication and Measuring Techniques

The furnace used for deposition consists of a tube (quartz) intersected by a branch tube as sketched in Fig. I-3. Four regions or zones are heated independently by nichrome heating coils. The desired temperature profile in the furnace is controlled by varying heater current with a variac. The temperature is measured with a thermocouple. The deposition tube and all containers which go in the deposition tube are thoroughly cleaned with white etch, water and alcohol just prior to the experiment. A large piece of Ge, thoroughly cleaned (with white etch and water) and dried, is put in zone II of the furnace as the "source", the iodine container is filled with solid iodine and inserted into zone I, a few grams of phosphorus is put directly in the branch tube, zone IV; and the GaAs seed, lapped to a desired thickness and cleaned with GaAs etchant is put on a quartz boat and placed in zone III. Then the hydrogen gas tubings are connected to the two entrances and the one exit and the flow rate is adjusted. After flushing with hydrogen, the power is applied to the heating coils and adjusted to obtain the desired temperature profile shown in Fig. I-4. The actual deposition process is as follows: (1) the solid iodine sublimes and the gaseous iodine is carried by the hydrogen toward zone II, (2) the gaseous iodine reacts with Ge in zone II and forms GeI_2 and GeI_4 and the two gasses are carried toward zone III, (3) phosphorus in zone IV evaporates and is carried into zone III by the hydrogen flow, and (4) in zone III Ge is deposited epitaxially on the GaAs seed by disproportionation of GeI_2 into GeI_4, and free Ge. This reaction can be expressed by the following chemical equation:

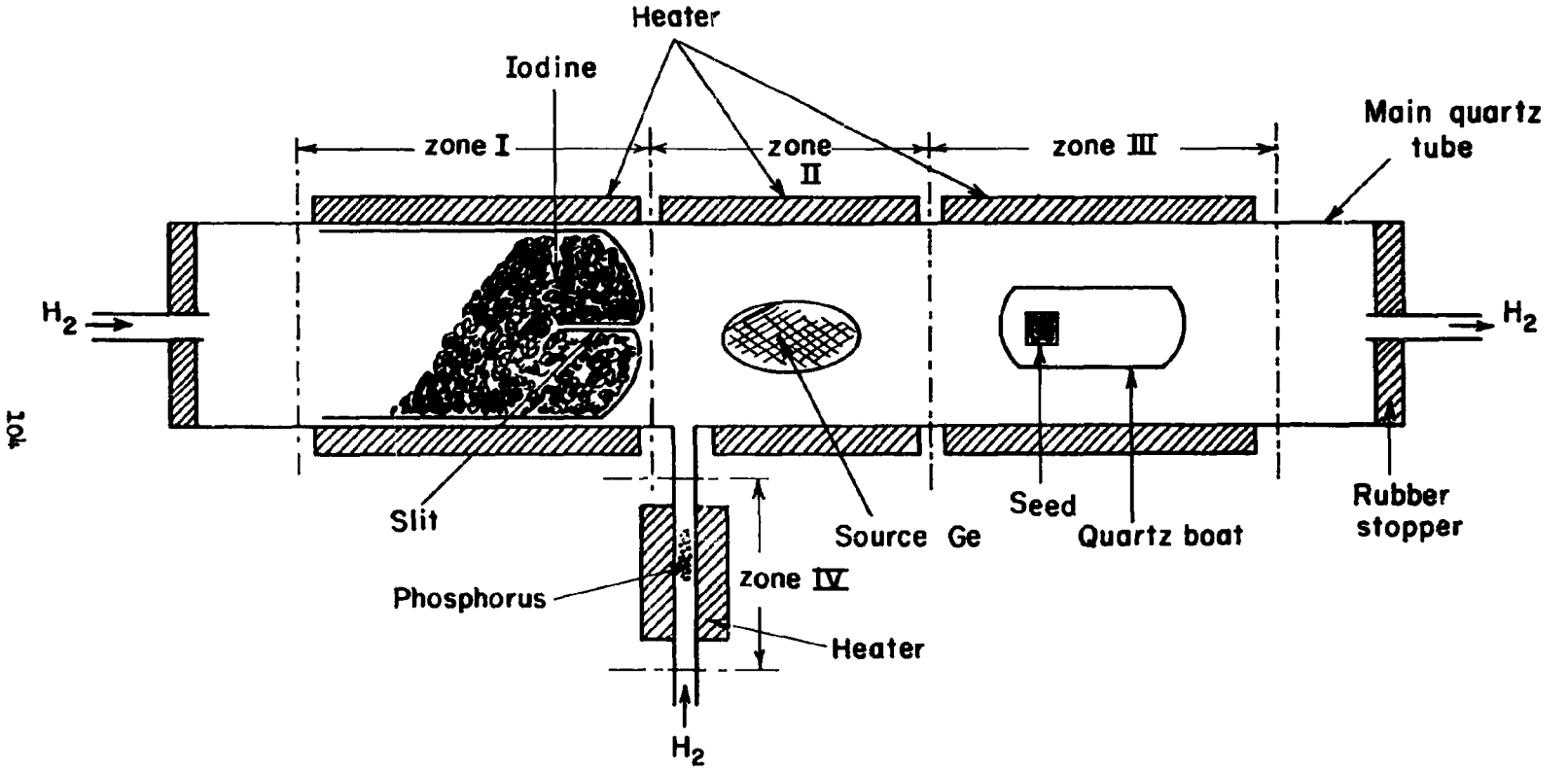

Fig. I-3. General Scheme of Deposition Furnace.

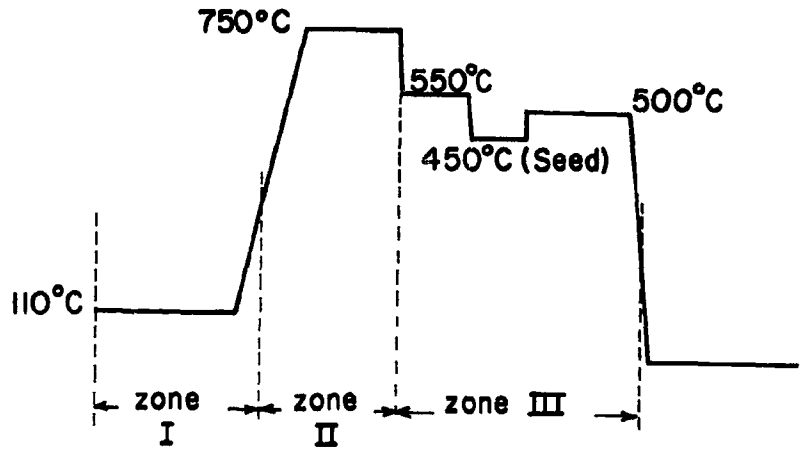

Fig. I-4. Temperature profile of the main deposition tube. The temperature of zone IV is 470 ~ 500°C.

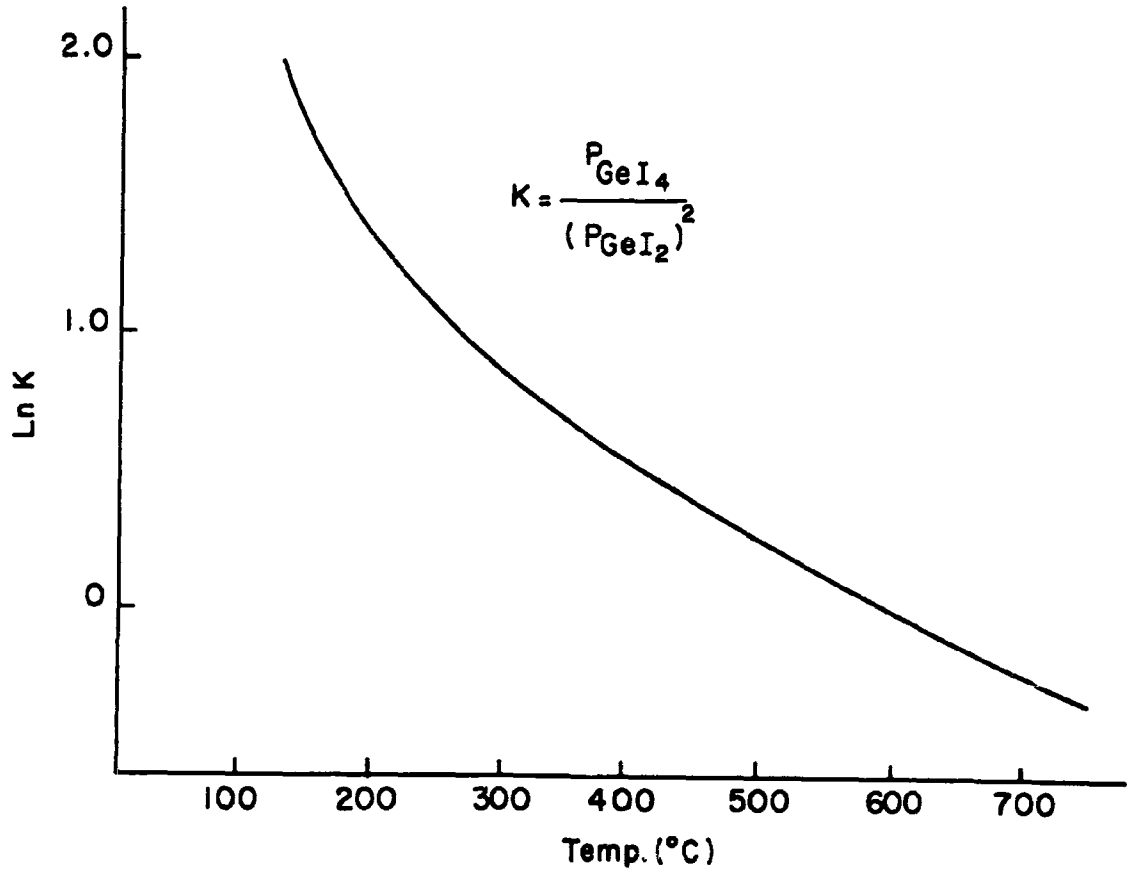

Fig. I-5. Variation of equilibrium constant K with temperature.

$$2GeI_2 \rightleftharpoons Ge(\text{solid}) + GeI_4$$

The equilibrium constant (k) of this disproportionation (defined as the ratio of the partial pressure of GeI_4 to the square of the partial pressure of GeI_2*) is determined by minimizing the free energy of the system.[2] This is plotted in Figure I-5 as a function of temperature. It is obvious that in zone II, where the maximum pressure of GeI_2 is required, the temperature should be high, and in zone III the temperature should be low in order to give the maximum pressure of GeI_4, or to give the maximum deposition of Ge. The limiting low temperature is that at which the GeI_2 crystalizes. The phosphorus from region IV is carried to region III where it becomes incorporated in the Ge and thus dopes the Ge n-type. The chemical reactions involved in the transport of impurities are not known.

The Ge from one side of the seed is removed by lapping. The remaining crystal is then cut into pellets about 20 mils square and mounted on transistor headers. Ohmic contacts are made to either side of the junction by alloying techniques. The junction is electrolytically etched (to reduce junction area) until the desired peak current is obtained (The I-V characteristics are monitored during etching.). After the device has been etched it is washed and dried and its area, capacitance, and its I-V characteristics are measured. The I-V characteristics are obtained by standard methods. The capacitance measurements are made at a frequency of 10^6 cps, using a Wayne Kerr Radio Frequency Bridge Type B601. The areas of the junctions are estimated by viewing them under a microscope using a calibrated eyepiece.

*The square is used because two molecules of GeI_2 are needed to form one molecule of GeI_4.

Experimental Results

A. I-V Characteristics

The typical I-V characteristics obtained at room temperature and at 77° Kelvin for tunnel heterodiodes are shown in Fig. I-6. The negative resistance is readily observable. The peak-to-valley current ratio on this unit is 1.6:1 at 300°K and 3.5:1 at 77°K. In the positive resistance region near the origin the forward tunneling current is almost independent of the temperature. The current in the valley region is much higher than that which would be expected from injection. In order to determine the source of this high excess current, the following experiment was conducted: In one deposition run in which n-type Ge was deposited simultaneously on degenerate p-type GaAs, the following classes of tunnel diodes were made:

(1) Ge-GaAs heterojunction from deposited Ge on GaAs seed

(2) Ge homojunction from deposited Ge on Ge seed

(3) Ge homojunction from alloying into the Ge seed of (2)

(4) Ge homojunction from alloying into the deposited Ge of (2)

(5) GaAs homojunction from alloying into the GaAs seed of (1).

The diodes from (3) and (5) above produced tunnel diodes having very good I-V characteristics, i.e., peak-to-valley current ratios in excess of 15. The diodes from (1), (2) and (4) above had degraded characteristics of the type mentioned earlier. This indicates that the deposited Ge is somehow at fault since if the difficulty were merely associated with the interface between seed and deposition, the diodes from (4) would be expected to have good I-V characteristics.

In some units a second negative resistance region is observed in the I-V characteristics. It is thought that this results from tunneling of electrons to (or from) an impurity band within the forbidden region. This second 'hump' has been observed both in Ge and in GaAs homojunctions.[3]

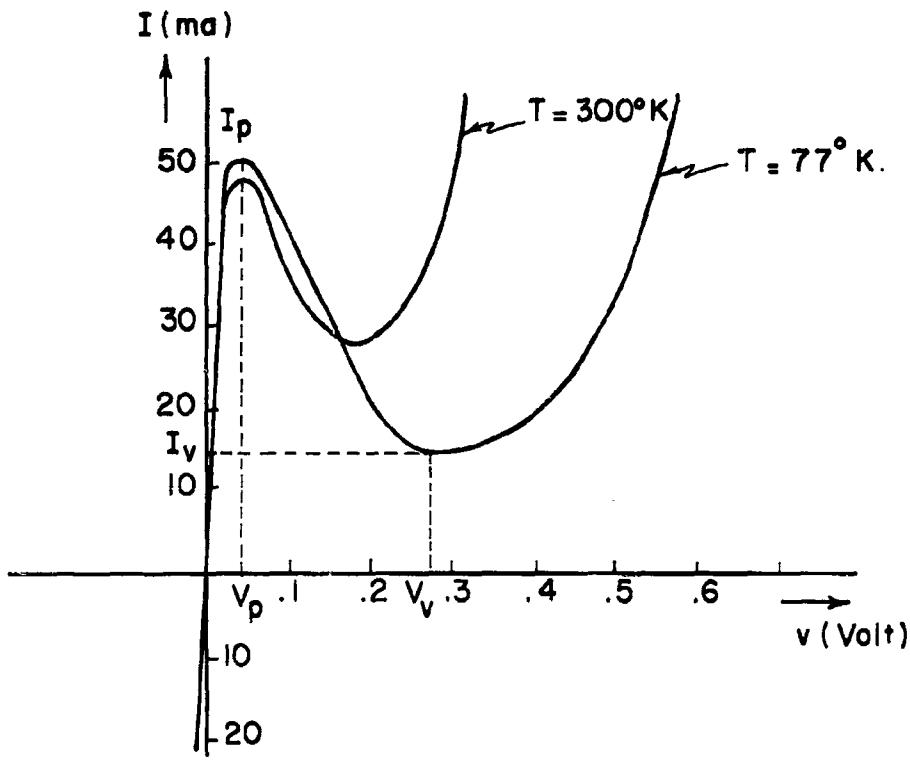

Fig. I-6. Typical I-V characteristic of a tunnel heterodiode obtained in the experiment at T = 300°K and T = 77°K.

B. C-V Characteristics

The results of the capacitance measurement and the estimated junction areas are listed in Table I-1 as ratios of the former to the latter. If we assume the Ge to be more lightly doped than the GaAs, the transition region will be mostly in Ge and the net donor concentration in Ge can be estimated from the measured capacity and a knowledge of the built-in

Unit No.	$C_1/A(pf/cm^2)$	W(A)	$J_p(A/cm^2)$	$N_D(cm^{-3})$
p - 1	1.3×10^6	110	74	9.5×10^{18}
r - 2	1.1×10^6	130	24	7.0×10^{18}
ℓ - 1	3.9×10^5	370	5.4	1.1×10^{18}

Table I-1. Capacitance per cm^2, junction width, peak current density and net donor density in the deposited Ge for three representable tunnel heterodiodes.

voltage (V_D), and the junction area. The expression for the net donor concentration (N_D) in the more lightly doped material (assuming homogeneous doping) can be related to the capacitance and the total barrier voltage as:

$$\frac{1}{C^2} = \frac{2(V_D - D)}{q \epsilon A^2 N_D}$$

where ϵ is the permittivity of this region and A is the junction area. Plotting $1/C^2$ against V then yields V_D(the voltage intercept), and N_D (related to the slope).

Results on three typical units are summarized in Table I-1. The junction width as estimated from capacitance measurements* and the peak current density

*The non-degenerate junction formula for junction width $W = \epsilon A/C$ is assumed to apply.

j_p is also shown. It is seen that the larger doping levels result in narrower junctions and higher peak current density diodes as is expected.

C. Reliability

Only one unit (p-1) has been life tested and so the results may not be indicative of Ge-GaAs heterojunctions. It appears, however, that before much meaningful data can be obtained, units having higher peak to valley current ratios must be obtained.

This unit was tested at three times the peak current for a total of 1000 hours. No changes in I-V characteristics were observed. Although the heterojunction tested did not fail on life test, this experiment did not shed much light on the mechanism of failure in GaAs tunnel homojunctions for two reasons: First the Germanium was much more lightly doped than was the GaAs and so the transition region was essentially entirely within the Ge. As a result, there is only a very small region in the GaAs subjected to the high electric field of the transition region; and second, because of the large excess current, the injection current was negligible and presumably the injection current is necessary for failure.

Discussion

It would be desirable to raise the peak to valley current ratio in the tunnel heterojunctions. Since the deposited Ge was determined to be the cause of the low ratio obtained, improvement in the quality of the Ge should improve the I-V characteristics. However, since it is not known how to improve quality, efforts were made to increase the doping level of the Germanium and therefore to decrease the transition region width. Although increasing the temperature of the dopant in region IV in the furnace increases the doping level, excess phosphorus produces a polycrystalline deposit.

Alternatively, more lightly doped GaAs seeds may be used. This would result in more of the transition region being in the GaAs and if the quality of this GaAs is good, the I-V characteristics may be improved.

A (p-Ge) - (n-GaAs) heterojunction would offer the advantage that tunneling would be "direct." It is, however, difficult to deposit heavily doped Ge by the process described.

If failure in GaAs tunnel diodes is a result of recombination of injected carriers, it is quite possible that heterojunctions will not fail in this manner. Because of the difference in band gaps in the two materials, injection current is expected only on the Ge side of the junction.

APPENDIX II

JUNCTION CAPACITANCE OF DEGENERATE p-n TUNNEL JUNCTIONS*

Introduction

Early investigators of tunnel diodes assumed that the variation of junction capacitance with voltage was given by the same expression as applies for ordinary abrupt nondegenerate p-n junctions. Thus

$$C_b = \frac{k_a}{(v_b - v)^{1/2}} \qquad \text{(II-1)}$$

where k_a is a constant of the device and v_b is the built-in voltage. Furthermore, capacitance measurements over a range of voltages on p-n tunnel junctions showed behavior as given by Eq. (II-1) . It was then assumed that Eq. (II-1) was valid over the entire range of voltages. It is our purpose here to show that Eq. (II-1) is valid only over a restricted range of voltages and that significant departures from the prediction of Eq. (II-1) are found in p-n tunnel junctions beyond this range. Experimental results are presented, and a theory is developed which explains these experimental results over almost the entire range of currents and voltages for which measurements were made.

Theory

It is useful to recall that Eq. (II-1) was derived by considering only the bound charge due to ionized acceptors and donors in the transition region of the junction. In a tunnel diode there are two additional kinds of charges not present in ordinary p-n junctions. These are the tunneling charges, and the free carriers (i.e., electrons and holes) that result because the Fermi

*In this appendix, R. P. Nanavati summarizes the masters thesis of Carlos Am deAndrade.

levels on the n and p sides are within the conduction and valence bands. These last two kinds of charges influence behavior for voltages less than the peak voltage, and the region of high forward current respectively. In the theory which follows all three kinds of charges are taken into account in solving Poisson's equation.

Figure II-1 shows where the free electrons and holes, and the tunneling electrons are located in the junction region. Figure II-2 shows approximately the distribution of charge density. The transition region is broken into five zones for computational convenience.

The junction capacitance can be calculated from the defining equation

$$C_j(v) = \frac{dQ}{dv} = \frac{dN_t}{dv} + \frac{dN_e}{dv} + \frac{dN_b}{dv} \qquad \text{(II-2)}$$

where Q is the total charge in the transition region of the junction

N_t is the charge due to tunneling electrons

N_e is the charge due to free electrons

N_b is the bound charge

and v is voltage.

In evaluating Eq. (II-2) only the negative charges will be considered. (Alternately only the positive charges could have been considered.) If the three charges can be obtained as a function of voltage, the junction capacitance can be evaluated.

The following are the major assumptions of the analysis. (1) The entire calculation is made at zero absolute temperature. (2) The carrier density at the top of valence band edge in the forbidden region is the same as the carrier density at the edge of the forbidden region at $x = w/2$ for each energy level. (3) The field is negligibly small outside the transition region. (4) The electrons tunneling from the n-side (i.e., between E_n and E_{cn}) towards the p-side are neglected.

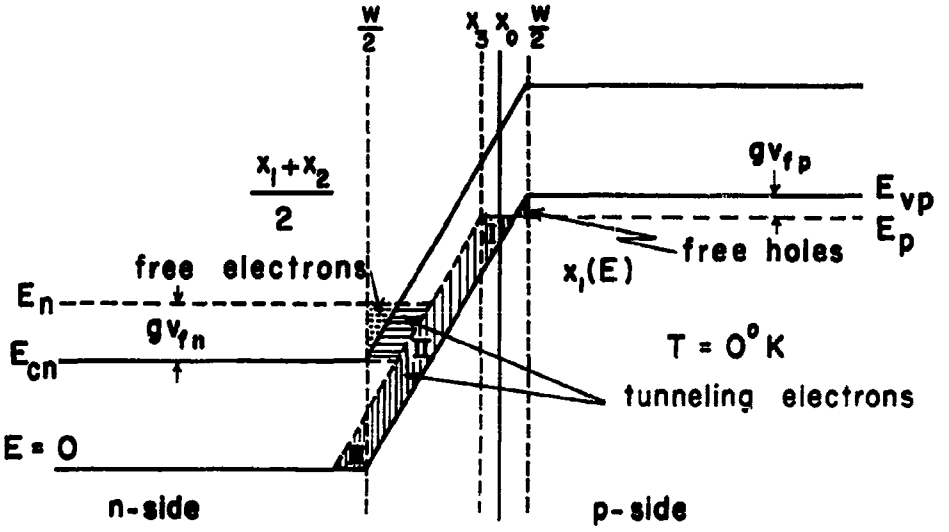

Fig. II-1. Free carriers and tunneling electrons in the transition region.

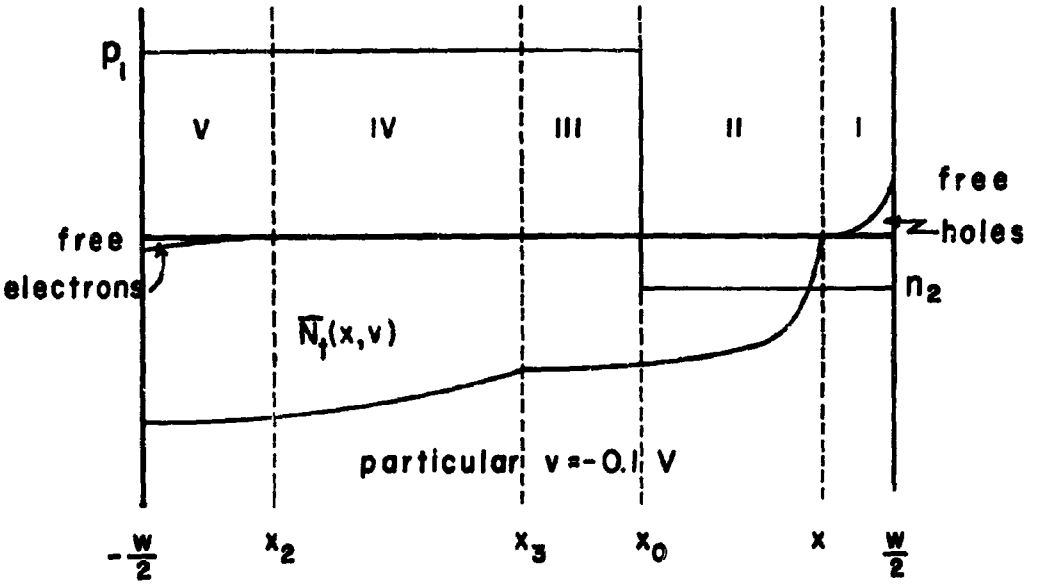

Fig. II-2. Distribution of charge in the transition region.

The first assumption allows us to carry out the integrations in closed form. The second assumption gives a higher than actual carrier density in the forbidden region. At present there is no satisfactory theory to calculate the actual carrier density. Assumption three is a very good one particularly because in tunnel diodes the doping levels are high. Calculations show that the fourth assumption too is a good one. It may be noted that the carrier density itself is not claimed to be small, only its variation with voltage is negligibly small.

The tunneling electron density can be calculated by solving Schrödinger's equation in all the regions of Fig. II-1 and requiring continuity of the wave function ψ across each boundary between two adjoining regions. When this procedure is followed, the tunneling charge N_t obtained is given below

$$N_t(v) = \frac{8\pi(2|m^*_h|)^{3/2}\, w\, E_{cn}{}^{q\,3/2}}{3h^3\, E_{vp}} \left[(v_b - v)^{3/2} - v_{fp}{}^{3/2}\right] \sum_{n=0}^{\infty} \frac{\left(-K_2 \frac{E_{cn}}{2\sqrt{2}}\right)^{3/2}{}^{n}}{n!\ (3n+2)} \qquad \text{(II-3)}$$

The free electrons N_e were found to be

$$N_e = \frac{16\,\pi}{15h^3} (2m^*_e)^{3/2} \frac{w}{E_{vp}} (E_n - E_{cn})^{5/2} \qquad \text{(II-4)}$$

The bound charge N_b was obtained as

$$N_b = n_2 \left[\frac{w(v)}{2} - x_o(v)\right] \qquad \text{(II-5)}$$

When Eqs. (II-3), (II-4) and (II-5) are substituted into Eq. (II-2) the result is

$$C_j(v) = \left\{ \frac{8\pi}{3h^3}(2|m^*_h|)^{3/2} v_g q^{5/2} - \frac{3w}{2(v_b - v)^{1/2}} \sum_{n=0}^{\infty} \frac{\left(-K \frac{E_{cn}^{3/2}}{2\sqrt{2}}\right)^n}{n!\,(3n+2)} \right.$$

$$\left. + [(v_b - v)^{3/2} - v_{fp}^{3/2}]\left[\frac{d}{dv}\left(\frac{w}{v_b - v}\right)\right] \sum_{n=0}^{\infty} \frac{\left(-K \frac{E_{cn}^{3/2}}{2\sqrt{2}}\right)^n (n+1)}{n!\,(3n+2)} \right\}$$

$$+ \left\{ qn_2 \left(\frac{1}{2} \frac{dw}{dv} - \frac{dx_o}{dv}\right) \right\}$$

$$+ \left\{ \frac{16\pi}{15h^3} (2m^*_e)^{3/2} q^{5/2} (v_{fn})^{5/2} \frac{d}{dv}\left(\frac{w}{v_b - v}\right) \right\} \qquad \text{(II-6)}$$

where

$$K = \frac{4\sqrt{2}\, w\, 4\sqrt{|m^*_h\, m^*_e|}}{3\hbar\, E_{vp}} \qquad \text{(II-7)}$$

In Eq. (II-6) the first $\{\ \}$ is the capacitance due to tunneling charge C_t, the second $\{\ \}$ is capacitance due to bound charge C_b, and the third $\{\ \}$ is capacitance due to free charge C_e. It is clear from Eq. (II-6) that to evaluate $C_j(v)$ explicitly a knowledge of dw/dv and dx_o/dv is essential. These two quantities can be calculated by solving Poisson's equation by integration.

Poisson's Equation

Poisson's Equation can be solved only if the boundary conditions are known. These boundary conditions are given below

$$\sum p(-\tfrac{w}{2}) - \sum n(-\tfrac{w}{2}) = 0 \qquad \text{(II-8)}$$

$$\sum p(w/2) - \sum n(w/2) = 0 \qquad \text{(II-9)}$$

$$\sum P - \sum N = 0 \qquad \text{(II-10)}$$

$$\left.\frac{d\phi_I}{dx}\right|_{x=w/2} = 0 \qquad \text{(II-11)}$$

$$\phi(0) = 0 \qquad \text{(II-12)}$$

$$\phi_V(-\tfrac{w}{2}) - \phi_I(\tfrac{w}{2}) = v_b - v \qquad \text{(II-13)}$$

where ϕ is the potential function

ϕ_I is the potential function in region I

ϕ_V is the potential function in region V

P and N are <u>total</u> charges due to electrons and holes in the transition region.

The first two follow because the field outside the transition region is zero, and hence net space charge neutrality must hold. The third merely says that the net positive charge must balance the net negative charge in the transition region. Equation (II-11) says the field is zero outside the transition region. Equation (II-12) is the voltage reference and Eq. (II-13) relates the total voltage across the transition region to the built-in voltage and the externally applied voltage v.

When Poisson's equation is integrated in each of the five regions of Fig. II-1 and the results combined, two equations are obtained with $x_o(v)$ and $w(v)$ as the two unknowns as follows

$$\frac{x_o}{w} = \frac{4.6v_{fp}^{3/2} - 0.33v_{fn}^{3/2} + 0.267v_{fn}(v_b-v)^{-1/2} - 3.68v_{fp}^{3/2}(v_b-v)^{-1/2} + 2.3\sum v_g(v_b-v)^{1/2} - 9.2v_{fp}^{3/2}\sum v_g(v_b-v)^{-1}}{13.8(v_b-v)^{1/2}\sum v_g + 0.67\, v_{fn}^{3/2} + 9.2\, v_{fp}^{3/2}} \qquad \text{(II-14)}$$

where $-q\, v_g = E_{cn}$

$$\frac{-q^{5/2}\, 4\pi(2m^*_e)^{3/2}\, w^2}{h^3\, k\, \epsilon_o}\left\{13.8(v_b-v)^{1/2}\sum v_g\left[\frac{1}{8} + \frac{x_o^2}{2w^2} + \frac{x_o}{2w} + \frac{2}{3}\left(\frac{v_{fp} + v_g/2}{v_b - v}\right)^{3/2} - \frac{6}{15}\left(\frac{v_{fp} + v_g/2}{v_b - v}\right)^{5/2} - \frac{4}{15}\right] + \frac{2}{3}v_{fn}^{3/2}\left(\frac{1}{8} + \frac{x_o^2}{2w^2} + \frac{x_o}{2w}\right)$$

$$+ \frac{13.8\left(\frac{1}{2} - \frac{x_o}{w}\right)^{1/2}}{(v_b - v)^{1/2}}\, v_g^2 \sum\left(\frac{v_{fp} + v_g/2}{v_b - v} - 1\right) - \frac{8v_{fn}^{7/2}}{105(v_b-v)^2}$$

$$+ \frac{13.8}{3}\, v_{fp}^{3/2}\, \frac{x_o}{w}\left(\frac{x_o}{w} + 1\right) - \frac{13.8}{6}\, v_{fp}^{3/2} + \frac{2(13.8)\, v_{fp}^{5/2}}{15\,(v_b - v)}$$

$$- \frac{13.8\left(\frac{1}{2} - \frac{x_o}{w}\right)^{1/2} v_g^3 \sum''}{(v_b - v)^{3/2}} - \frac{8(13.8)\, v_{fp}^{7/2}}{105(v_b - v)^2}$$

$$+ \frac{2(13.8)\, v_{fp}^{5/2}}{15(v_b - v)} - \frac{13.8\, v_{fp}^{3/2}}{12}\Bigg\} = v_b - v \qquad \text{(II-15)}$$

Equations (II-14) and (II-15) are quite formidable and, except for the capacitance C_e, defy solution in a closed form. The series used in these

equations turn out to be only slowly converging and hence a computer solution is necessary.

The capacitance C_e can however be calculated as follows

$$C_e = \frac{dN_e}{dv} = \frac{16\pi(2m^*_e)^{3/2}(qv_{fn})^{5/2}}{15\ h^3}\left[\frac{(v_b - v)\frac{dw}{dv} + w}{(v_b - v)^2}\right] \qquad \text{(II-16)}$$

In the next section we shall see that in Eq. (II-16)

$$(v_b - v)\frac{dw}{dv} << w \qquad \text{(II-17)}$$

in the vicinity of built-in voltage. Thus

$$C_e = \frac{(\frac{16\pi}{15h^3})(2m^*_e)^{3/2}\ (q\ v_{fn})^{5/2}\ w}{(v_b - v)^2} = \frac{k_e}{(v_b - v)^2} \qquad \text{(II-18)}$$

The last part of the equation can be permitted if w can be considered essentially constant in the small voltage range in the vicinity of the built-in voltage v_b.

It should be mentioned here that the calculations of x_o/w and w are valid only for $0.1 < v < 0.5$ volt. For $v > 0.5$ volt, x_2 overlaps x_3 (See Fig. II-2), and Poisson's equation would need to be formulated and solved.

Numerical Calculations and Experimental Results

We shall consider a GaAs tunnel diode made in our laboratory, many of whose parameters are known either from experimental measurements or from the best available published information. The device constants of this tunnel diode are listed below

$|m^*_h| = 0.5m$ where m is the free electron mass.

$$m^*_e = 0.087m$$

$$v_D = 1.4 \text{ volts}$$

$$W = 0.5 \times 10^{-8} \text{ meter}$$

$$v_g = 1 \text{ volt}$$

Corresponding to these values the series can be numerically evaluated and the variables x_o, w, and their derivatives can be computed with the help of the computer. Figure II-3 and II-4 show the result of these computations. In Fig. II-3 the series are plotted, for convenience, against an auxiliary variable C_o, given by

$$C_o = \frac{-K E_{cn}^{3/2}}{2\sqrt{2}} = \frac{-4\sqrt{2}\sqrt{|m^x_h \; m^x_e|}\,(q\, v_g)^{3/2}\, w}{3\hbar\, q\, 2\sqrt{2}\,(v_b - v)} \qquad \text{(II-19)}$$

For the tunnel diode being considered

$$C_o = -11.8\,(10^8 w)/(v_b - v)$$

The capacitance measurements were made with a high-frequency bridge, and utilized the circle diagram[1] technique modified so that it was not necessary to determine the series inductance or resistance which are often difficult to determine accurately.

Figure II-5 shows the nature of experimental $C_j(v)$ curve and that predicted by Eq. (II-1). It is clear that the form of the prediction of Eq. (II-1) fits the experimental observation over a range of voltages from just beyond the peak voltage to within about 0.2 volt of the built-in voltage. Outside this range of voltage, however, the experimental behavior is markedly different. The theory of the preceding sections in this Appendix is an attempt to find a model to explain the entire curve. It turns out that though the calculations are quite complex, the formulation of the $C_j(v)$ as given here predicts the straight-line behavior

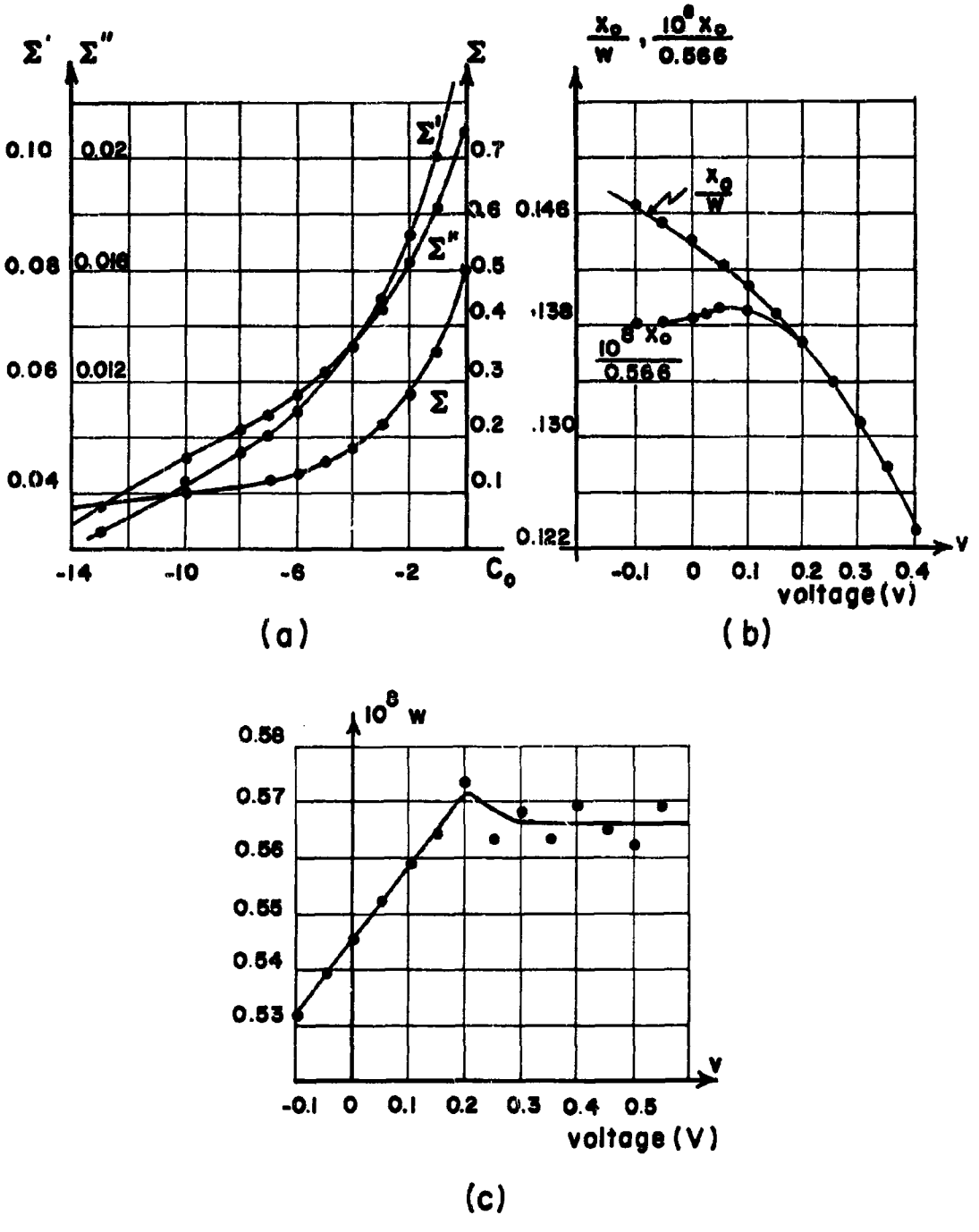

Fig. II-3. Numerical computations of parameters for a GaAs tunnel diode.

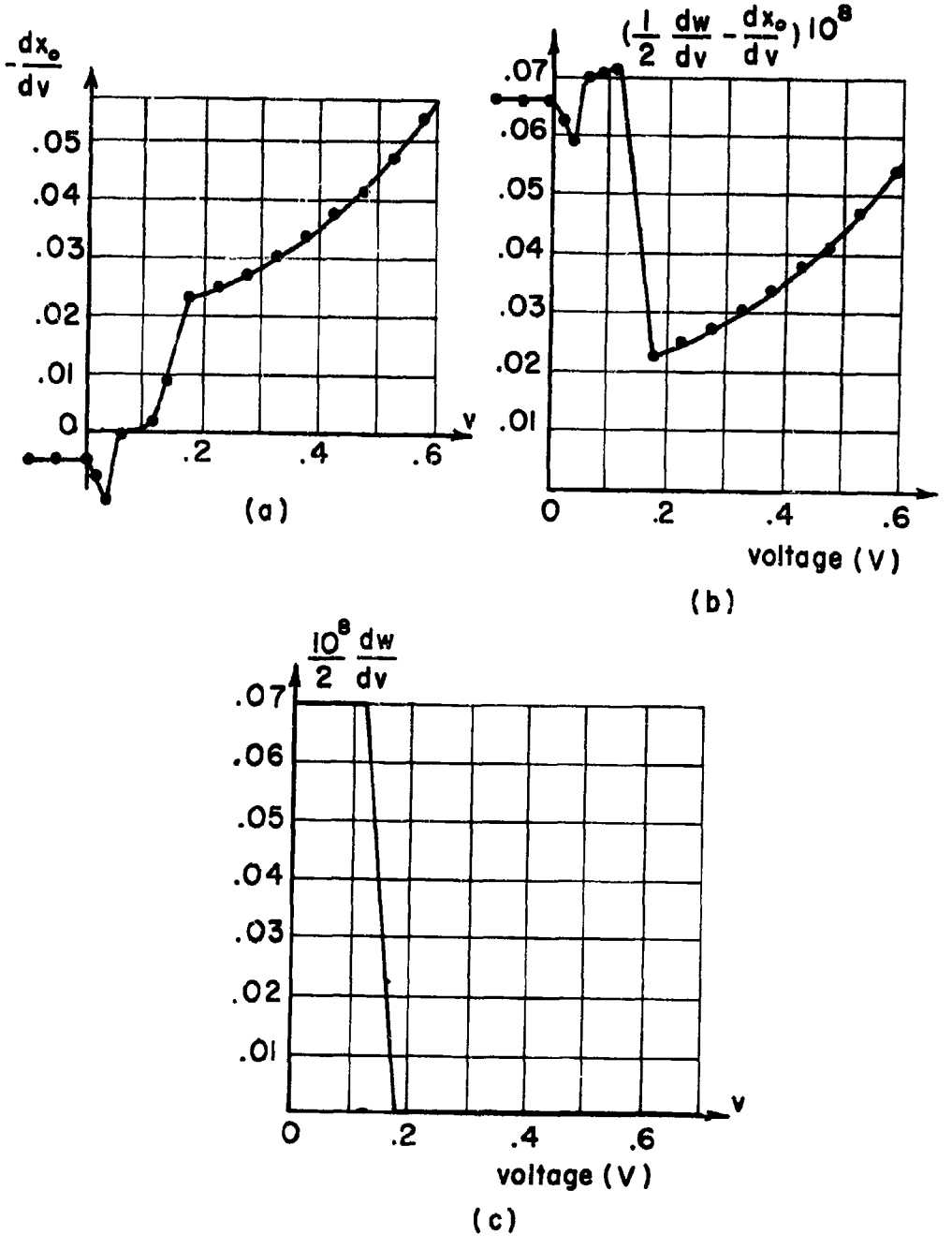

Fig. II-4. Numerical computations for derivatives for a GaAs tunnel diode.

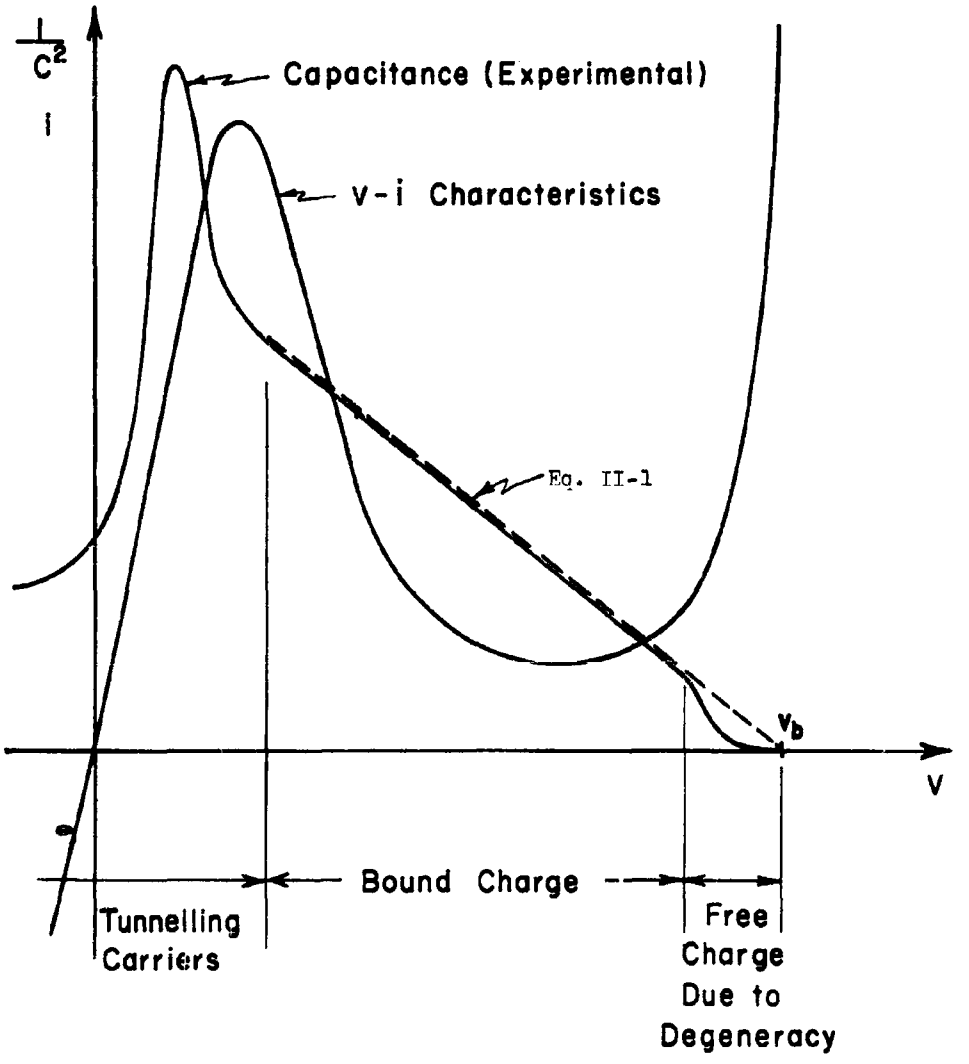

Fig. II-5. Junction capacitance for a degenerate p-n tunnel junction.

of $1/|C_j|^2$ for the range of voltages mentioned above. Except in the vicinity of the built-in voltage the calculations of Fig. II-4 indicate that $C_e << C_b$. In the vicinity of v_b, however C_e predominates over C_b. Figure II-6 shows two regions in log C_j vs. $\log10(v_b - v)$ plot obtained experimentally. It can be seen that the prediction of Eq. (II-18) is indeed experimentally verified because of the slope being 2. Many tunnel diodes including germanium ones showed similar behavior with the slope being quite close to 2 in the vicinity of the built-in voltage. The change of slope beyond the dotted line results because beyond about 0.2 volt away from v_b the capacitance C_b dominates.

Interestingly enough the theory of the preceding section predicts the experimentally observed capacitance minimum and the sharp rise for lower voltages. For instance, the theoretically predicted capacitance minimum for the diode in question is at 0.1 volt whereas the experimentally observed minimum occured at 0.065 volt.

Considering the very approximate nature of the device parameter values used, the agreement is considered fairly good. The general shape of the curve predicted by the theory and observed experimentally is the same for the entire range of positive voltages.

For negative voltages the agreement is not as good. The model would need to be refined to obtain a better agreement with experimental observations for the negative voltages. For instance assumption (2) of the Theory leads to an overestimate of the tunneling carrier density. A refinement of this assumption may produce better agreement between theory and experimental results.

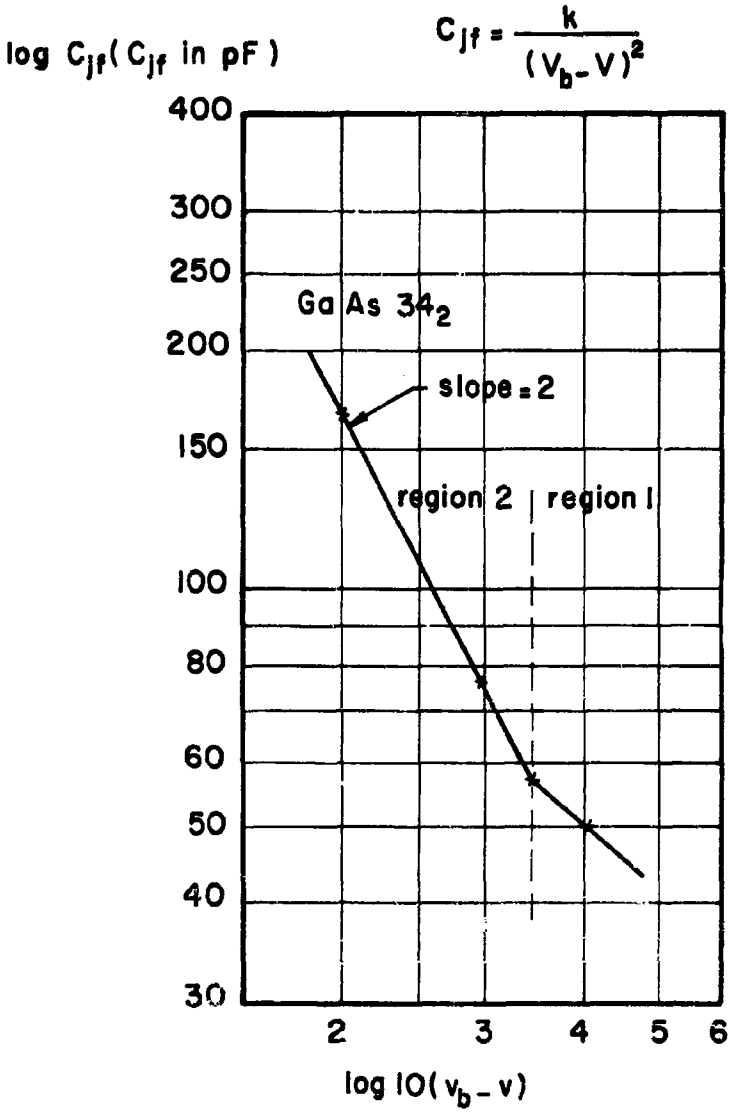

Fig. II-6. Experimental Data of the Junction Capacitance of a GaAs Tunnel Diode in the Vicinity of Built-in Voltage.

Conclusions

A fairly simple model has been proposed to explain the $C_j(v)$ for tunnel diodes. The theory and experiment agree qualitatively for all voltages, and have close quantitative agreement for positive voltages (in spite of only approximate knowledge of important device parameters such as E_g, carrier densities, and Fermi levels). The best agreement with experimental results was for C_e and C_b. The tunneling component of capacitance C_t was less accurately known quantitatively. It may be mentioned that the sharpness of the capacitance minimum (or the $1/|C_j|^2$ peak) is strongly sensitive to carrier density on both sides of the junction. Unfortunately these are known only approximately. Incidentally the sharpness of the capacitance minimum (essentially occurring within about 10 millivolts) is probably the most likely cause of the scattered data obtained by others for voltages less than the v-i peak voltage in tunnel diodes.

REFERENCES

Section 2

1. K. M. van Vliet, "Noise in Semiconductors and Photoconductors," Proc. IRE, vol. 46, (June, 1958), pp. 1004-1018.
2. See for example, E. L. Grant, "Statistical Quality Control," McGraw-Hill Book Company, Inc., New York, 1946.
3. Instruction book for Quan-Tech Model 310 Transistor Noise Analyzer, Quan-Tech Laboratories, Boonton, New Jersey.
4. D. Bell, "Electrical Noise," D. Van Nostrand Company, Inc., Princeton, New Jersey, 1960, pp. 258-262.
5. W. B. Davenport and W. L. Root, "Random Signals and Noise," McGraw-Hill Book Company, Inc., New York, 1958, pp. 41-42.
6. D. Bell, ibid. pp. 239-240.
7. P. L. Kirby and G. P. Sibilia, "An Investigation of Current Noise in Fixed Resistors," Proceedings of Symposium on Noise in Fixed Resistors, 5 March 1959, issued by Royal Radar Establishment, Great Malvern, England, pp. 1-25.
8. E. L. Grant, ibid.
9. P. L. Kirby and G. P. Sibilia, ibid., Fig. 1.13.
10. "Electrical Noise and Integrity of Semiconductor Devices," m/i Systems Design, February, 1963, Fig. 1.
11. P. L. Kirby and G. P. Sibilia, ibid., Fig. 1.14.
12. J. G. Curtis, "Current Noise Measurements as a Failure Analysis Tool for Film Resistors," Physics of Failure in Electronics, edited by M. F. Goldberg and J. Vacarro, Spartan Books, Inc., Baltimore, Maryland, 1963, pp. 204-213.

Section 2 (continued)

13. W. Feller, "Probability Theory and Its Applications," John Wiley and Sons, New York, 1950, Chapters 6 and 7.
14. Davenport and Root, ibid., p. 36
15. A. L. McWhorter, "1/f Noise and Germanium Surface Properties," Semiconductor Surface Physics (R. H. Kingston Editor) University of Pennsylvania Press, 1957, pp. 207-227.
16. Davenport and Root, ibid., Chapter 6.
17. A. Erdelyi (editor), "Tables of Integral Transforms," McGraw-Hill Book Company, Inc., New York, 1954, volume I, p. 8, entry 12.
18. See for example, E. Jahnke and F. Emde, "Tables of Functions," Dover Publications, New York, 1945, p. 2, 6-9.
19. A. Van der Ziel, "On the Noise Spectra of Semiconductor Noise and of Flicker Effect," Physica, vol. 16, 1950, p. 359.
20. W. H. Card, et.al. "Theoretical and Experimental Studies Relating to Mechanisms of Failure of Semiconductor Devices," Syracuse University Research Institute Report No. EE 751-625TN-3, 1962, pp. 2-15 to 2-21.

Section 3

1. R. H. Campbell and R. A. Chipman, "Noise from Current-Carrying Resistors 20 to 500 KC, Proc. IRE, vol. 37, 1949, pp. 938-942.
2. D. A. Bell, "Electrical Noise," D. Van Nostrand Co., Inc., Princeton, New Jersey, 1960, pp. 258-262.
3. W. B. Davenport and W. L. Root, "Random Signals and Noise," McGraw-Hill Book Company, Inc., 1958, pp. 267-273.
4. See for example, W. R. Bennett, "Methods of Solving Noise Problems," Proc. IRE, vol. 44, May, 1956., pp. 609-638.

Section 3 (continued)

5. Davenport and Root, ibid., pp. 145-170.

6. ibid, pp. 267-273.

7. R. R. Bennett and A. S. Fulton, "The Generation and Measurement of Low Frequency Random Noise," Journal of Applied Physics, vol. 22, September, 1951, pp. 1187-1191.

8. W. Howard Card, et.al., "Theoretical and Experimental Studies Relating to Mechanisms of Failure of Semiconductor Devices," Syracuse University Research Institute Report No. EE 751-625TN-3, 21 May 1962, pp. 3-1 to 3-17.

9. Davenport and Root, ibid., pp. 81-84.

Section 4

1. H. J. Henkel, "Aging Effects in GaAs Tunnel Diodes," Z. Naturforsch, vol. 17a, April, 1962, pp. 358-360.

2. N. Holonyak, Jr., T. Selig, and J. Smith, "Hump Current Dependence upon Trapping Effects and the Relationship to some Aspects of Forward-Injection Failure of GaAs Tunnel Diodes," IRE Trans. vol. ED-8, September, 1961, pp. 427 and 428.

3. R. D. Gold and L. R. Weisberg, "The Degradation of GaAs Tunnel Diodes," IRE Trans., vol. ED-8, September, 1961, p. 428.

4. D. Meyerhofer, G. A. Brown, and H. S. Sommers, Jr., "Degenerate Germanium I. Tunnel, Excess and Thermal Current in Tunnel Diodes," Physical Review, vol. 126, May 15, 1962, pp. 1329-1341.

5. R. L. Anderson, "Radiation from GaAs Tunnel Diodes," Proc. IEEE, vol. 51, April, 1963, p. 610.

Section 5

1. R. J. Keyes and T. M. Quist, "Recombination Radiation emitted by Gallium Arsenide," Proc. IRE, vol. 50, August 1962, pp. 1822-1823.
2. J. I. Pankove and J. E. Berkeyheiser, "A Light Source Modulated at Microwave Frequencies," Proc. IRE, vol. 50, September, 1962, pp. 1976-1977.
3. R. N. Hall, G. E. Fenner, J. D. Kingsley, T. J. Soltys, and R. O. Carlson, "Coherent Light Emission from GaAs Junctions," Phys. Rev. Letter, Vol. 7, November, 1962, pp. 366-368.
4. M. I. Nathan and G. Burns, "Recombination Radiation in GaAs by Optical and Electrical Injection," Applied Phys. Letter, Vol. 1, December 1, 1962, pp. 89-90.
5. T. M. Quist, R. H. Rediker, R. J. Keyes, W. E. Krag, B. Lax, A. L. McWhorter, and H. J. Ziegler, "Semiconductor Maser of GaAs," Applied Phys. Letter, vol. 1, December, 1962, pp. 91-92.
6. R. L. Anderson, "Radiation from GaAs Tunnel Diodes," Proc. of IEEE, Vol. 51, April, 1963, p. 610.
7. R. P. Nanavati, "Some Physical Mechanisms Contributing to Tunnel Diode Failure," Physics of Failure in Electronics, Proceedings, Spartan Books, Inc., p. 214, 1963.
8. T. Yajima and L. Esaki, Journal Phys. Soc., Japan, vol. 13, 1958, p. 128.
9. E. O. Kane, "Theory of Tunneling," Journal of Applied Physics, vol. 32, January, 1961, pp. 83-92.
10. A. G. Chynoweth, W. I. Feldman and R. A. Logan, "Excess Current in Silicon Esaki Junctions," Physical Review, vol. 121, No. 3, February 1, 1961, pp. 684-694.
11. W. Franz, vol. 17, p. 155, in J. Flugge (ed.), "Handbuch der Physik," Springer-Verglag OHG, Berlin, 1956.

Section 5 (continued)

12. M. Cardona, "Electron Effective Masses in InAs and GaAs as a function of Temperature and Doping," Physical Review, vol. 121, No. 3, 1 February 1961, pp. 752-758.

Appendix I

1. R. L. Anderson, Solid State Electronics, vol. 5, pp. 341-351, 1962.
2. W. L. Jolly and W. M. Lathimer, J. Amer. Chem. Soc., 74, 1952, p. 5754 and 5752.
3. N. Holonyak, Jr., I. A. Lesk, R. N. Hall, J. J. Tiemann, and H. Ehrenreich, Phys. Rev. Letters, vol. 3, No. 4, August, 1959, pp. 167-8.
4. W. Schottky, Z. Physik, 118, pp. 539 (1942).

Appendix II

1. W. H. Card, "Bridge Measurement of Tunnel Diode Parameters," IRE Trans. on Electron Devices, vol. ED-8, pp. 215-220, May 1961.